BUMBY, ADAM JOHN

THE GEOLOGY OF THE RUSTENBURG FAULT

MSc UP 1997

The geology of the Rustenburg Fault

by

ADAM JOHN BUMBY

Submitted in partial fulfilment of the requirements for the degree

MAGISTER SCIENTIAE

in the Faculty of Science
University of Pretoria

PRETORIA

August 1997

THIS THESIS REPRESENTS THE ORIGINAL WORK OF THE AUTHOR, EXCEPT WHERE SPECIFIC ACKNOWLEGEMENT IS MADE TO THE WORK OF OTHERS

AUGUST 1997

ABSTRACT:

The N.N.W.-S.S.E. striking Rustenburg Fault zone, in the western Transvaal Basin, South Africa, has been mapped, in order to unravel its tectonic history. Thickness differences in the Daspoort Formation of the Pretoria Group on opposite sides of the Fault suggest that the Fault was active during Pretoria Group sedimentation, with normal faulting producing localised second-order basins on the down-thrown side of the Fault.

In post-Pretoria Group times, but before the intrusion of the Bushveld Complex at ~2050 Ma, the area surrounding the Fault zone underwent two compressive events. The first was directed N.E.-S.W., producing S.E.-N.W. trending folds, and the second was directed N.W.-S.E., producing N.E.-S.W. trending folds. The second set of folds refolded the first set to form typical transitional Type 1-Type 2 interference folding, and this compression ultimately caused reactivation of the Rustenburg Fault, so that dextral strike-slip movement displaced the Pretoria Group sediments by up to 10.6 km.

The subsequent intrusion of the Bushveld Complex into the adjacent strata intensely recrystallised, and often assimilated, the strata along the Fault zone. The fault rocks within the Fault zone were also recrystallised, destroying any pre-existing tectonic fabric. Locally, the Fault zone has been assimilated by the Bushveld Complex

After the intrusion of the Bushveld Complex, little movement has occurred along the Fault, especially where the Fault passes under areas occupied by the Bushveld Complex. It is thought that the crystallisation of the Bushveld Complex has rheologically strengthened the neighbouring strata, preventing them from being refaulted.

This model presented above is at variance with previous assumptions that continuous regional extension during Pretoria Group sedimentation culminated in the intrusion of the Bushveld Complex.

SAMEVATTING:

Die N.N.W.-S.S.O. strekkende Rustenburgverskuiwing, in die westelike Transvaalkom, Suid-Afrika, is gekarteer om sy tektoniese geskiedenis te bepaal. Dikte verskille in die Daspoort Formasie, van die Pretoria Groep, aan weerskante van die verskuiwing dui daarop dat dit aktief was tydens Pretoria Groep sedimentasie. Die afskuiwing het dus gelokaliseerde tweede-orde komme gevorm aan sy sakkant.

In na-Pretoria Groep tye, maar voor die indringing van die Bosveldkompleks teen ~2050 Ma, is die omgewing waarin die verskuiwing voorkom aan twee kompressiewe deformasie gebeurtenisse onderwerp. Die eerste was N.O.-S.W. gerig en het S.O.-N.W. neigende plooie tot gevolg gehad; die tweede was N.W.-S.O. gerig en het N.O.-S.W. neigende plooie tot gevolg gehad. Die tweede generasie plooie het die eerste generasie herplooi om oorgangs Tipe 1 - Tipe 2 interferensie plooie te vorm, en hierdie kompressie het ook uiteindelik gelei tot die heraktivering van die Rustenburgverskuiwing as 'n regs-laterale strekkingsglipverskuiwing met tot 10.6 km verplasing van Pretoria Groep sedimente.

Die daaropvolgende indringing van die Bosveldkompleks het gelei tot die herkristallisasie en assimilasie van gesteentes langs die verskuiwingsone. Die gesteentes in die verskuiwingsone is ook geherkristalliseer en voorafbestaande tektoniese maaksels is grootliks vernietig. Op plekke is die verskuiwingsone ook geassimileer deur die Bosveldkompleks.

Na indringing van die Bosveldkompleks het baie min beweging plaasgevind langs die Rustenburgverskuiwing, veral in die gebiede waar die verskuiwing deur die Bosveldkompleks oorlê word. Dit word voorgestel dat die kristallisasie van die Bosveldkompleks gelei het tot die reologiese versterking van die naasliggende strata en dat dit nie die ontwikkeling van nuwe verskuiwings sou bevorder nie.

Die voorgestelde model verskil van vorige aannames dat regionale uitrekking tydens Pretoria Groep sedimentasie voortgeduur het en uiteindelik gekulmineer het in die indringing van die Bosveldkompleks.

TABLE OF CONTENTS.

LIST OF TABLES.

1: INTRODUCTION.

1.1: Location of the Rustenburg Fault:

The Rustenburg Fault is situated in the North-West Province, Republic of South Africa (Figure 1.1) and strikes N.N.W.-S.S.E. over a distance of 200 km, with its northern termination 80 km W.S.W. of the town of Thabazimbi, and the southern limit 15 km S.E. of the town of Carletonville (Geological Survey of South Africa 1:250 000 sheets 2426 [Thabazimbi], 2526 [Rustenburg], 2626 [Wes-Rand]). Midway along its length, the Fault passes close to the mining town of Rustenburg, from which it derives its name.

1.2: Location of the field area:

The northern extent of the investigation was 25^0 20.5' S, 27^0 E, where the Fault meets the Pilanesberg mountains and 26^0 S latitude was taken as the southern limit of investigation (Figure 1.2). The eastern and western margins of the field area were drawn approximately 5 km away from each side of the Rustenburg Fault zone (Figure 1.2). The area west of Pilanesberg, containing the Liliput segment (Vermaak, 1970) (Figures 1.1 and 1.2) of the Rustenburg Fault, was excluded from this study, due to its offset from the main segment of the Fault. The southern limit of the chosen field area was determined by outcrop quality.

The topography of the area north of Olifantsnek Dam (Figure 1.2) is often hilly, as much of the field area lies in the Magaliesberg mountain range (local elevation up to 1600m). South of Olifantsnek Dam, the topography is flatter. The field area is easily accessible by roads.

1.3: General geology of the field area:

The lithological units encountered within the field area are correlated with the sedimentary and volcanic strata of the Pretoria Group of the Transvaal Supergroup (Table 1.1) and with the igneous rocks of the Bushveld Complex (Table 1.2) (S.A.C.S., 1980). The field area was specifically chosen for the excellent outcrop afforded by the Fault as it cuts the Pretoria Group strata. Before considering the detailed geology of the Pretoria Group in the proximity of the Fault (Chapters 2

and 3), a brief outline of the geology of the Transvaal Supergroup and Bushveld Complex will provide a framework in which to study the Rustenburg Fault.

1.3.1: The Transvaal Supergroup:

The Neoarchaean-Palaeoproterozoic Transvaal Supergroup is preserved in three structural basins on the Kaapvaal Craton of southern Africa, the largest of which is the Transvaal Basin (Eriksson & Reczko, 1995). The field area is located in the centre of the Kaapvaal Craton, and on the southern side of the preserved Transvaal basin, where the succession youngs to the north (Figure 1.3).

The base of the Transvaal Supergroup, along the northern and eastern margin of the preserved basin, is marked by protobasinal rocks; initial rift-related volcanic rocks and immature sediments give way to more mature basinal deposits, reflecting the onset of deeper fault-controlled basin conditions (Eriksson et al., 1996). Only one zircon age has been determined in lava in these rocks, 2657-2659 Ma (Eriksson et al., 1996). Rocks of the 2714±8-2709±4 Ma (Armstrong et al., 1991) Ventersdorp Supergroup underlie the Transvaal basin elsewhere. It is possible that the protobasinal successions, preserved in discrete fault-controlled basins, reflect equivalent tectonic conditions to those inferred for the Ventersdorp volcanism (Eriksson & Reczko, 1995).

The onset of widespread Transvaal Supergroup sedimentation across the basin is marked by the Black Reef Formation, comprising a basal conglomerate overlain by feldspathic quartzite and shale (S.A.C.S., 1980). This unit succeeds the proto-basinal successions unconformably across the preserved basin (Eriksson & Reczko, 1995). The overlying Chuniespoort Group (dated at~2585-2430 Ma by U- Pb zircon: Altermann & Nelson, in press) contains a lower Malmani Subgroup, comprising stromatolitic dolomite with chert interbeds. The upper unit of the Chuniespoort Group across most of the Transvaal basin is the Penge Formation, consisting of banded iron formations (B.I.F.s), but it is not preserved in the study area. In the northeastern Transvaal basin, mixed clastic and carbonate rocks of the Duitschland Formation overlie the Penge Formation (S.A.C.S., 1980). The Chuniespoort Group has been interpreted as a carbonate ramp deposit formed in an epeiric sea, with supratidal, subtidal and shallow basinal or shelf facies (e.g. Clendenin, 1989).

The Pretoria Group unconformably overlies the Chuniespoort Group (Eriksson & Reczko, 1995), burying a palaeokarst landscape developed on exposed dolomites. This depositional hiatus, due to uplift, weathering and erosion, is estimated to have lasted at least 80 Ma (Eriksson & Reczko, 1995). The Pretoria Group comprises an alternation of sandstones (e.g., Daspoort and Magaliesberg Formations) and mudrocks (e.g., much of the Timeball Hill and Silverton Formations) (Table 1.1), reflecting sedimentation due to successive epeiric marine transgressions and alluvial regressions, in an intracratonic basin on the Kaapvaal Craton (Eriksson & Reczko, 1995). Interbedded with the sandstones and mudrocks are minor conglomerates, diamictites and carbonate rocks (Eriksson et al., 1995). Superimposed on this sedimentation are significant volcanic units, comprising thin andesitic lavas of the Bushy Bend Member and thick amygdaloidal andesites of the Hekpoort Formation (Table 1.1). The pyroclastics of the Machadodorp Member in the Silverton Formation are found only in the east of the preserved Transvaal basin.

The pattern of sedimentation and volcanism in the Pretoria Group has been interpreted as reflecting deposition within an extensional tectonic setting, either within half-grabens, controlled by movement along ancient fault zones such as the Thabazimbi-Murchison Lineament (Eriksson et al., 1991.), or the beginning of a continental rift (Schreiber et al., 1992). More recently Eriksson and Reczko (1995) suggested an intracratonic sag basin due to thermal subsidence during incipient continental break-up. The essentially extensional tectonic setting of the Pretoria Group was considered by Eriksson et al. (1995) to be compatible with the intrusion of the Bushveld Complex into the basin at ~2050 Ma (Harmer & Von Gruenewaldt, 1991).

1.3.2: The Bushveld Complex:

The approximately 2050 Ma (Harmer & Von Gruenewaldt, 1991) Bushveld Complex is the world's largest mafic layered intrusion (66,000 km^2 x 8-11 km in present thickness) and hosts large economic deposits of chromium, vanadium and platinum-group elements (Von Gruenewaldt & Harmer, 1993).

Sills intruded into upper Pretoria Group sedimentary rocks (Cawthorn et al., 1981; Sharpe, 1982), can be interpreted as a precursor to the main Bushveld event. The Bushveld mafic magmas of the Rustenburg Suite (Table 1.2) also intruded the Pretoria Group rocks, often exploiting the

Magaliesberg quartzite as a floor rock. The uppermost Transvaal Supergroup strata, the Rooiberg Group lavas (only preserved in the central and eastern Transvaal basin), were lifted to form the roof of the Complex. Syn-Bushveld sills also intruded along bedding planes in the Pretoria Group (Cawthorn et al., 1981). Where earlier tectonic activity had caused interference folding in the Transvaal sedimentary sequence, Bushveld magmas solidified around these localised domes to form preserved inliers of Transvaal rocks (Hartzer, 1995) (Figures 1.4 and 1.5).

The Bushveld Complex can be subdivided into two main units; the Rustenburg Layered Suite and the slightly younger rocks of the Rashoop Granophyre and the Lebowa Granite Suites. Mafic tc ultramafic layered Rustenburg rocks outcrop in four lobes, as well as in the western Nietverdiend intrusion, and are cross-cut by the acidic rocks, which also form part of the roof of the Complex in the centre of the intrusion (Figure 1.4). The Rustenburg Layered Suite was subdivided by Wager and Brown (1967) into informal zones (Table 1.2), some of which are bounded by economically important horizons (e.g., Merensky reef), and these zones be correlated in the different lobes.

The intrusion of the Bushveld Complex produced a contact metamorphic aureole in the surrounding Transvaal Supergroup country rocks (Vermaak, 1970; Cawthorn et al., 1981; Sharpe, 1982; Nell, 1985; Engelbrecht, 1986, Wallmach et al., 1989), so that arenaceous rocks became recrystallised to quartzite and argillaceous rocks were changed to hornfelses. Evidence for contact metamorphism in the Transvaal strata extends laterally for up to 20 km away from the contact with the Bushveld Complex (Sharpe, 1982). Primary sedimentary structures were often destroyed during recrystallisation (Vermaak, 1970). The extent of recrystallisation is highly variable between outcrops (see Section 2.7.2).

The shallow dip of layered Bushveld rocks towards the centre of the complex, and the approximately similar dip of the Transvaal Supergroup floor rocks (10^0 to 25^0), reflect thermal collapse after the emplacement of the intrusion (Harmer & Von Gruenewaldt, 1991).

1.3.3: The Pilanesberg Complex:

Although located outside of the field area, the proximity of the Pilanesberg Complex to the

Rustenburg Fault (Figures 1.2 and 1.4) warrants its consideration in the general geology of the area. The Pilanesberg Complex is a 1250 Ma alkaline pipe and consists of a central core of red foyaite, surrounded by ring dykes of green and white foyaite, tinguaite and syenite, with interlayered volcanics (Lurie, 1986). A swarm of radiating late-Pilanesberg (Lurie, 1986) dykes intruded away from the complex into the surrounding host rocks, and a set of syn- to late-Pilanesberg faults radiating westwards from the intrusion affected the Liliput segment of the Rustenburg Fault (Vermaak, 1970).

1.4: Previous work on the Rustenburg Fault:

The Rustenburg Fault has received little attention in the geological literature. Coertze (1962) and Bloy (1986) suggested contrasting movement directions on the Fault. Coertze (1962), working in the area between Boshoek and the Pilanesberg Complex (Figure 1.2), suggested post-Bushveld normal faulting, with downthrow to the east, due to the presence of sheared Bushveld gabbro, the displacement of chromitite seams, and the intrusion of late Bushveld bodies (e.g. magnetite and sulphide pipes) along the Fault zone. In a discussion of this paper, Cousins (1962) argued that evidence for the post-Bushveld age of the Fault was inconclusive, and ascribed any post-Bushveld fault movement in the area to Pilanesberg-aged faults. Cousins (1962) also questioned the sense of displacement proposed by Coertze (1962), as it could not account for the presence of Pretoria Group rocks on the eastern 'downthrown' side of the Fault. Bloy (1986) investigated the area between Rustenburg and Olifantsnek Dam (Figure 1.2) and interpreted the Rustenburg Fault as a dextral strike-slip fault, but offered no constraint on the timing of the Fault.

Vermaak (1970) mapped the area immediately west of the Pilanesberg Complex, including the N.W. striking Liliput segment of the Rustenburg Fault (Figure 1.2). Vermaak concluded that the Liliput Fault is a post-Bushveld normal fault with downthrow to the east, and he proposed that it was a northerly extension of the Rustenburg Fault which was displaced by Pilanesberg-aged faults.

Du Plessis and Walraven (1990) proposed a post-Bushveld age for normal faulting on the Fault, and related this to sinistral movement on the Thabazimbi-Murchison Lineament (T.M.L.) (Figure 1.5). They noted that such movement could not have occurred, as demonsrated by the inferred post-Bushveld strain ellipse for the T.M.L., and concluded that the post-Bushveld movement on

the Fault was probably due to reactivation of a pre-Bushveld structure. They also suggested that such pre-existing fractures acted as feeders for the Bushveld magmas.

Friese et al. (1995) considered general tectonic processes on the Kaapvaal Craton, and proposed a sinistral, Kibaran-aged (1400-1140 Ma), reactivation of the previous normal Rustenburg Fault. This interpretation is based on the apparent 5 km of sinistral offset by the Rustenburg Fault of two Pilanesberg-aged dykes north of Carletonville (A.E.W. Friese, pers comm., 1997).

It can therefore be seen that there is no consensus regarding the timing or sense of displacement of the Rustenburg Fault. All workers agree, however, on a post-Transvaal Supergroup age for the Fault. It is also apparent that each interpretation is based on investigation of limited areas along the strike of the Fault, rather than considering evidence from a large segment of the Fault.

1.5: Previous work on the tectonic history of the Kaapvaal craton relevant to this study:

While the Rustenburg Fault itself has not been the subject of detailed study, other structures within the Transvaal basin and surrounding areas on the Kaapvaal Craton have been more thoroughly investigated and recorded. An outline of the structures observed in the area adjacent to the Fault zone is given here to act as a framework into which a model for the evolution of the Rustenburg Fault may later be accommodated.

In view of their widespread usage among South African-based researchers, terms like pre-Transvaal, syn-Pretoria Group and post-Bushveld are utilised in the text to describe events that occurred pre- syn- and post- the deposition or development of the lithostratigraphic unit in question.

1.5.1: Summary of pre-Transvaal Supergroup deformation:

The core of the Kaapvaal craton had stabilised by 3100 Ma, to be followed by a period of terrane accretion around the northern and western margins of the shield until 2650 Ma (McCourt, 1995). This period of terrane accretion culminated in the Limpopo Orogeny (~2700 Ma; Barton & Van

Reenen, 1992) as the Zimbabwe craton collided with the northern margin of the Kaapvaal craton (McCourt, 1995). By the start of the Proterozoic (2500 Ma) the craton was firmly established (McCourt, 1995), already containing N.N.W.-S.S.E. and E.N.E.-W.S.W. orientated structural grains (Stanistreet & McCarthy, 1991) defined by the orientation of greenstone belts (Figure 1.5). These zones of weakness were reactivated during basin development throughout the rest of the Proterozoic history of the craton (Stanistreet & McCarthy, 1991). The E.N.E.-W.S.W. Thabazimbi-Murchison Lineament (T.M.L.) (Figure 1.5) was one of these major lineaments to have developed by this time, and defines a suture between two Archaean terranes (McCourt, 1995).

Coeval with terrane accretion, the late-Archaean also produced the first records of large scale cratonic sedimentation on the Kaapvaal craton. Basins, perhaps caused by collision-related impactogenic stresses within the craton, created depositories for the 3096-3074±6 Ma (Armstrong et al., 1991; Robb et al., 1991) Dominion Group volcanics and minor sediments, the ~3000-2914±8 Ma (Barton et al., 1989) Witwatersrand sediments and volcanics, Pongola Supergroup sediments and volcanics (2940-2870 Ma; Hegner et al., 1984), and for Ventersdorp Supergroup (2714±8-2709±4 Ma; Armstrong et al., 1991) volcanic and subordinate sedimentary lithologies. The Nsuze Group of the Pongola Supergroup, and the Dominion Group appear coeval and, similarly, the Mozaan Group of the Pongola Supergroup and the West Rand Group of the Witwatersrand Supergroup are coeval (Beukes & Cairncross, 1991). In contrast to the lower Witwatersrand and Pongola extensional basins, the Central Rand Group of the upper Witwatersrand Supergroup is thought to have been deposited within a compressional regime, either in a foreland (Burke et al., 1986) or hinterland (Coward et al., 1995) basin, in response to the start of Limpopo tectonics. Stanistreet and McCarthy (1991), and Eriksson and Reczko (1995) suggest instead that this compressional regime led to tectonic escape of the basement of the Witwatersrand basin to the S.W., with movement having occurred by reactivation of the Archaean lineaments.

The initiation of the Ventersdorp basin was accompanied by Klipriviersberg flood basalts at 2714±8 Ma (Armstrong et al., 1991), along N.E.-S.W. orientated fissures (Burke et al., 1985). Sinistral strike-slip movement along the T.M.L. (Figure 1.5) is thought to have reactivated Witwatersrand thrusts to produce N.E.-S.W. trending extensional rifts across the craton (Burke et al., 1985; Stanistreet & McCarthy, 1991), directly crossing the area later occupied by the

Rustenburg Fault. Burke et al. (1985) directly relate this event to the Limpopo Orogeny. However, many syn-Ventersdorp grabens also trend E.-W., which cannot be reconciled with this model. Hatton (1995) suggested that the Ventersdorp magmatism may have been related to a mantle plume, which would account for the variety in orientation of the grabens.

It is therefore apparent that the Archaean basement underlying the Transvaal basin contains lines of fundamental weakness, resulting from terrane accretion (E.N.E.-W.S.W. and N.N.W-S.S.E. directions) and impactogenic stresses resulting from the Limpopo orogen (N.E.-S.W. orientated lines of weakness). Many of these lineaments were reactivated as synsedimentary faults during the development of the Dominion, Pongola, Witwatersrand and Ventersdorp depositories (Stanistreet & McCarthy, 1991), and were potential sites for fault reactivation during and after Transvaal Supergroup deposition.

1.5.2: Summary of syn-Transvaal Supergroup deformation:

The onset of Transvaal Supergroup protobasinal sedimentation and volcanism prior to 2657 Ma (Eriksson et al., 1996) reflects an initial continuation of the tectonic setting inferred to have created the 2709±4 Ma (Armstrong et al., 1991) Ventersdorp grabens (Eriksson & Reczko, 1995). Eriksson et al. (1996) suggested that strike-slip faulting along the Thabazimbi-Murchison lineament produced small, deep pull-apart basins in which the protobasinal rocks of the Transvaal Supergroup were deposited. The W.N.W.-E.N.E. orientated Kanye axis (Figure 1.5), probably related to the 2770-2780 Ma (Grobler & Walraven, 1993) Kanye volcanism in Botswana, also appears to have played a role controlling depository location, as the early Transvaal Supergroup sedimentation up to and including the Black Reef Formation (Table 1.1) appears to have followed this axial trend (Eriksson et al., 1996). The Black Reef Formation reflects peneplanation and fluvial deposition after gentle north-directed thrusts had produced a northerly palaeoslope in the region of the preserved Transvaal basin (Eriksson & Reczko, 1995). Thermal subsidence above pre-existing lines of tectonic weakness in the Kaapvaal Craton, particularly those related to Ventersdorp volcanism (Figure 1.5), led to the formation of an epeiric marine basin, which accommodated the Chuniespoort Group carbonates and B.I.F.s (Clendenin, 1989; Eriksson & Reczko, 1995). Potgieter (1992) proposed that deposition of the Black Reef and Chuniespoort lithologies was followed by northward-verging folding and thrusting, evident in the Mhlapitse fold

belt in the northeast of the preserved Transvaal basin. This deformation led to positive inversion of the Black Reef-Chuniespoort Basin, and, following a period of erosion, the Pretoria Group was deposited on an angular unconformity on these older rocks (Potgieter, 1992).

The presence of thick volcanic units in the Pretoria Group suggest that rifting was probably active at this time, though in contrast, the sheet-like nature of the entire volcano-sedimentary sequence indicates a process of thermal subsidence. It seems likely, therefore, that both mechanical and thermal subsidence controlled the Pretoria Group basin development (Reczko et al., 1995; Eriksson & Reczko, 1995). Generally, the Pretoria Group sediments represent deposition distal to the source areas, indicating that any syn-sedimentary faults were located largely outside the present preservation of the basin, and the more proximal sediments have since been eroded. However, immature Pretoria sediments with apparent northern source areas (e.g. Boshoek and Dwaalheuwel Formations) suggest that the T.M.L. was active during Pretoria Group deposition (Eriksson & Reczko, 1995).

Thus, the tectonic activity leading to the creation of the Transvaal Supergroup basin encompased a combination of mechanical and thermal subsidence, along lines of pre-existing tectonic weakness created during the formation of the Kaapvaal Craton.

1.5.3: Summary of post-Transvaal Supergroup deformation:

Of particular structural importance are inliers of Transvaal Supergroup rocks within the Bushveld Complex (Figure 1.5), namely the Crocodile River, Marble Hall, Dennilton, Rooiberg and Stavoren 'fragments' (Figure 1.4). These structures have been variously interpreted as xenoliths (Daly, 1928: Truter, 1955), floor-attached domes (Wagner, 1927; Cousins, 1959), and roof pendants (Willemse, 1959; Verwoerd, 1963). All the inliers show evidence for multiple deformation (Hartzer, 1995). Du Plessis and Walraven (1990) noted that the eastern and western lobes of the Bushveld Complex contain evidence for different tectonic histories. For the purpose of this work, only the history of the area surrounding the western lobe, near the Rustenburg Fault, will be discussed.

Vermaak (1970) and Du Plessis and Walraven (1990) proposed that the folding, in the Transvaal

inliers and in the floor rocks of the Bushveld Complex, resulted from stresses generated during the emplacement of the complex. The stress field necessary to produce the observed folding must have been orientated with σ_1 (maximum compression) trending horizontally in a N.E.-S.W. direction. This produced folds in the floor rocks with a N.W.-S.E. trending fold axis (Table 1.3) (Du Plessis & Walraven, 1990). However, this stress field fails to account for post-Bushveld extensional features, such as the Brits Graben (Figure 4.1) and the Rustenburg Fault, which lie perpendicular to the inferred σ_1 direction. Du Plessis and Walraven (1990) proposed that these anomalous directions were the result of reactivation of pre-Bushveld structures.

In contrast to the syn-Bushveld deformation of the inliers proposed by Du Plessis and Walraven (1990), Hartzer (1995) provided strong evidence that the western inliers (Crocodile River and Rooiberg) were the product of pre-Bushveld interference folding within the Transvaal Supergroup floor. Hartzer (1995) proposed that the Crocodile River and Rooiberg fragments represent a floor dome and a synformal roof pendant, respectively. Other smaller inliers in the western lobe of the Bushveld Complex, such as those between the Pilanesberg Complex and the South Africa-Botswana border and those N.W. of Rustenburg (Figure 1.2), were also interpreted as folded floor rocks exhibiting the same directions of interference folding as shown in the larger inliers (Table 1.4) (Vermaak, 1970; Schürmann, 1991). Hartzer (1995) therefore concluded that these identical patterns of interference folding in inliers throughout the western Bushveld reflect pre-Bushveld regional scale compression. Hartzer's proposed regional pre-Bushveld folding directions around the western lobe are shown in Table 1.4.

There is a fundamental difference between the two models of Du Plessis and Walraven (1990) and Hartzer (1995). Hartzer (1995) proposed that the long-lived stress field (σ_1 trends N.E.-S.W.) of Du Plessis and Walraven (1990) was interrupted by a perpendicular compressional event (σ_1 trends N.N.W.-S.S.E.) and the intrusion of the Bushveld Complex. Hartzer (1995), however, did not consider how the activity of nearby faults may fit into his model.

Shortly after the intrusion of the ~2050 Ma Bushveld Complex (Von Gruenewaldt & Harmer, 1993), the 2023±4 Ma (Reimold & Gibson, 1996) Vredefort Dome was formed (Figure 1.5). The nature of this event has been the subject of much debate. Some workers (e.g. Coward et al.,1995) proposed that the Vredefort dome is an Eburnian-aged (1800-2000 Ma) pop-up

structure, due to lateral shearing resulting from plate collision on the north-west margin of the Kaapvaal Craton; others (e.g. Brock & Pretorius, 1964) proposed that the dome represents a diapiric mantle upwelling. Most other workers, however, agree that the Vredefort structure is an eroded astrobleme, a view supported by the presence of shatter cones (Hargraves, 1961), coesite and stishovite (Martini, 1978), and pseudotachylite (Shand, 1916). The Dominion, Witwatersrand and Transvaal strata forming the collar of the dome are highly deformed, and often overturned. Whilst the tectonic effects of the Vredefort event are intense in the areas adjacent to the structure, they have few correlates elsewhere on the Kaapvaal craton (Roering et al., 1990).

The Bushveld Complex and Vredefort events were followed, at about 1900-1700 Ma, by deposition of the Waterberg-aged red beds, in fault-controlled basins (Callaghan et al., 1991). The main Waterberg Basin lies directly to the north of the T.M.L. (Figure 1.5), and derived much of its detritus from uplifted Bushveld granites in the south (Callaghan et al., 1991). The Middelburg Waterberg Basin lies in the eastern Bushveld Complex, just to the south of the Dennilton Dome, approximately along the Kanye axis (Eriksson et al., 1996) (Figure 1.5). The third Waterberg-aged basin, in which the Soutpansberg Group was deposited, comprises a graben developed in the southern part of the Limpopo Mobile Belt (Figure 1.5).

The intrusion of the Pilanesberg Alkaline Complex at 1250 Ma (Lurie, 1986) was the next significant structural event to have affected the Kaapvaal Craton in the area of the western Bushveld Complex (Figure 1.5). It intruded along a pre-existing line of basement weakness, possibly defined by the Kanye axis (Eriksson et al., 1996), or along a N.W.-S.E. trending Kibaran-aged lithospheric weakness (Friese et al., 1995). Its emplacement caused radiating faults and dykes, which reactivated and exploited, respectively, pre-existing faults (Vermaak, 1970; Meadon, 1973).

The Permian sediments of the Karoo Supergroup in the Springbok Flats Basin (Figure 1.5) unconformably overlie the rocks of the Bushveld Complex in the central region, between the five Transvaal inliers. The minimal tectonic activity recorded since these rocks were deposited is not considered relevant to this study.

1.6: Aims and objectives:

Although the geology of the Rustenburg area is well known (e.g. Walraven, 1981) on account of the extensive mining operations in the area, the investigations concentrated on the economic deposits of the Bushveld Complex, rather than the neighbouring apparently uneconomic Transvaal Supergroup lithologies. As a result, the history of fundamental structural features such as the Rustenburg Fault remains largely unknown. The summary of previous work in Section 1.4 serves to emphasise the lack of consensus of opinion on both the timing and sense of displacement of the Fault. The controlling effects of the Rustenburg Fault on the rocks of the Bushveld Complex are also largely unresolved, due to the poor time constraints established for Fault activity. The aim of this work is therefore to produce a detailed geological map (Appendix) of the Rustenburg Fault within the chosen study area, in order to determine its geological history, and especially to constrain the age of movement, the type of faulting which has occurred, the amount and sense of displacement, and the possibility of reactivation having occurred.

Though not exhaustive in its treatment of the whole length of the Fault zone (Figure 1.2), this study does cover the largest portion thereof, and that with the best outcrops. It should thus be possible to resolve some of the differences of opinion expressed in past literature, which were based on examination of significantly smaller portions of the Fault, regarding the tectonic history of the Rustenburg Fault.

1.7: Methodology:

The stratigraphy for the study area is already well established and is easily available from the published maps of the Geological Survey of South Africa (e.g, 1:250,000 sheet 2626 [Wes-Rand]). Field mapping was preceded by a study of aerial photographs and the compilation of a photogeological map. The latter was then used as a base map for the detailed field mapping.

1.7.1: Photogeology:

The different lithologies in the field area each undergo weathering and erosion at a variety of rates,

particular to each individual lithology. The topography of the field area was therefore found to bear considerable relationship to underlying geology, and allowed for accurate remote mapping of major stratigraphical units and large-scale structural phenomena.

The epeiric marine and regressive alluvial sedimentary systems inferred for the Pretoria Group (e.g., Eriksson & Reczko, 1995) tend to produce repetitions of shale / hornfels and sandstone / quartzite. The shales erode quickly to produce low-lying flat areas, and weather easily to produce thick soils. Sandstones and quartzites were found to weather and erode considerably more slowly, producing lines of hills approximately parallel to the line of strike of the sandstone beds, with maximum relief being developed in the Magaliesberg mountains associated with Magaliesberg quartzite, and in the lower hills crossing the field area at 25 ^{0}58' S: 27 ^{0}28' E, associated with the Daspoort quartzite (Appendix). Locally, variation in soils, reflecting the underlying geochemistry, gives rise to contrasting natural vegetation between neighbouring lithologies. A change in the density or type of trees identifiable from aerial photographs could be used to signal a geological contact (e.g. the small indigenous Sugarbush tree favours growth on areas underlain by quartzite).

When stereo-pairs of aerial photographs were viewed under a stereoscope, the resultant vertical exaggeration enabled accurate estimation of geological contacts between lithologies of contrasting properties, which could not be gained by mesoscopic investigation in the field, due to poor outcrop. This process was not possible where lithologies of similar weathering and erosion rates are juxtaposed. The Timeball Hill shales and Hekpoort lavas are in contact in the field area at around S 25^0 59' latitude. The relief and vegetation produced from these lithologies do not differ appreciably. Mafic sills intruding the Magaliesberg quartzite (e.g. at 25 ^{0}44' S: 27 ^{0}14' E) had no visible effect on relief, whereas similar sills intruding Silverton shale (e.g. at 25 ^{0}50' S: 27 ^{0}16' E) were more easily identifiable on aerial photographs by their resistance relative to the Silverton shales.

The durable nature of the Magaliesberg quartzite allows for individual bedding planes to be manifest in the topography; often the geometry of hillslopes in the Magaliesberg mountains is coincident with the angle of dip and strike of the quartzite bedding on that hillslope. Therefore aerial photographic interpretation of the Magaliesberg mountains could often be used as an indicator of the angle of dip. Although the vertical exaggeration, when viewed stereoscopically,

visually increased angles of dips, it did still allow for comparisons (i.e. relative steepening of beds) to be made. Fold structures, such as those at Olifantspoort farm (25^0 48' S: 27^0 16.50' E) and Rietvlei (25^0 39.00' S: 27 ^{0}11.30' E) were easily identifiable stereoscopically, allowing for the trend of the fold axes to be estimated.

Stereoscopic analysis of aerial photographs was of particular use in identifying the contact between Magaliesberg quartzite and the Bushveld Complex lithologies. The easily weathering nature of the mafic Rustenburg Layered Suite produces flat topography and thick soils, e.g. 11 metres of cover above the Bushveld norite found at 25^0 35.71' S: 27^0 08.47' E (information gained from a crew drilling water boreholes in the township of Phokeng). Locally, cobbles of mafic Bushveld rock could be found at the surface in stream beds (e.g. at 25^0 40.84' S: 27^0 11.12' E.) but no solid outcrops were found within the field area. Fortunately, the marked topographical contrast between the Magaliesberg quartzite and flat lying Bushveld mafics allowed for accurate lines of contact to be inferred.

Aerial photographs again proved useful in the identification of a thrust fault at 25^{0}47.50' S: 27^0 17.50' E, where the Magaliesberg quartzite was found to be anomalously thick (see Section 3.1.3.4). Similarly, other features observable as lineaments on the surface, were traced using aerial photographs. At 25^0 53' S: 27^0 18' E and 25^0 56.00' S: 27 ^{0} 20.50' E, faults strike 030 ^{0}, and tend to be exploited by streams, and could thus be followed by their topographical expression.

1.7.2: Field work:

Field work was carried out between February and December 1996. The 80 km^2 field area shown in Figure 1.2, was mainly mapped on foot, and geological data were recorded in notebooks and plotted on field base maps. A transparent overlay on 1:20,000 aerial photographs provided a basemap of suitable scale for detailed field mapping. Navigation in the field was accomplished by use of a G.P.S. (global positioning system) receiver.

General geological data were collected during the course of the field work, and mostly comprised primary sedimentary structures and secondary (tectonic) structures. Dip and dip-direction of bedding was frequently recorded. Where present, the orientation of tectonic structures along the

Fault zone, such as slickensides, foliations, lineations and veins were recorded. Primary sedimentological features were recorded for the identification of sedimentary facies and marker beds, in order to correlate strata across the Fault. Soft-sediment deformation structures and current direction indicators, such as ripple-marks and cross-bedding directions were recorded, to provide evidence for synsedimentary activity of the Fault. The degree of recrystallisation in the Bushveld aureole was determined by relative quartz crystal size. This was mapped in the Magaliesberg Formation quartzites, so that any noticeable offset of the recrystallisation pattern by the Fault could be identified.

Much of the data collected are shown on the accompanying 1:50,000 geological map (Appendix), which is divided into three sheets, numbered from south to north along the Fault zone. However, not all collected data (e.g. recorded bedding geometry) is shown. This map was compiled from the basemaps and scaled down onto South Africa 1:50,000 topographical map sheets 2526BD (Mabaalstad), 2527AC (Sun City), 2527CA (Rustenburg West), 2527CB (Rustenburg East), 2527CC (Derby), and 2527 CD (Maanhaarrand). A small-scale copy of the field geological map is also included in chapters 2 and 3 (Figures 2.1 and 3.1) for easier reference. Many small-scale minor structural data collected during the fieldwork are not presented on these maps due to lack of space. Instead they are presented on large-scale maps which accompany the text in chapter 3 (Figures 3.5, 3.8 and 3.46). The map was compiled through a combination of aerial photograph interpretation, the collection of field data and subsequent thin-section analysis.

1.7.3: Laboratory work:

Lithological samples from all the main stratigraphic units (including the Fault zone) encountered in the field area were collected for thin section analysis. Orientated samples were taken in order to determine kinematic directions, fault and recrystallisation history.

Bedding orientation data were analysed stereographically to identify any dominant fold trends. Stereographic projections of poles to bedding were constructed and analysed using *SpheriStat 2* software. Each stereographic projection presented in this work is a lower hemisphere projection on a Schmidt (equal area) net. Density distribution analyses of bedding data were undertaken using SpheriStat, with contour intervals at 0, 1, 2, 5, 8, 13, 18 and 23 % of poles per 1% area,

using the contouring method of Schmidt (1925). The orientation of fold axes were calculated using Eigenvector analysis. As the position of each data point could be entered in three dimensions (U.T.M. grid reference and altitude), the SpheriStat software allowed for the construction of maps. Rotation of the pre-determined fold axis to vertical, and replotting the map using the same rotation axis, gave a down-plunge projection of the fold. This was done in order to classify and compare different fold structures, and to aid with the determination of the orientation of the fold axial surface.

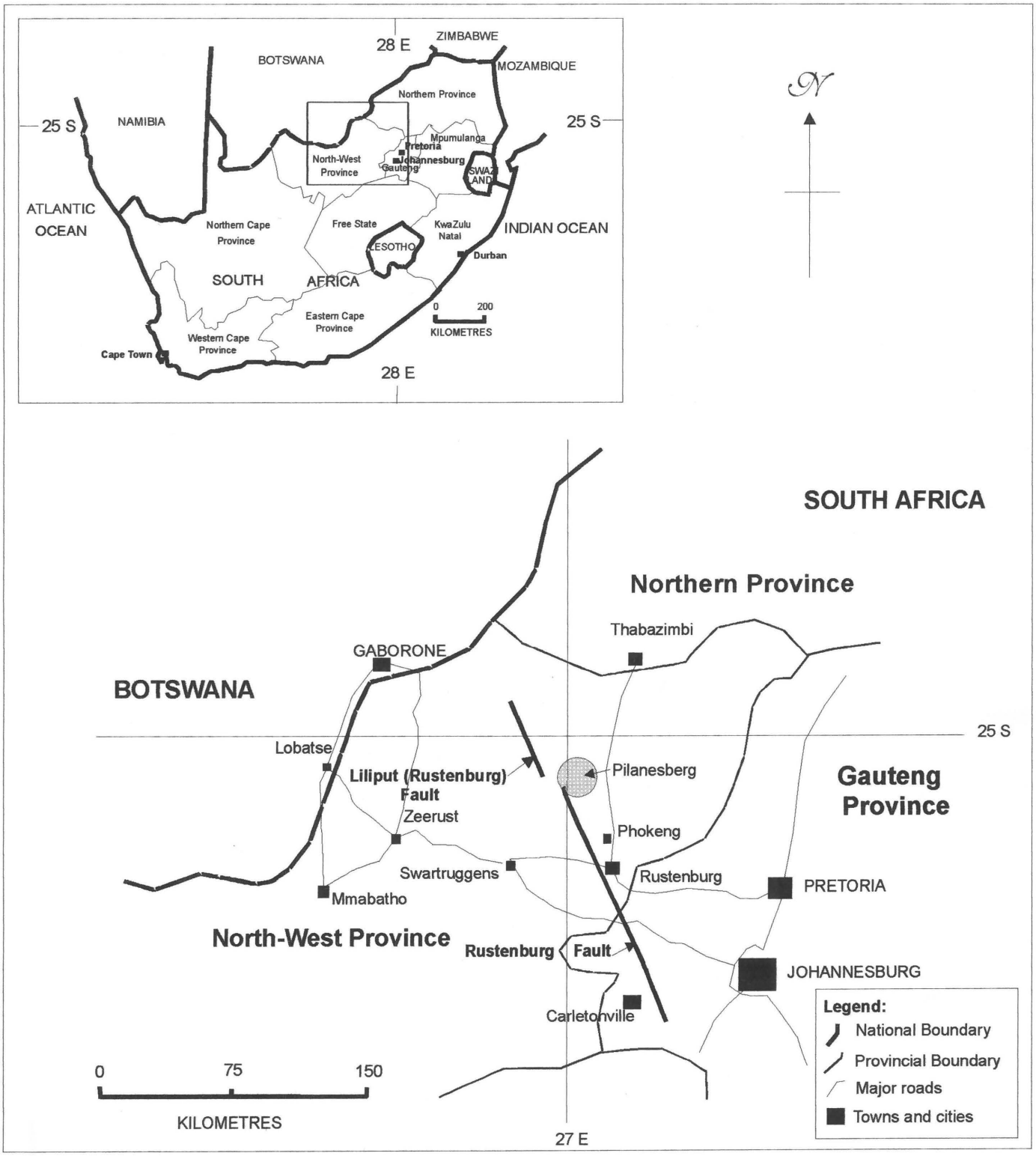

Figure 1.1: Geographical location of the Rustenburg Fault.

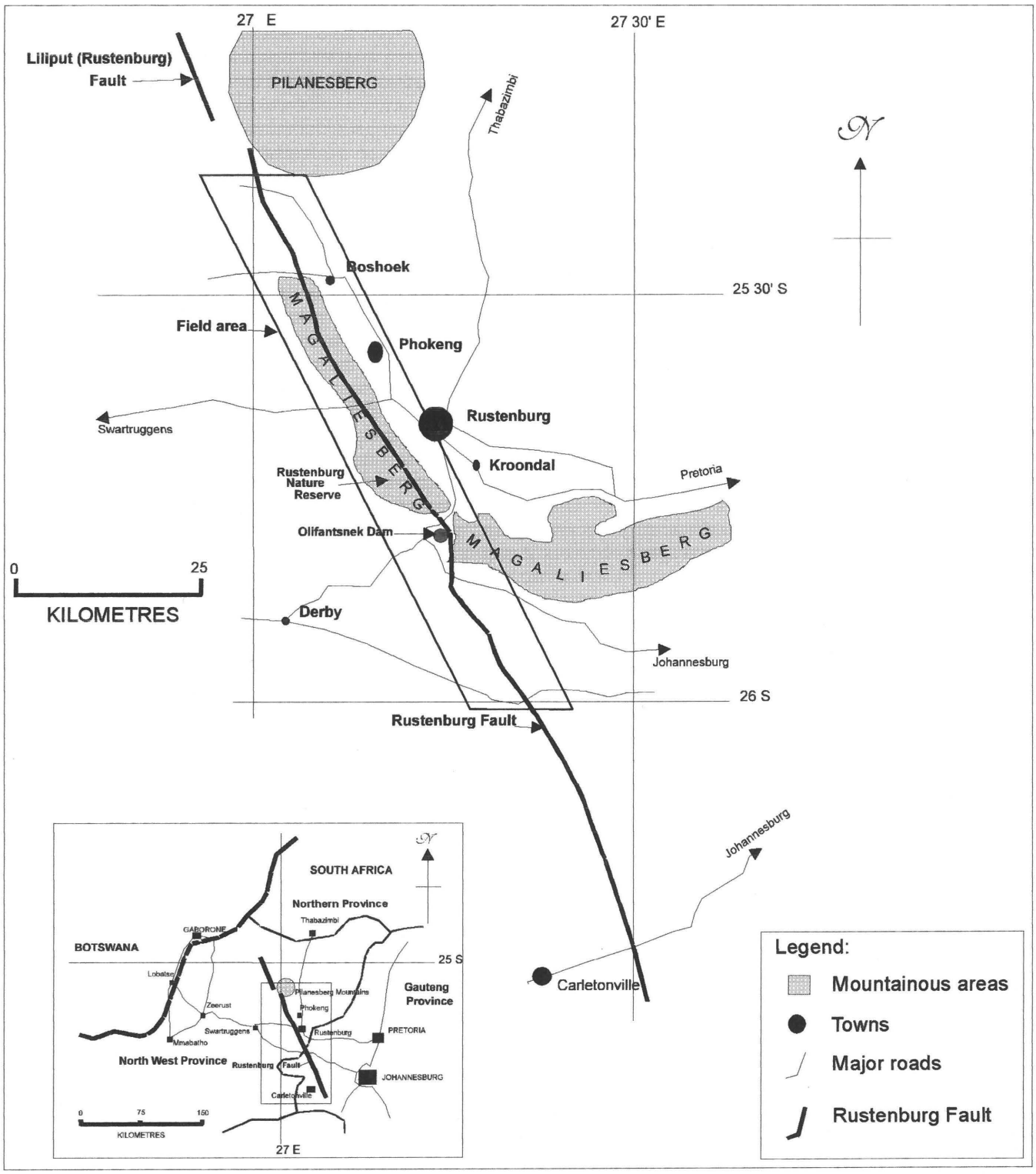

Figure 1.2: Location of the field area.

	GROUP	FORMATION	LITHOLOGY	APPROXIMATE THICKNESS (m)
TRANSVAAL SUPERGROUP	PRETORIA	Woodlands	Sandstone and mudrock	200m
		Magaliesberg	Sandstone	0-200m
		Silverton	Mudrock	300 (min)
		Daspoort	Sandstone (minor mudrock)	90
		Strubenkop	Mudrock and siltstone	130
		Dwaalheuwel	Conglomerate and sandstone	0-120m
		Hekpoort	Amygdaloidal andesitic lava	500
		Boshoek	Conglomerate, sandstone and mudrocks	0-55m
		Timeball Hill	Mudrock and sandstone	500-800
		Rooihoogte	Sandstone, mudrock and conglomerate	50-200
	CHUNIESPOORT	Penge	Banded iron formation	320
	CHUNIESPOORT / Malmani Subgroup	Frisco	Chert-poor dolomite	30
	CHUNIESPOORT / Malmani Subgroup	Eccles	Chert-rich dolomite	490
	CHUNIESPOORT / Malmani Subgroup	Lyttelton	Chert-poor dolomite	290
	CHUNIESPOORT / Malmani Subgroup	Monte Christo	Chert-rich dolomite	740
	CHUNIESPOORT / Malmani Subgroup	Oaktree	Dark coloured dolomite	330
		Black Reef	Sandstone and mudrock	25

N.B. Sandstones are often recrystallised to quartzite

Table 1.1: Stratigraphy of the Transvaal Supergroup in the western Transvaal Basin (modified after S.A.C.S., 1980).

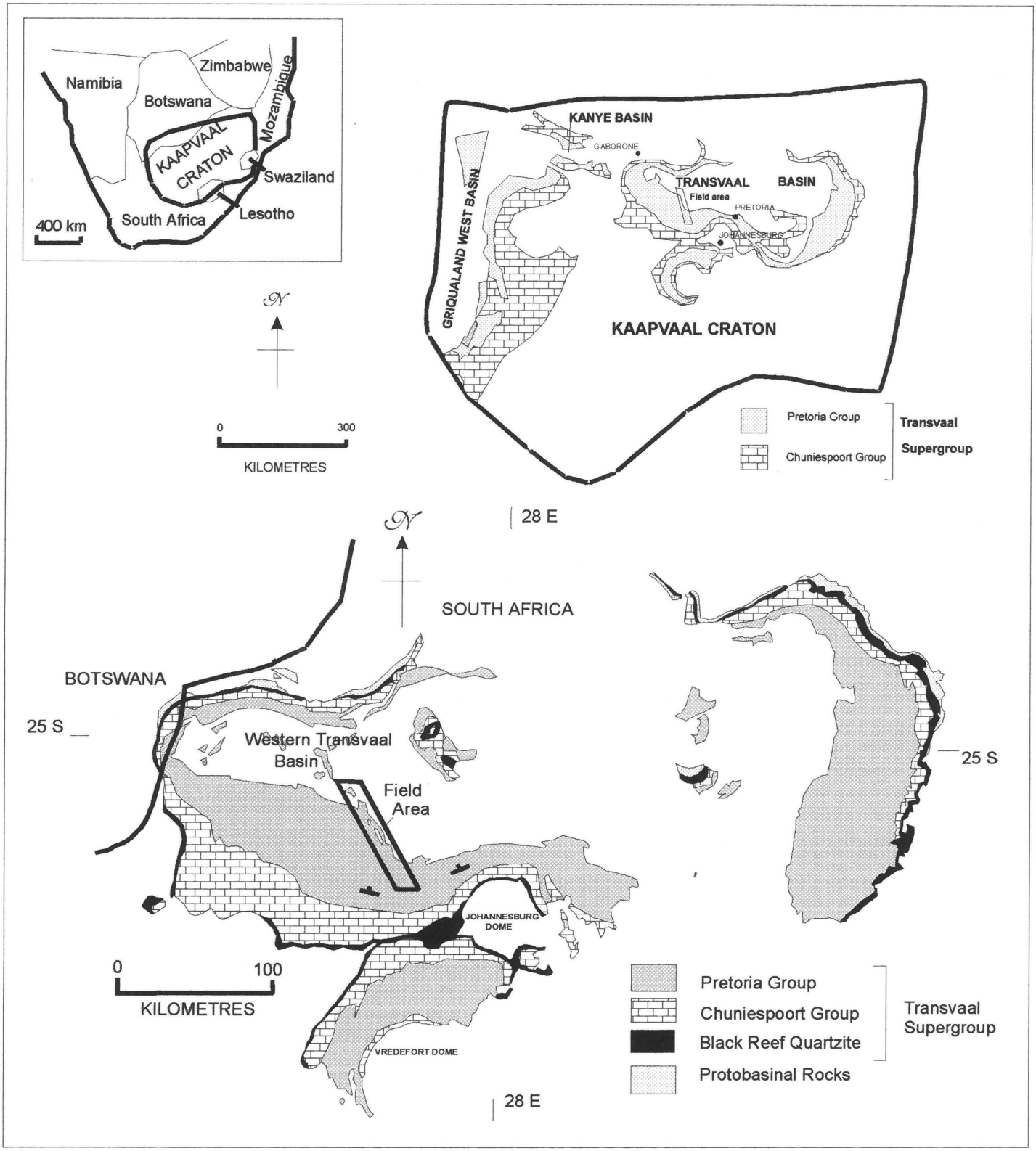

Figure 1.3: Map showing the Transvaal Supergroup on the Kaapvaal craton (After Eriksson & Cheney, 1992; Eriksson et al., 1993).

	SUITE	ZONE
BUSHVELD COMPLEX	Lebowa Granite Suite	
	Rashoop Granophyre Suite	
	Rustenburg Layered Suite	Upper Zone Main Zone Critical Zone Lower Zone
		Marginal Zone (Kolobeng Norite)

Table 1.2: Lithostratigraphic subdivision of the Bushveld Complex (simplified after S.A.C.S., 1980).

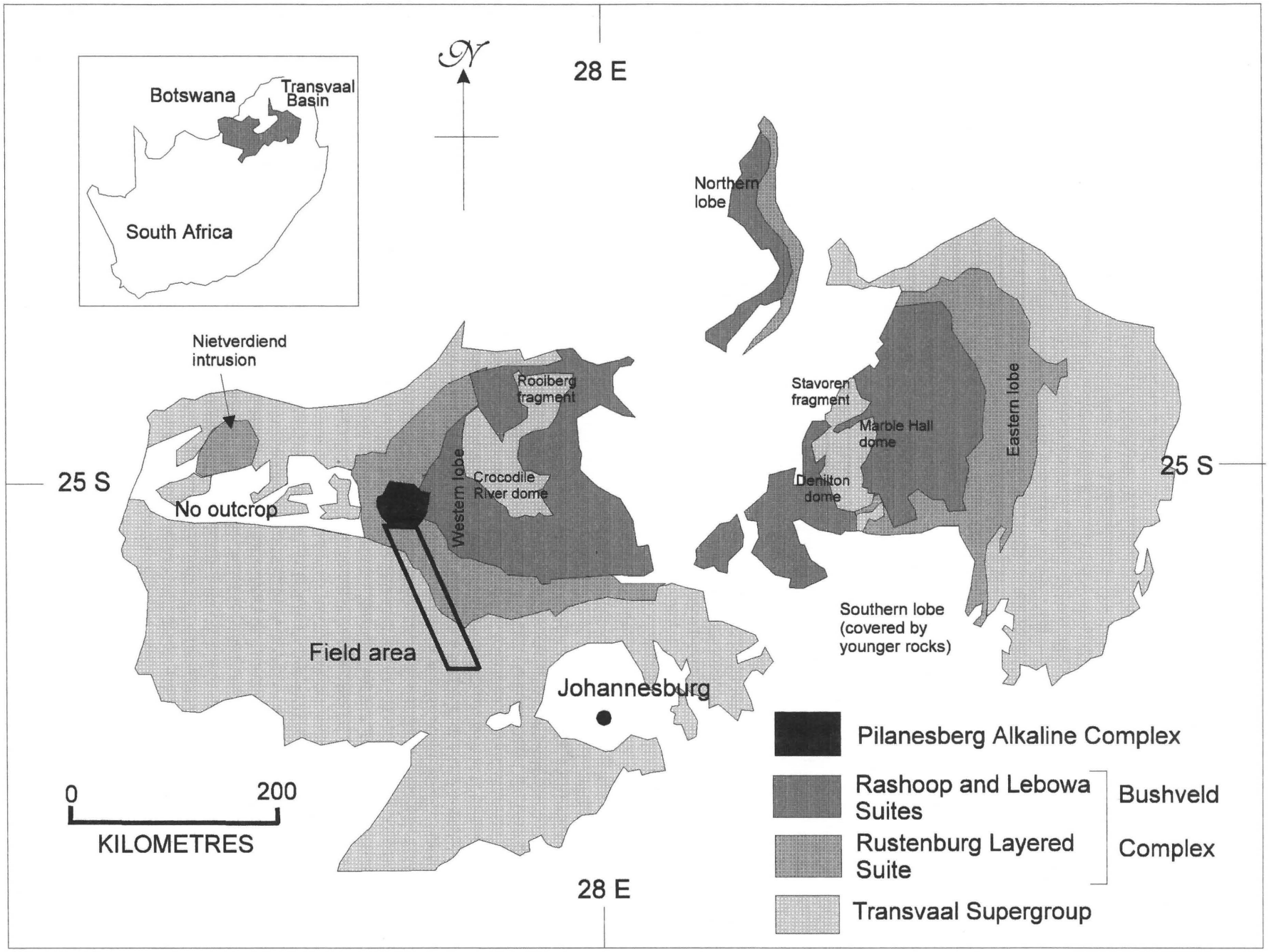

Figure 1.4: Map of the Bushveld Complex (After Eriksson et al., 1995).

Tectonic Event	σ_1 direction	Trend of fold-axis	Strike of inferred extensional faults	Timing
D_1	N.W.-S.E.	F_1 = E.N.E.-W.S.W.	N.W.-S.E.	Pre-Bushveld
D_2	N.E.-S.W.	F_2 = N.W.-S.E.	N.W.-S.E. continued	Syn- and Post-Bushveld (long-lived)

Table 1.3: Sequence of structural events in the vicinity of the western lobe of the Bushveld Complex, as proposed by Du Plessis and Walraven (1990).

Tectonic Event	σ_1 direction	Trend of fold-axis	Timing
D_1	N.E.-S.W.	F_1 = N.W. to S.E.	Pre-Bushveld
D_2	N.N.W.-S.S.E.	F_2 = E.N.E. to W.S.W.	Pre-Bushveld
D_3	N.E.-S.W.	F_3 = N.W. to S.E. F_1 tightened and Bushveld folded	Post-Bushveld

Table 1.4: Sequence of structural events in the vicinity of the western lobe of the Bushveld Complex, as proposed by Hartzer (1995).

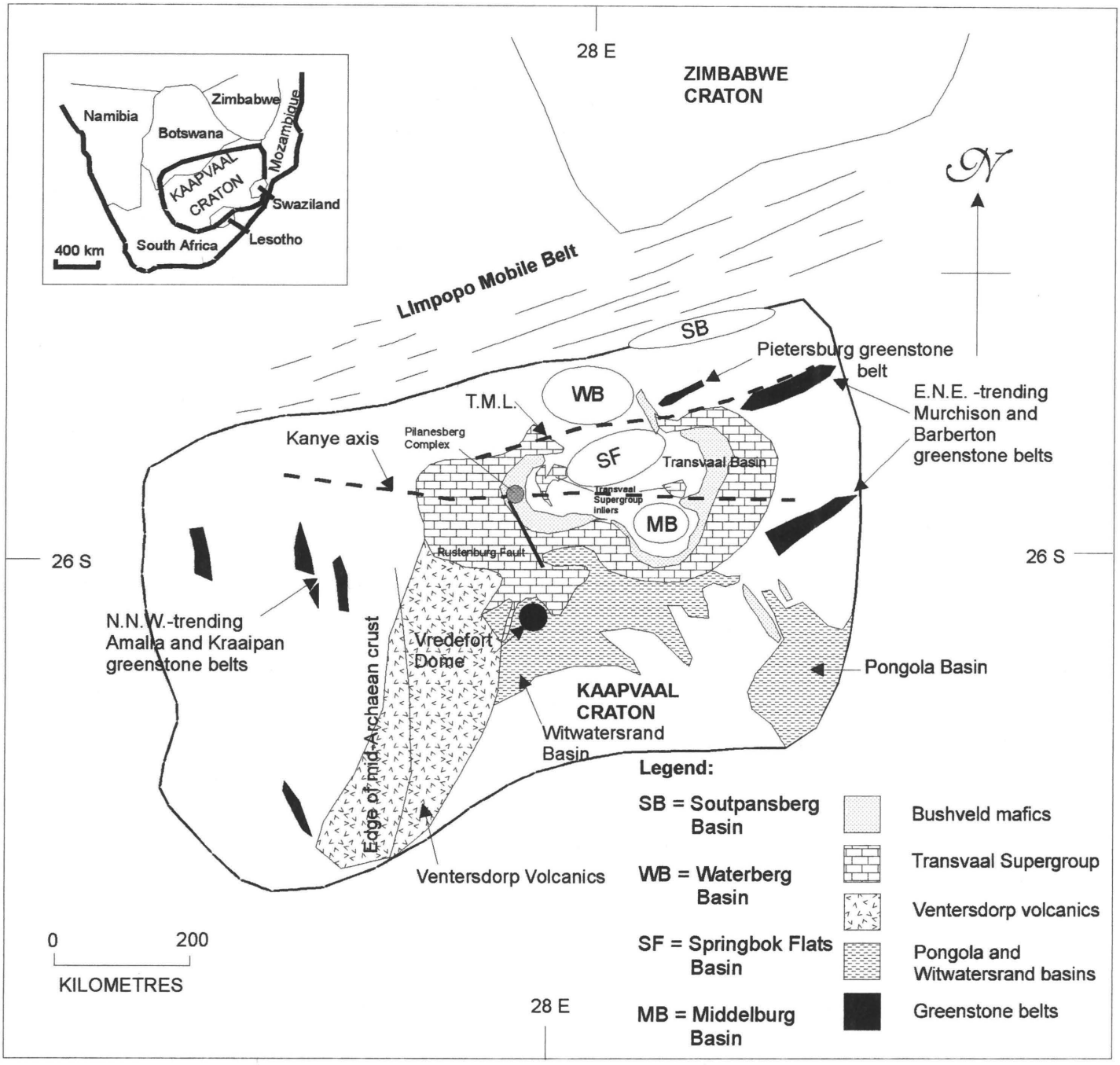

Figure 1.5: Major structural elements of the Kaapvaal craton (after Burke et al., 1985; Stanistreet & McCarthy, 1991; de Wit et al., 1992; Eriksson et al., 1995).

2: STRATIGRAPHY AND LITHOLOGY.

The stratigraphic sequence of the Pretoria Group is well established (S.A.C.S., 1980), and the depositional environments have been investigated by many workers (e.g. Button, 1973; Van der Neut, 1990; Schreiber, 1991; Eriksson & Reczko, 1995). It is not the purpose of this thesis to elaborate on these studies, but only to report on the nature of the Pretoria Group rocks found within the field area. Figure 2.1, Table 1.1 and the map in the Appendix show the general stratigraphy within the field area. The localities of figures used to illustrate this section are given by latitude and longitude, and grid lines at 5' spacing are provided on Figure 2.1 to aid in the location of these localities.

The lowermost unit of the Pretoria Group encountered in the field area is the Timeball Hill Formation. In the southern section of the field area (Appendix), the Pretoria Group strata generally strike E.-W. with a northerly dip, so that successively younger Pretoria Group strata are exposed northwards. These are intruded by pre- and syn-Bushveld sills (Cawthorn et al., 1981), and ultimately by the Bushveld Complex, which caused contact metamorphism of the Pretoria Group rocks. Each of the stratigraphic units will be examined in order of deposition or intrusion.

2.1: Timeball Hill Formation:

The Timeball Hill Formation consists of lower and upper shale members, separated by a medial arenaceous Klapperkop Member (S.A.C.S., 1980). The field area contains only the upper shales. These are dark grey, laminated (2-7 mm) mudrocks, locally exhibiting lenticular bedding. Microscopic examination of thin-sections indicates that laminae commonly have normal grading. They are generally fissile along these laminations, though in places (e.g. S 25^0 58.84': E 27^0 21.25') the shales have lost their fissility, and are more durable, possibly due to low-grade contact metamorphism within the aureole of nearby sills (Figure 2.2). These indurated areas of shale often create the only outcrops, with more fissile shales being buried beneath soils.

2.2: Boshoek Formation:

A disconformity generally marks the base of the Boshoek conglomerate in the Western Transvaal basin (Schreiber et al., 1990). In the field area, however, there is some evidence (Appendix) that the unconformity may locally be angular (e.g. the area around 25^0 59' S: 27^0 21' E). Only two small outcrops of Boshoek conglomerate were found in the field area (at 25^0 58.84' S: 27^0 20.97' E and 25^0 58.89' S: 27^0 21.34' E), together providing about $20m^2$ of outcrop, both outcrops being less than 1m thick. The Boshoek Formation thus forms laterally restricted lenses on the contact between the Timeball Hill and Hekpoort Formations (Schreiber et al., 1990). The nature of the lithology is the same at both localities. The conglomerate is poorly sorted, and consists of chert (often banded) pebbles and cobbles in a fine-grained sandy matrix. The conglomerate is generally matrix-supported. Chert pebbles are well rounded with low sphericity (Figure 2.3). Pebble size is variable, from 2 mm (granules) up to a maximum axial length of 7cm (small cobbles). No imbrication or preferred orientation is noticeable, and no sedimentary structures were observed.

2.3: Hekpoort Formation:

The Hekpoort andesites overlie the Boshoek conglomerate locally, but more commonly directly overlie the Timeball Hill shale, possibly on an angular unconformity (Oberholzer, 1995). The outcrops of the lavas are poor. The lavas are generally basaltic andesites, with a mineralogy of plagioclase, quartz and amphibole (hornblende and tremolite-actinolite) (Oberholzer, 1995). Surface boulders of Hekpoort andesite show numerous vesicles, up to 5cm in diameter, filled with quartz amygdales. Often, vesicles are elongated in the direction of upward gas escape (Figure 2.4). At one location (25^0 58.32' S: 27^0 20.88' E), 2m of intercalated weathered sandstone and shale occur in the Hekpoort lava, reflecting sedimentation during a temporary hiatus in eruption. No pillow lavas were observed, probably indicating predominantly subaerial eruption. No pyroclastic deposits were found in the field area. The lavas commonly contain younger quartz veins.

2.4: Dwaalheuwel and Strubenkop Formations:

No outcrops of either recrystallised Dwaalheuwel quartzitic sandstone or Strubenkop mudrocks were found in the field area. They are either absent or only thinly developed in the stratigraphy at this location (Schreiber et al., 1992), and any small outcrops possibly present were most likely covered over by soils and scree from the overlying Daspoort Formation.

2.5: Daspoort Formation:

The Daspoort Formation lies conformably above the Strubenkop Formation shales in most of the Western Transvaal basin (Eriksson et al., 1993), and consists of planar stratified grey sandstone (often recrystallised), which weathers to a dull cream colour. Where diagenetic haematite occurs, the rock is more rusty-brown in colour. In thin section, it is difficult to determine original roundness and sphericity of grains. Many of the grains appear to be angular, though this is not an indication of textural immaturity, but rather due to pressure solution. In all samples examined, no cement was visible, and no quartz overgrowths were observed. Lithification appears to have occurred almost exclusively by pressure solution at grain boundaries.

The sandstones are medium- to coarse-grained (Figure 2.5), with individual grain sizes occasionally approaching 0.7mm diameter. The rocks are generally well to moderately sorted (Figure 2.5), though locally they show poor sorting. Lithic fragments are rare, and feldspars are absent. More than 95% of the grains are quartz, indicating a quartz arenite. Many of the larger quartz grains show undulose extinction, reflecting either a tectonised source area, or straining *in situ*. Though much of the Daspoort Formation in the study area is metamorphosed to quartzite, none of the examined thin-sections show evidence for significant recrystallisation.

Where the Rustenburg Fault cuts the Daspoort Formation, there is a pronounced difference in thickness of the unit on either side of the Fault. The width of outcrop on the eastern side of the Fault is 1.45 km, with bedding dipping at 10^0 to the north; this indicates a formation thickness of 250m. Immediately west of the Rustenburg Fault, outcrop width is 4.5 km, with bedding dipping at 10-11^0 to the N.E.; this indicates a formation thickness of 850m. Four kilometres west of the Fault, the width of outcrop has thinned to 3.5 km, with no change in dip. This indicates a

formation thickness of 600m.

2.6: Silverton Formation:

Outcrop of the Silverton Formation mudrocks is poor in the broad valley between the hills formed by the Magaliesberg and Daspoort Formations. Where strata were indurated by thermal metamorphism, outcrop is better, and dark grey spotted hornfelses are seen. Unmetamorphosed shales are usually highly weathered at the surface, and may be reddish brown in colour, indicating diagenetic alteration.

Shales metamorphosed to hornfels show a typical low-pressure contact-metamorphic mineral assemblage for pelites, with biotite and cordierite or andalusite replacing the clay minerals (Figures 2.6 and 2.7). This assemblage resulted from the following reaction:

$$\text{chlorite} + \text{muscovite} \rightarrow \text{cordierite} + \text{biotite} + \text{quartz} + H_2O$$

The presence of this assemblage represents a burial depth of over 2km (Engelbrecht, 1976). The growth of andalusite without cordierite is indicative of the presence of large amounts of Fe, related to the presence of secondary haematite in the groundmass (Figure 2.6).

2.7: Magaliesberg Formation:

The durable nature of the Magaliesberg Formation has led to the formation of a long mountain range around the rim of the Bushveld intrusion. In many areas (e.g. the E. and S.E. Transvaal basin), contact metamorphism of the Magaliesberg Formation by the Bushveld intrusion is not intense, due to the presence of the overlying Rayton Formation and equivalent units of the Pretoria Group (Schreiber et al., 1992), and consequent distance from the heat source. Most original lithofacies are therefore preserved in many areas (e.g. Schreiber, 1991). In the western Transvaal basin, however, the Magaliesberg Formation commonly forms the top of the Pretoria Group, and is in contact with the intrusives of the main Bushveld Complex, except near the Botswana border, where the Nietverdiend Bushveld intrusive lobe (Figure 1.4) intruded into the Woodlands Formation (Table 1.1). Consequently, the effects of the thermal aureole associated with the

intrusion are most intense in the Magaliesberg Formation in the study area. This section will examine preserved sedimentological features of the Magaliesberg Formation, and then consider the effects of the Bushveld contact metamorphism.

2.7.1: Sedimentological features:

A study based on the facies and architectural elements of the Magaliesberg Formation (Eriksson et al., 1995) identified three architectural elements. These are (1) medium- to coarse-grained sandstone sheets, (2) fine- to medium-grained sandstone sheets, and (3) mudrock elements. It is not possible to recognise these architectural elements in the field area, as recrystallisation during the Bushveld event caused much of the pre-existing internal structures of the Magaliesberg Formation to be destroyed. Large-scale bedding features often appear to have acted as barriers to crystal growth, and thus coarse-grained recrystallised beds, ripple marks and desiccation cracks are often preserved, whereas less robust internal features, such as laminations and cross-strata are lost (Figures 2.8, 2.9 and 2.10). Individual beds within the Formation may be identifiable by differential degrees of recrystallisation between subsequent beds (Figure 2.12).

The thickness of the Magaliesberg Formation in the field area must be calculated assuming that the top of the Formation is marked by the contact between the Magaliesberg Formation and the Bushveld Complex, and assuming no assimilation by the Bushveld magma. Therefore the original stratigraphic thickness of the formation may have been greater than the calculated thickness. East of the Rustenburg Fault, a formation thickness of >850m is calculated. West of the Fault zone, a thickness of >650m is calculated. An example of the minimum thickness can be seen in Figure 2.11. However, it is important to note that considerable assimilation of the top of the Magaliesberg Formation is envisaged (Section 4.1), and the present contact between the Magaliesberg Formation and the Bushveld Complex is unlikely to represent the stratigraphic top of the Formation.

2.7.2: Metamorphism and recrystallisation:

Figure 2.12 shows that the degree of recrystallisation is often specific to individual beds of sandstone, with initial recrystallisation probably being controlled by the original permeability of the bed to quartz-rich fluids. Such fluids are envisaged as providing the extra SiO_2 necessary to fill

pore-spaces during metamorphism.

Locally in the study area, individual beds have completely escaped recrystallisation, providing evidence of the original lithology of the Magaliesberg sandstone. Figure 2.13 shows an example of Magaliesberg sandstone with little evidence for recrystallisation, and exhibiting well rounded, spherical grains. In contrast to this, the rock appears mineralogically immature, with many interstitial feldspars and micas, and localised muddy matrix. There are no cement or overgrowths visible and lithification appears to have occurred by pressure solution (in common with Daspoort sandstones) (Figure 2.13).

The size of quartz crystals in the Magaliesberg quartzite appears to correlate indirectly with the percentage of sillimanite or other inclusions (Figures 2.14, 2.15 and 2.16). Chemical diversity of less mature sandstones (sublitharenites or subarkoses) would produce sillimanite and muscovite as a metamorphic mineral. Such impurities would have hindered the recrystallisation of quartz during grain boundary movement, hence producing smaller quartz crystals (Spry, 1969). In all thin-sections, later pressure solution, caused by compaction, has destroyed the original grain or later crystal boundaries.

The effect of a generally mineralogically mature protolith, and recrystallisation possibly assisted by the presence of silica-rich fluids has created a rock of exceptionally high SiO_2 content in the field area. Figure 2.17 shows white (no haematite) Magaliesberg quartzite with over 99.6% SiO_2, which is quarried and crushed for glass manufacture.

Though only seen outside the field area, occasional pelitic horizons in the Magaliesberg Formation (Figure 2.18) have also undergone metamorphism comparable to the low pressure metamorphism seen in the Silverton shales.

2.8: Pre-and syn-Bushveld sills:

The strata of the Pretoria Group are host to a variety of usually concordant sills of varying thickness. These have been interpreted as precursor intrusions to the main Bushveld event, though a substantial volume may have been intruded during the Bushveld event, as many show no

evidence of metamorphism (e.g. Cawthorn et al., 1981). In the field, sills rarely outcrop, but are usually indicated by large rusty red-coloured, rounded boulders on the surface. The boulders are usually very hard, and do not weather easily. The samples collected in the field area for thin section analysis showed that most sills are meta-diabases (Figure 2.19) containing randomly-oriented tremolite needles, largely obliterating any previous granularity. The thickest of the pre-Bushveld sills are intruded concordantly into the Silverton shales, south of Olifantsnek Dam (Appendix).

Locally, closer to the main Bushveld Complex, norite sills were injected into Pretoria Group sediments from the main noritic body of the lower Rustenburg Layered Suite (Cawthorn et al., 1981). In a thin-section from a sill at 25^0 38.5' S: 27^0 08.5' E, norite shows euhedral laths of hypersthene, with, quartz, augite, hornblende and biotite as interstitial minerals (Figure 2.20). Plagioclase was locally present in the thin section.

2.9: Bushveld Complex:

The layering of the Rustenburg Layered Suite of the Bushveld Complex includes a basal layer of norite at the contact with the Pretoria Group sediments. The basal norite is rarely exposed, but a sample was collected from the edge of a pegmatitic pipe at S25^0 25.89': E 27^0 05.36' for illustration of lithology (Figure 2.21).

GEOLOGICAL MAP OF THE RUSTENBURG FAULT

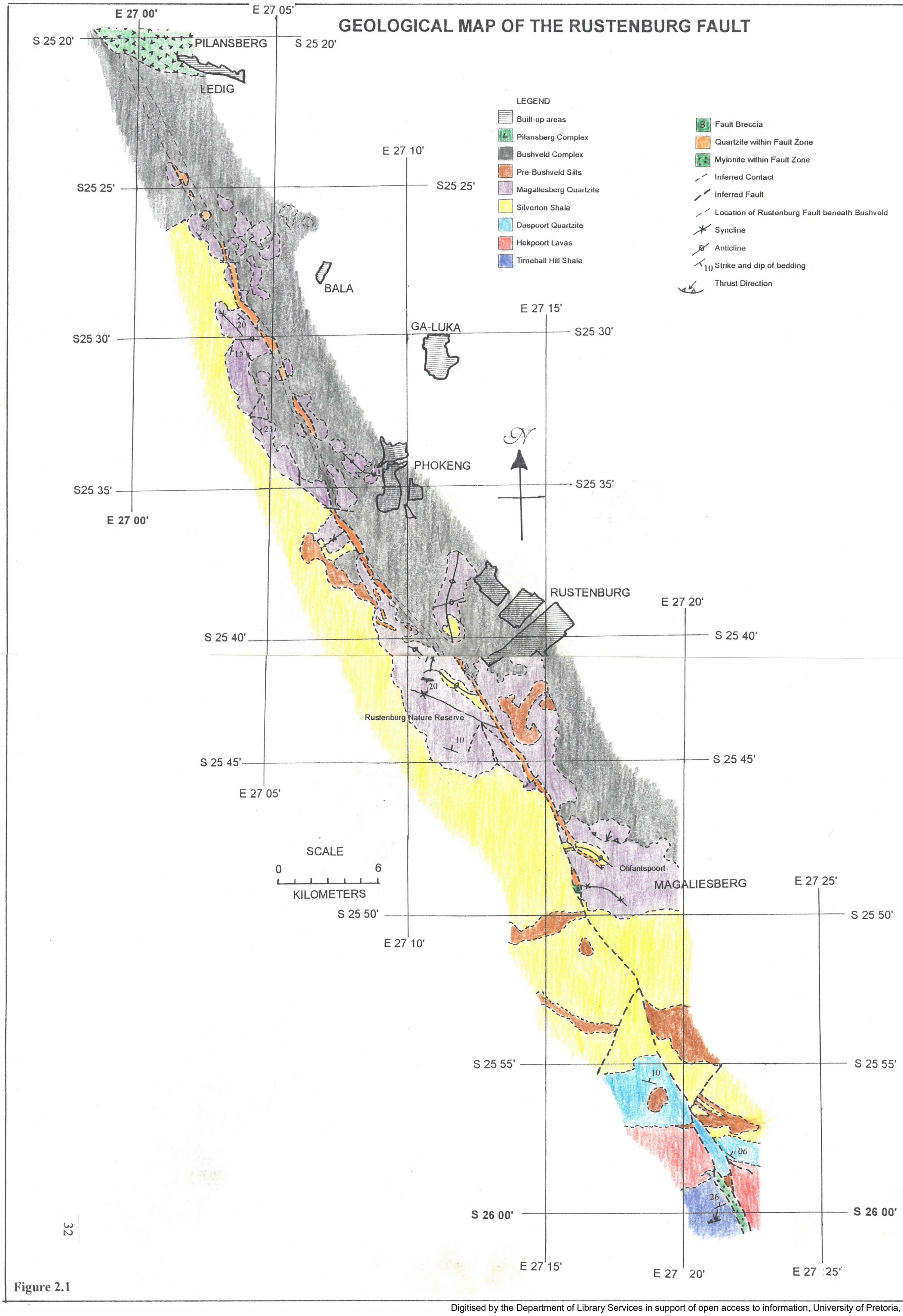

Figure 2.1

Figure 2.2: Timeball Hill shales at 25° 58.84' S: 27° 21.25' E. The view is towards the S.E., up the bed of the Hex river. In hand specimen these rocks appear to have been indurated, possibly by metamorphism. A small sill is located 20m to the S.E. of this locality, with a chilled margin evident against the shales. The grasses in the foreground are 0.5m high.

Figure 2.3: Boshoek conglomerate at 25° 58.84' S: 27° 20.97' E, showing poorly sorted, well rounded chert pebbles with low sphericity, and no imbrication or preferred orientation of clasts.

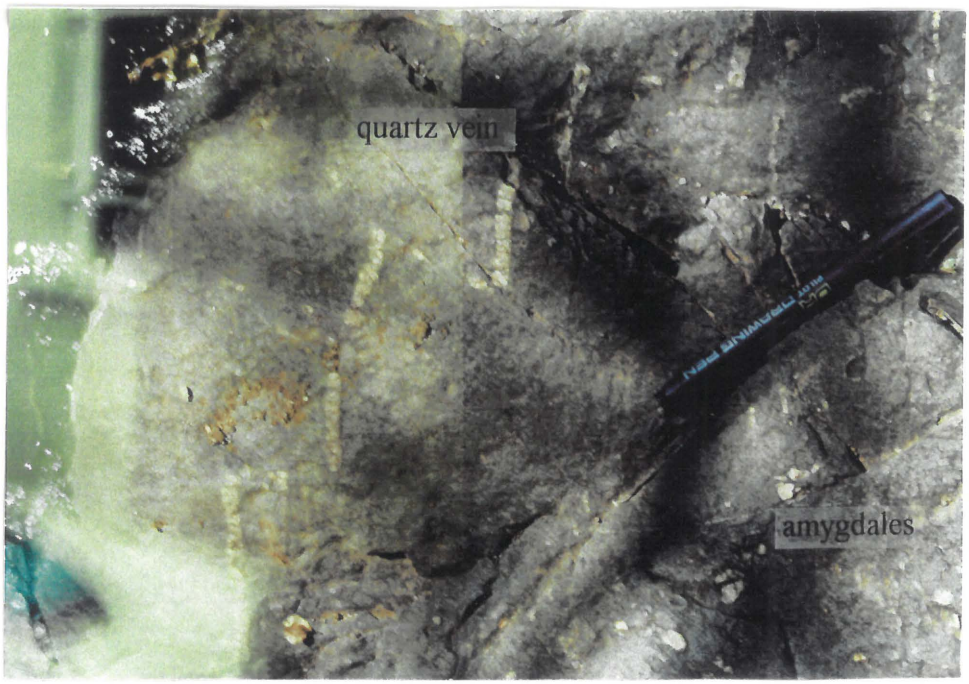

Figure 2.4: Amygdaloidal Hekpoort lava at 25^0 58.36' S: 27^0 21.03' E, also showing subsequent quartz veins.

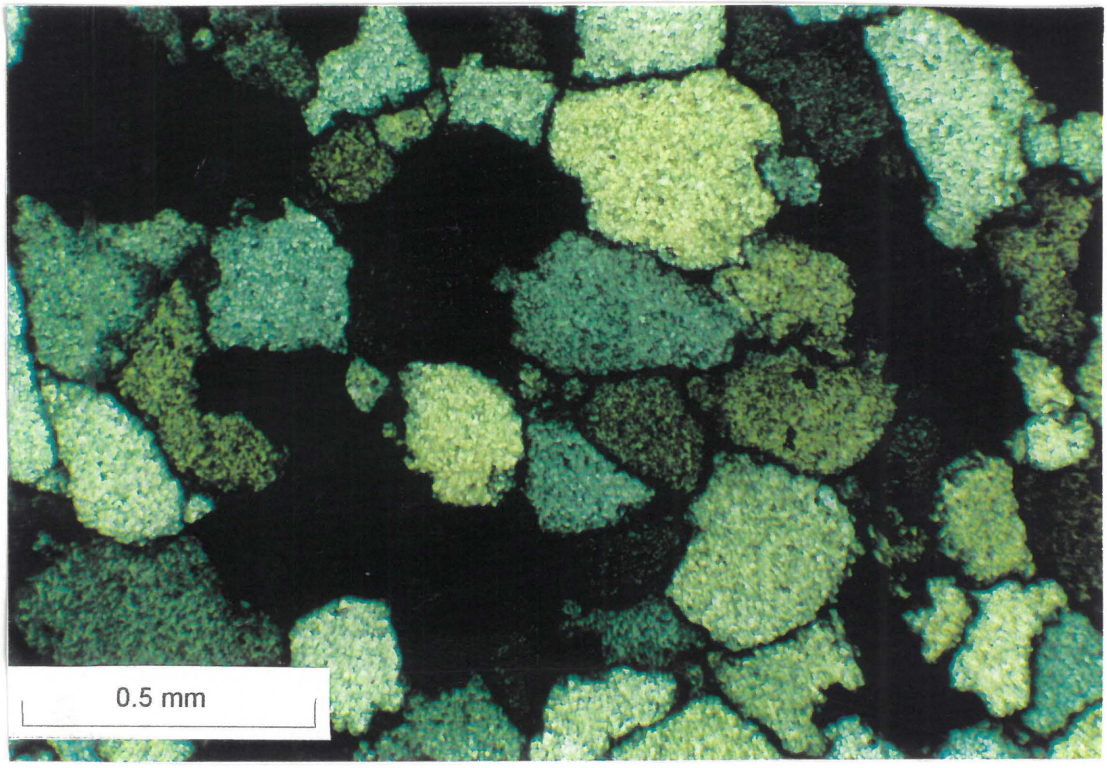

Figure 2.5: Photomicrograph of Daspoort sandstone at 25^0 58.41' S: 27^0 21.26' E, showing good sorting of medium-sized quartz grains, a lack of cement, and pressure solution at grain boundaries creating angular grain shapes (crossed poles).

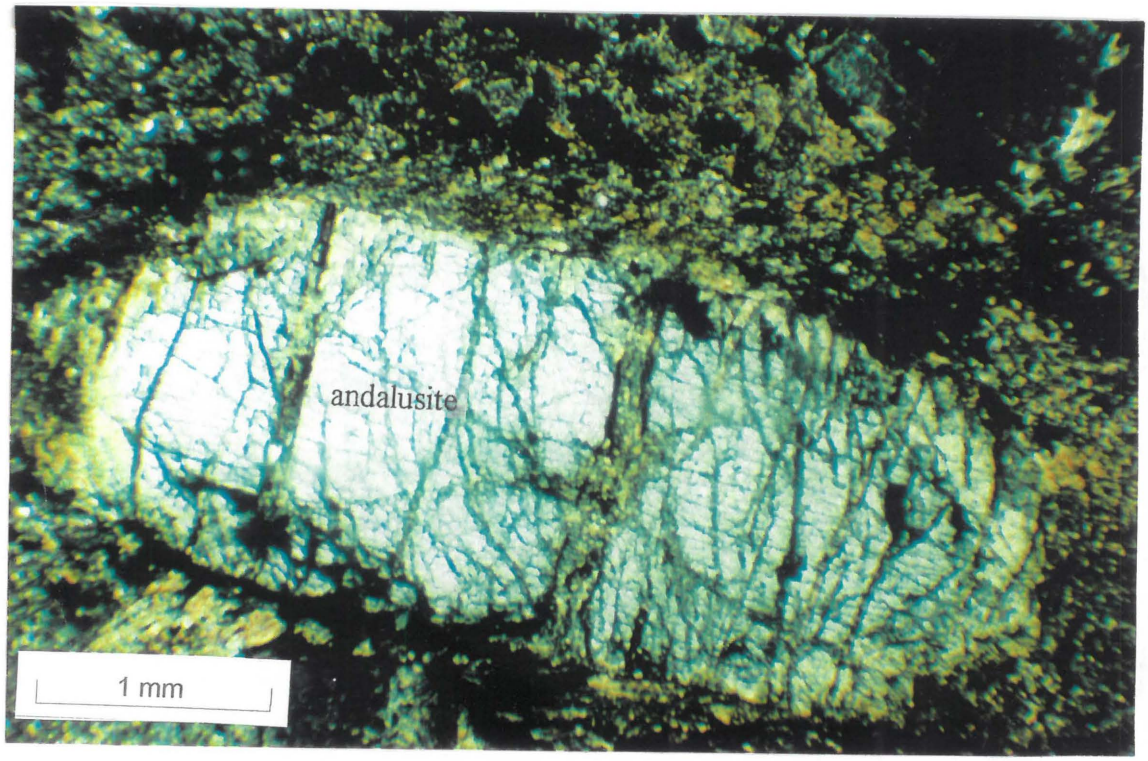

Figure 2.6: Photomicrograph of an andalusite hornfels in the Silverton Formation at 25^0 56.00' S: 27^0 20.50' E. Groundmass is quartz, haematite and secondary biotite. The large andalusite crystal shows the diagnostic cruciform pattern of chiastolite. The andalusite has a strong cleavage, along which biotite has grown (crossed poles).

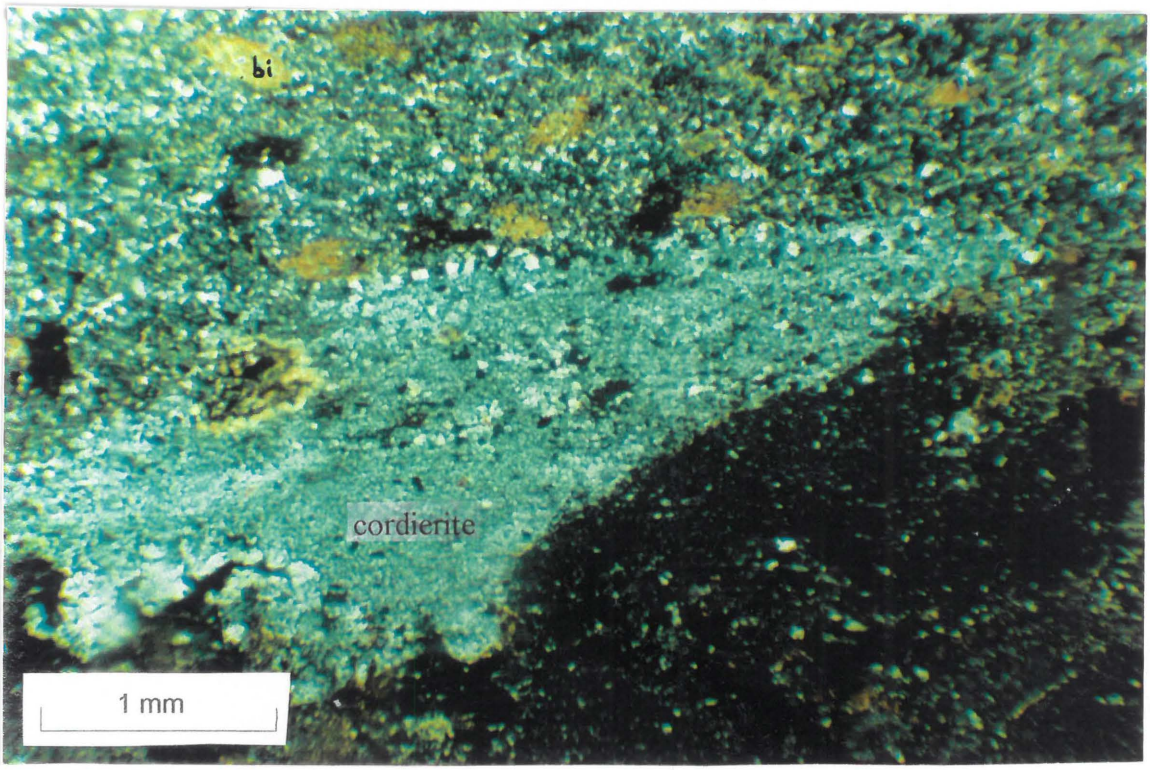

Figure 2.7: Photomicrograph of a cordierite-biotite hornfels in the Silverton Formation at 25^0 56.25' S: 27^0 20.10' E. Cordierite has grown in preference to andalusite due to lack of Fe (less secondary haematite compared to Figure 2.6). The large, partly pinitised cordierite poikiloblast shows diagnostic twinning (crossed poles). The poikiloblasts of either cordierite or andalusite give the characteristic 'spots' in hornfels.

Figure 2.8: Bedding preserved in very coarse-grained recrystallised Magaliesberg quartzite at 25^0 47.68' S: 27^0 17.16' E. The view is to the west, showing northwards-dipping bedding.

Figure 2.9: Large mudcracks preserved in Magaliesberg quartzite at 25^0 42.63' S: 27^0 11.39' E.

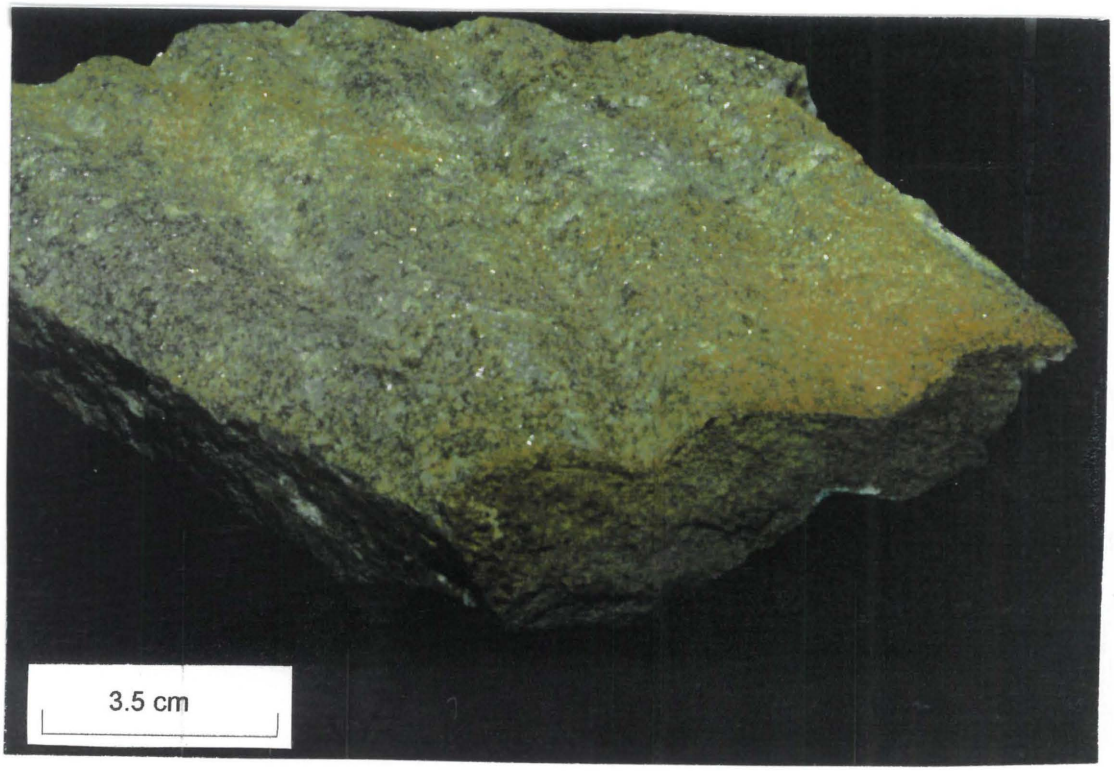

Figure 2.10: Asymmetric ripple marks in Magaliesberg quartzite.

Figure 2.11: Steeply dipping bedded Magaliesberg quartzite overlying Silverton shale (see left of Figure) at 25° 42.60' S: 27° 12.20' E. To the top right of the Figure, the flat topography marking the Bushveld Complex can be seen. The thickness of the Magaliesberg Formation shown in this Figure is ~650 m. View is to the N.W..

Figure 2.12: Differential degrees of recrystallisation in beds of Magaliesberg quartzite (25^0 42.97 S: 27^0 12.12' E).

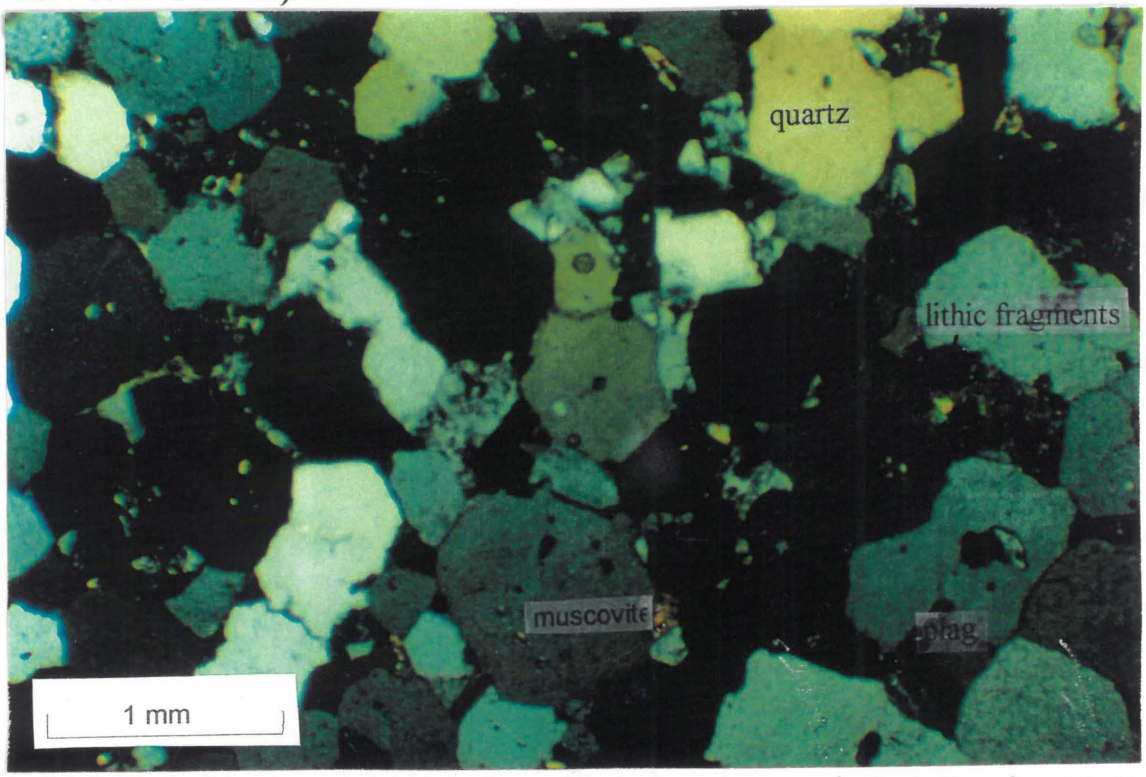

Figure 2.13: Photomicrograph of Magaliesberg sandstone from 25^0 47.50' S: 27^0 16.84' E, showing quartz, plagioclase, lithic fragments and secondary sillimanite and muscovite (crossed poles).

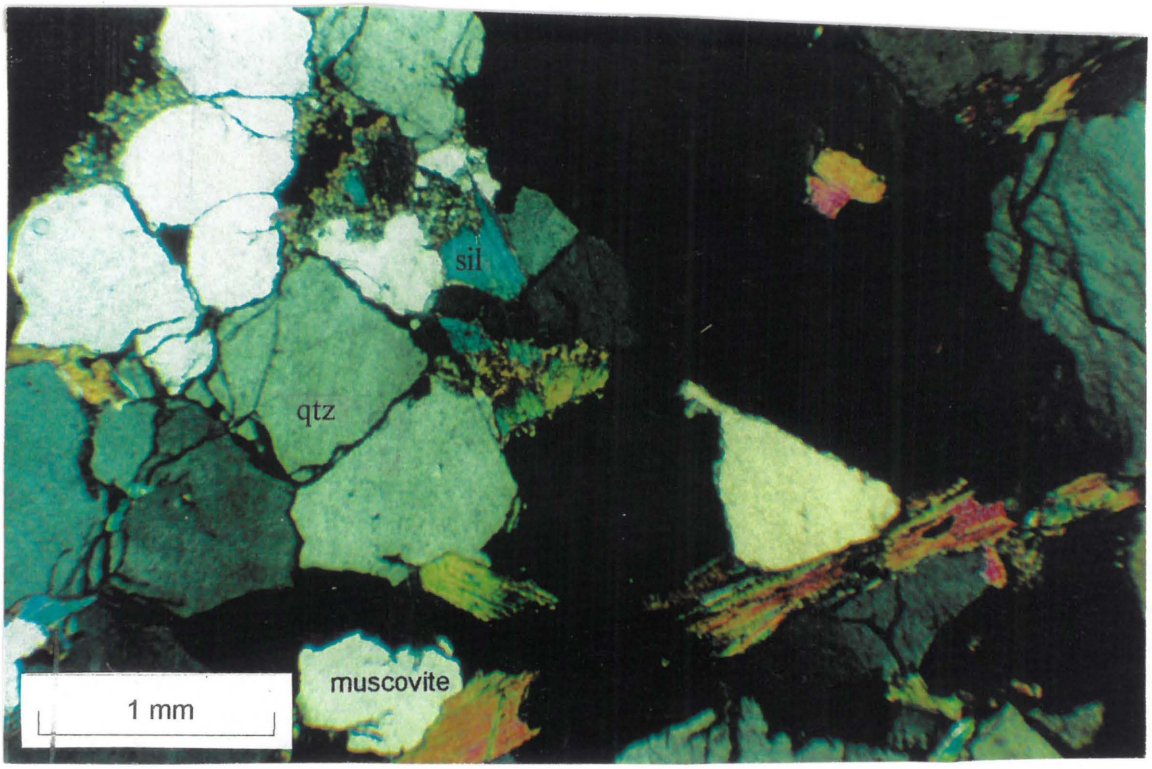

Figure 2.14: Photomicrograph of slightly recrystallised Magaliesberg quartzite from 25^0 39.80' S: 27^0 09.60' E, with high percentage of sillimanite, muscovite and primary matrix. Note the original rounded grain boundaries at the crystal/matrix interfaces in the top left hand corner (crossed poles).

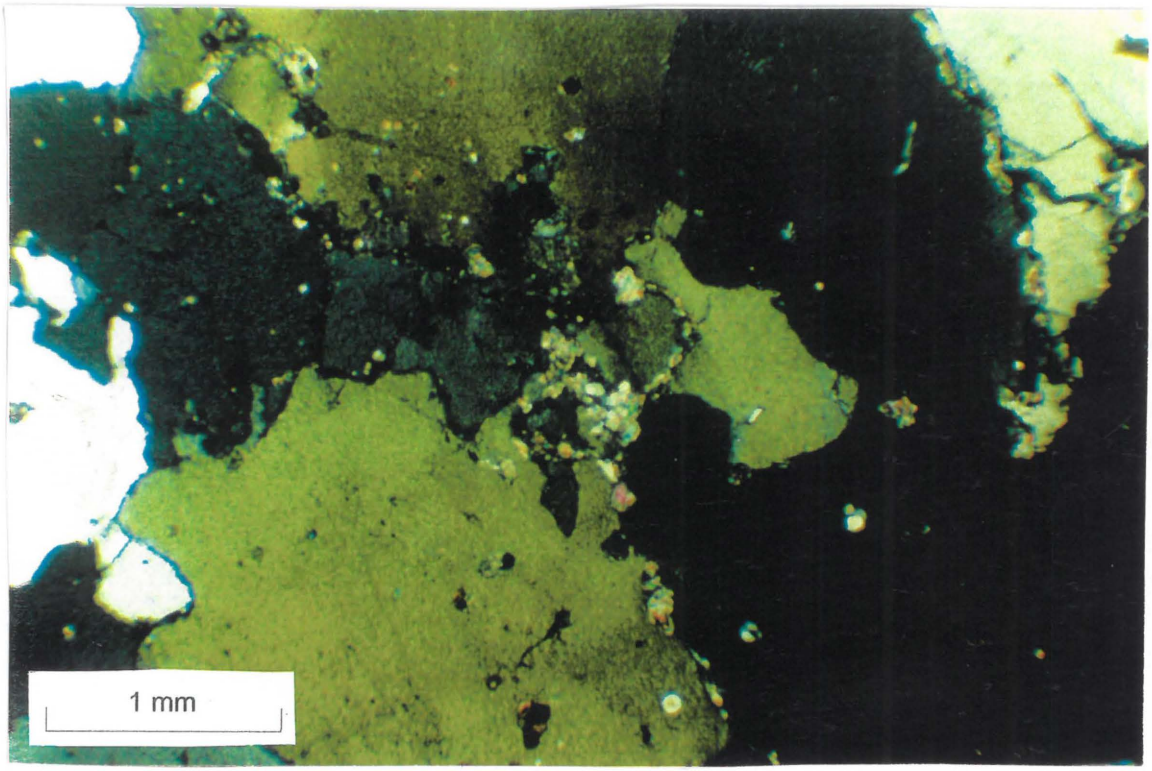

Figure 2.15: Photomicrograph of coarse recrystallised Magaliesberg quartzite from 25^0 47.32' S: 27^0 16.66' E, showing frequent small inclusions and plentiful small secondary metamorphic mineral crystals impeding quartz crystal growth (crossed poles).

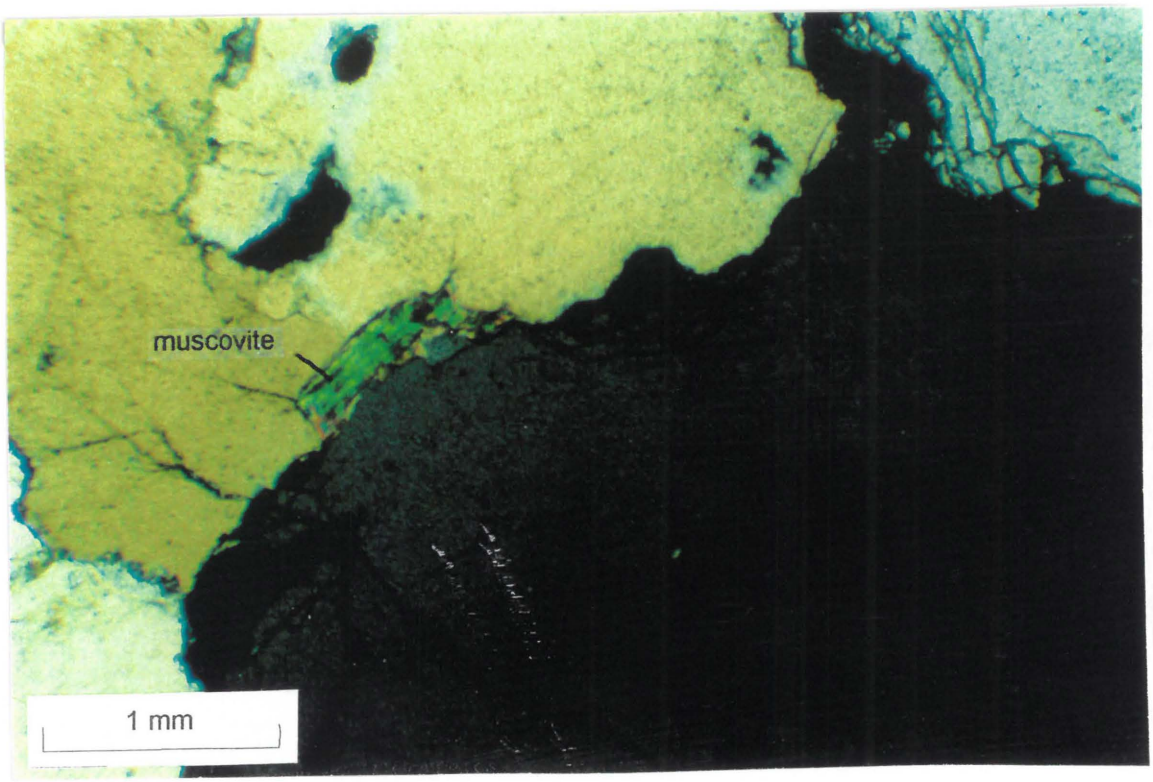

Figure 2.16: Photomicrograph of very coarsely recrystallised Magalieberg quartzite from 25 ^{0} 47.52' S: 27^0 17.12' E. Note lack of inclusions in quartz crystals and rare muscovite (crossed poles).

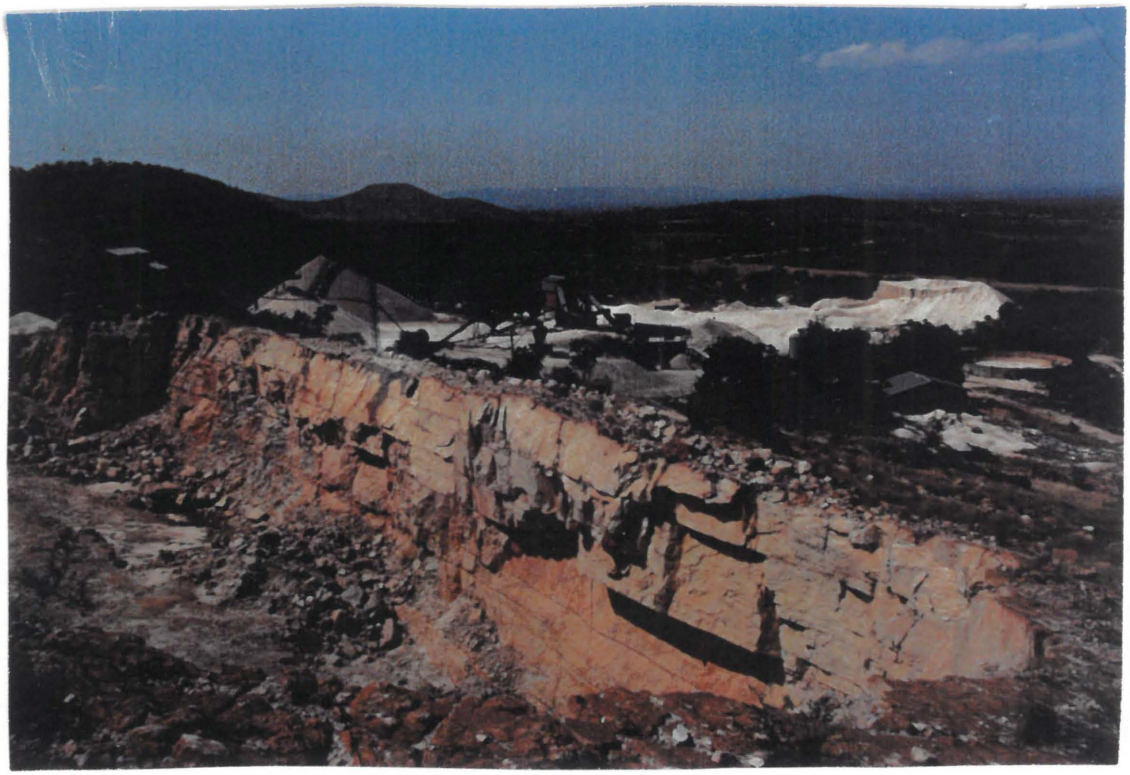

Figure 2.17: Sand quarry at 25^0 32.32' S: 27^0 04.69'E, exploiting high SiO_2 percentages of Magaliesberg quartzite. View is towards the N.E., showing eastwards dipping bedding.

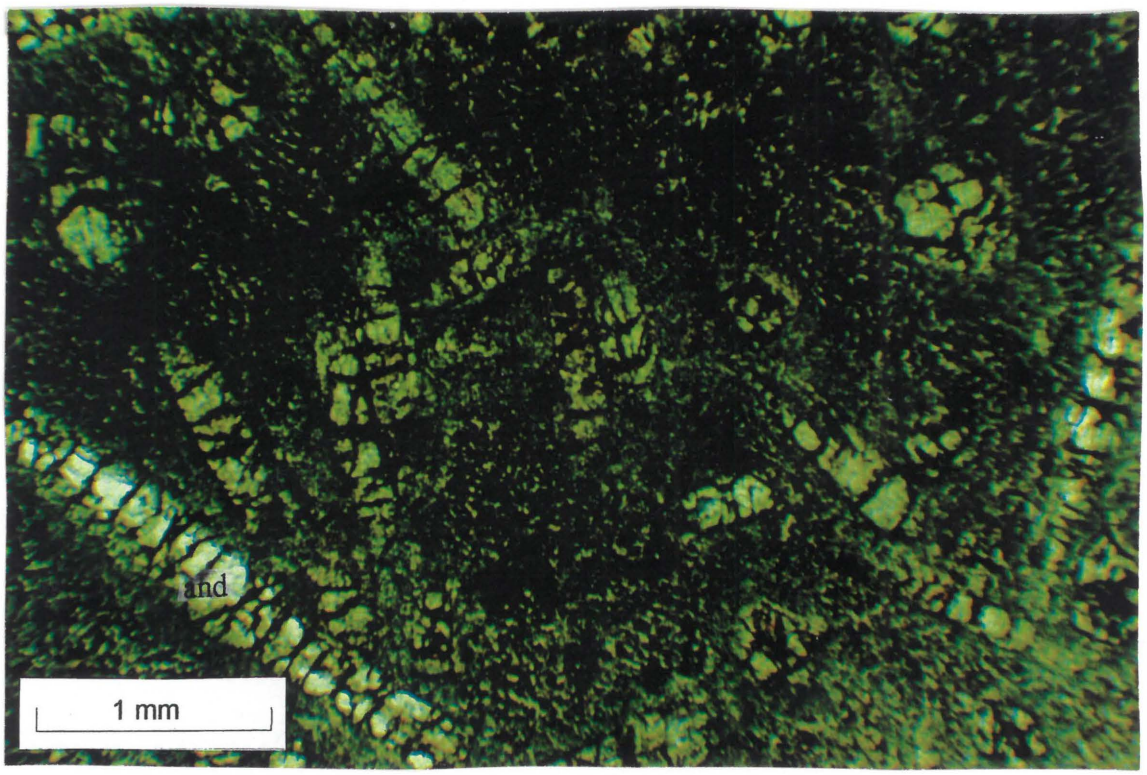

Figure 2.18: Photomicrgraph of hornfels in the Magaliesberg Formation, showing acicular andalusite crystals in a fine-grained chloritic groundmass (plane poles).

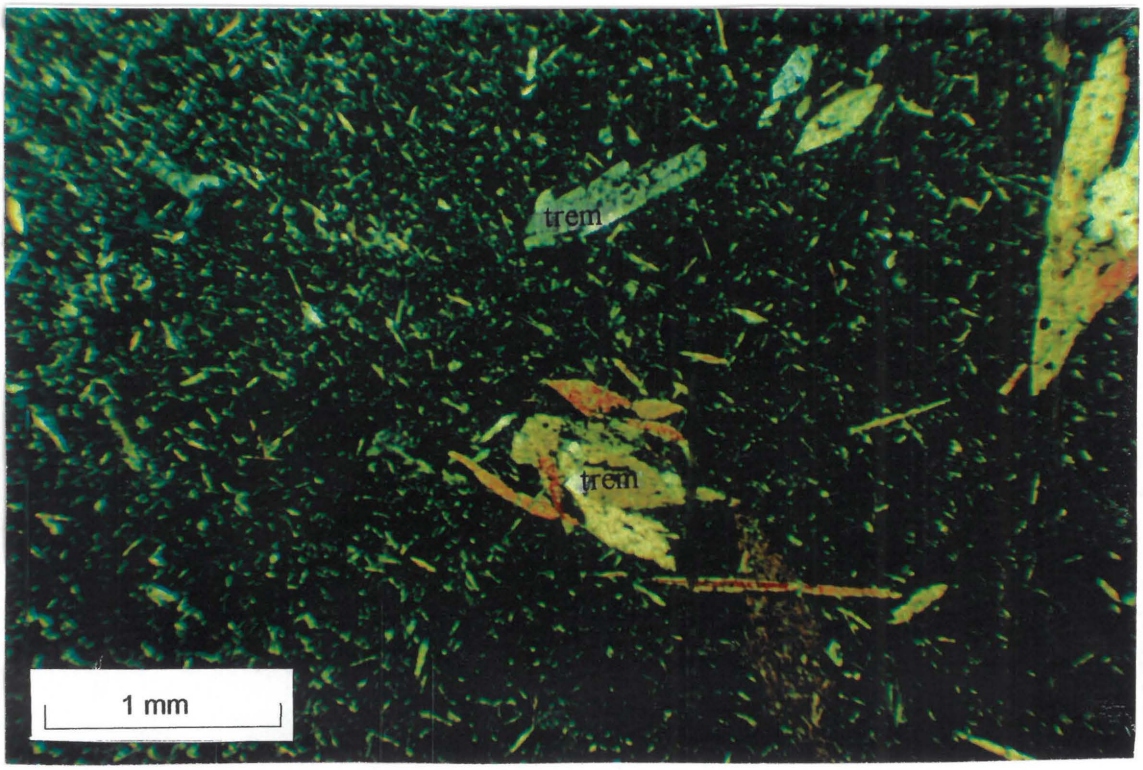

Figure 2.19: Photomicrograph of meta-diabase consisting of needles of tremolite, and glomerocrysts of tremolite at 25^0 55.60' S: 27^0 20.50' E (crossed poles).

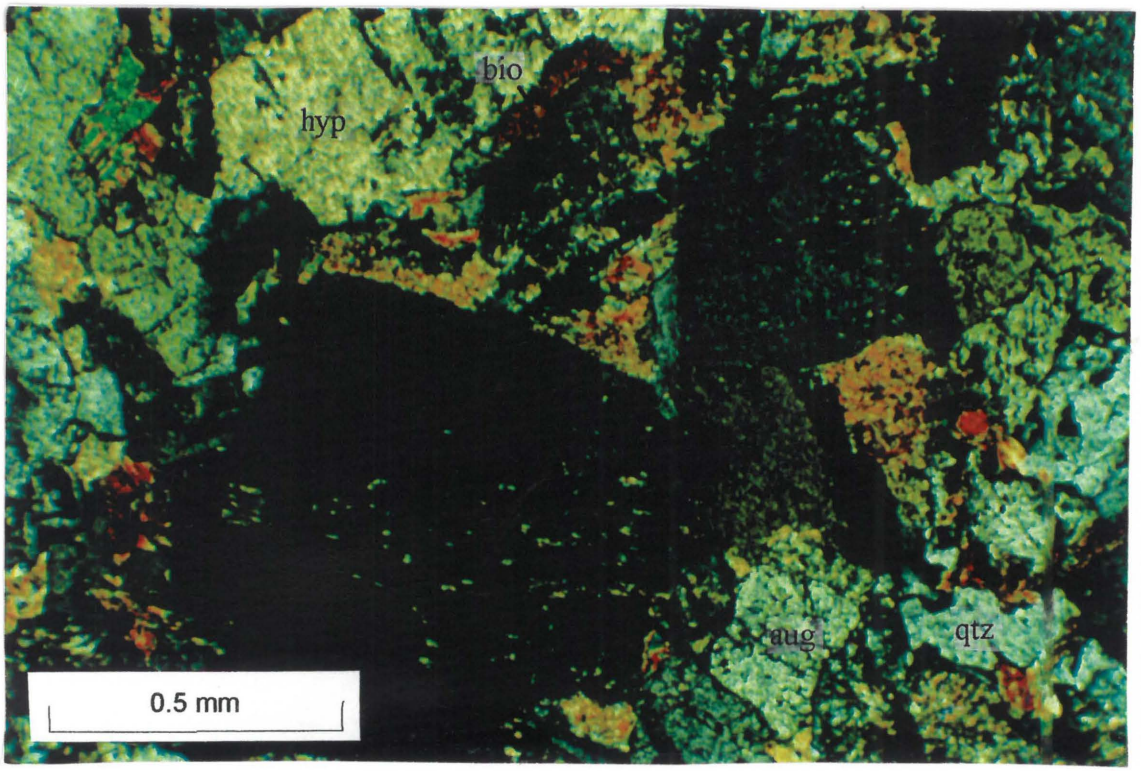

Figure 2.20: Photomicrograph of a norite sill at 25^0 38.50' S: 27^0 08.50' E, showing hypersphene laths, surrounded by interstitial quartz, augite and biotite (crossed poles).

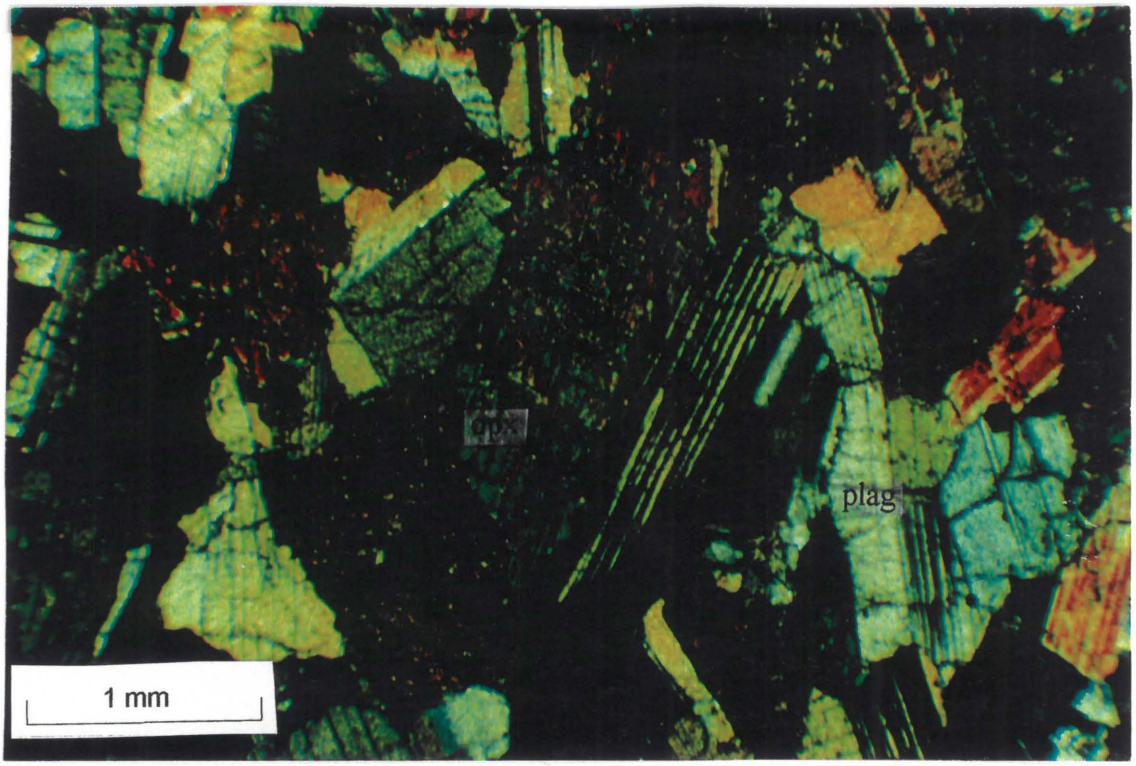

Figure 2.21: Photomicrograph of a lower, contact norite from the Bushveld Complex, showing plagioclase and orthopyroxexe. The hand specimen from which this was taken shows layering of orthopyroxenes (crossed poles).

3: STRUCTURAL GEOLOGY.

Tectonic structures along the Rustenburg Fault zone and in the adjacent areas were examined in order to unravel the kinematic history of the Fault zone. The structural data will be presented separately for two discrete areas: Area 1, the largest of the two, encompasses the field area between Olifantspoort in the south, to the northern edge of the field area, in the Pilanesberg mountains. This area contains mainly Magaliesberg Formation quartzite and the rocks of the Bushveld Complex (Appendix, and Figure 3.1). Area 2 encompasses the area from Olifantspoort to the southern edge of the field area, at S 26^0. This area contains the lower formations of the Pretoria Group (Appendix and Figure 3.1).

Location numbers of structural phenomena mentioned in the text are shown on the map in the Appendix, and on more detailed maps (Figures 3.1, 3.5, 3.8 and 3.46) which are included in this chapter.

3.1: Structural data from Area 1 (Olifantspoort to Pilanesberg):

The strata in this area are on the western margin of the western lobe of the Bushveld Complex. The major lithologies within this area are the basal (Kolobeng) norites of the Bushveld Complex and the Magaliesberg Formation quartzite (lying within the Bushveld metamorphic aureole). In this area, the Bushveld mafic rocks rarely outcrop, so the structural data in this area were mainly collected from the Magaliesberg Formation. Reports from underground mining in the Rustenburg area, however, suggest that the regular layering of the Complex is undisturbed, apart from shallow dips into the centre of the Complex (e.g. Leeb-du Toit, 1986; Viljoen & Hieber, 1986), and does not show evidence for any of the structures presented below.

3.1.1: Soft sediment deformation in Area 1:

Locally (e.g. location 1), sedimentary structures, such as slumping of bedding and dewatering structures, such as sand pipes, may be seen in unrecrystallised strata of the Magaliesberg Formation (Figure 3.2). These features may have formed due to dewatering of unconsolidated Magaliesberg sands under loading by succeeding layers, or may have been induced as a result of

shock during earthquake movement. However, as most of the Magaliesberg quartzite is recrystallised, small-scale sedimentary structures are generally not preserved. As described in section 2.7.2, individual beds may escape recrystallisation, and small-scale features (Figure 3.2) may thus locally be preserved.

3.1.2: Folding in Area 1:

The Magaliesberg Formation around the edge of the Bushveld Complex is generally regarded as possessing planar geometry (i.e. not locally folded), and having beds dipping towards the centre of the intrusion (e.g. Eriksson et al.,1995), reflecting loading of the stratigraphy by the Complex. While this is usually true around most of the rim of the Bushveld Complex, in the present field area the Magaliesberg Formation strata were found to be characterised by large-scale open folds, often with a fold-wavelength and amplitude of several hundred metres.

3.1.2.1: Field description of large-scale folds:

Large-scale folding is well developed at Olifantspoort farm, just east of Olifantsnek dam and east of the Rustenburg Fault zone (Appendix, Figure 3.1, and Figure 3.5). Here the Magaliesberg quartzites are folded into a sequence consisting of an anticline in the north and a syncline in the south (wavelength 3.5 km). The Silverton shales are exposed along the core of the anticline. In the field, the overall form of the fold can be described as upright, open, symmetrical folding (as defined by Fleuty, 1964) (Figures 3.3 and 3.4). Bedding orientation at the crest of the anticline (location 2 in Appendix, Figure 3.1, and Figure 3.5) suggest that the folds are gently plunging to the S.E.. Plotting bedding geometry of the folds on a map shows that the axial trace of this fold system has an average trend of 296^0 (Appendix, Figure 3.1 and Figure 3.5). The orientation of the fold axial surfaces are therefore approximately $296^0 90^0$. However, the fold axial trace appears to have a variable trend, which is discussed below. The detailed structure of the Olifantspoort area is shown in the geological map in Figure 3.5, which shows the non-linear trend of the fold axial trace.

Folding on a similar scale was observed west of the Rustenburg Fault zone in Rustenburg Nature Reserve (Appendix, Figure 3.1 and Figure 3.8), where the Magaliesberg and Silverton Formations

and possibly also diabase sills are folded. In the field, the fold system appears to bear much resemblance to the style of folding at Olifantspoort. Again, the fold system consists of an anticline to the north and a syncline to the south, and Silverton shales are exposed along the core of the eroded anticline. The folds are also upright, open and symmetrical (Figures 3.6 and 3.7). The orientation of the fold axial surfaces in the Rustenburg Nature Reserve fold system are approximately 305^0 90^0. The detailed structure of the Rustenburg Nature Reserve area is shown in Figure 3.8. The curved trend of the axial trace of the anticline is in common with the fold system at Olifantspoort.

In the extreme north of Rustenburg Nature Reserve (location 3 and 4), folding is of a smaller scale, though generally more complex, with two intersecting trends of fold axial traces producing crescent-shaped fold structures. The first set trends 130^0, and the second set trends 030^0-050^0., and it is apparent that set one (F_1) is refolded by set two (F_2). This pattern is also probably responsible for the curved nature of the Olifantspoort and Rustenburg Nature Reserve fold axial traces, which seem to have been slightly refolded around a second fold axial trace trending 035^0 (Figures 3.5 and 3.8). Such crescent-shaped folds, caused by intersecting upright folds which are perpendicular to each other can be classified as transitional between Type 1 interference folding (two perpendicular sets of upright folds create basin and dome structures) and Type 2 interference folding (a recumbent fold set is refolded by an upright fold set to produce crescent-shaped folds), as described by Ramsay (1967).

This pattern of transitional Type 1-Type 2 interference folding (Ramsay, 1967) is evident throughout much of the field area. At locations 5 and 6 (Appendix and Figure 3.1), Magaliesberg quartzite is folded into anticlines along axial traces with an original trend of approximately 140^0 (F_1), which have subsequently been refolded along axial traces trending 040^0-070^0(F_2). Erosion along the core of the set 1 anticline at location 5 (Appendix, Figure 3.1 and Figure 3.8) has exposed Silverton shale. Similarly at location 7, a synclinal axial trace trending 150^0 is refolded by a later anticlinal axial trace trending 090^0.

3.1.2.2: Field description of bedding in other outcrops of the Magaliesberg Formation in Area 1:

Data on the orientation of bedding in all other Magaliesberg Formation strata in the field area, with apparently no systematic fold structures (e.g the area east of the Fault zone in Rustenburg Nature Reserve, and the northern part of the field area, between Phokeng and Pilanesberg), were also recorded. Though visible folding was never encountered in the field in these areas, and collected field data did not suggest any particular pattern to the trends of fold axial traces, stereographic analysis (Section 3.1.2.3) suggests that these areas are systematically folded with similar fold axes to those identified above.

3.1.2.3: Stereographic projections of folded strata in area 1:

Stereographic projections of poles to bedding defining the Olifantspoort anticline and syncline are shown in Figures 3.9 and 3.10, respectively. Comparison of these figures shows that both structures were formed by parallel folding around a fold axis of $07^0 \rightarrow 296^0$ (mean fold axis). This N.W.-directed plunge contrasts with the S.E.-directed plunge identified at location 2, but can be explained by invoking interference folding to vary the plunge direction. Accurate orientations of fold axial planes could not be determined accurately from the available data by using Ramsay's (1967) method, due to the shallow plunge of these folds. The distribution of poles to bedding define a broad girdle, and statistical analysis (Eigenvector analysis) gives a best-fit great circle (π circle). The pole of the π circle defines the fold axis. The scatter of data within the π girdle of the Olifantspoort fold system may indicate either sub-cylindrical folding, or the effects of refolding of an initially cylindrical fold.

The geometry of the Rustenburg Nature Reserve anticline and syncline is shown stereographically in Figures 3.11 and 3.12, respectively. Poles to bedding tend again plot within a broad π girdle, indicating sub-cylindrical folding or interference folding, similar to the folding style at Olifantspoort. These stereographic projections show near parallel fold axes, with the plunge direction for the anticline and syncline being $00^0 \rightarrow 127^0$ and $01^0 \rightarrow 125^0$ respectively. Again, Ramsay's (1967) method for determining the orientation of fold axial planes could not be used, due to the shallow plunges plotted on the stereographic projections.

The remaining areas of outcrop of the Magaliesberg Formation show little evidence for systematic folding in the field (Section 3.1.2.2). For analysis by stereographic projection, these areas were subdivided into four separate domains. These are the area east of the Rustenburg Fault in Rustenburg Nature Reserve, the area between Olifantsnek dam and Rustenburg Nature Reserve, and both east and west of the Rustenburg Fault zone in the area between Phokeng and Pilanesberg, in the north of the field area (Appendix and Figure 3.1). The orientation of bedding in each of these areas were plotted stereographically and analysed. The bedding geometry of Magaliesberg quartzite in the area east of the Rustenburg Fault in Rustenburg Nature Reserve (location 8) is presented in Figure 3.13. Though no large-scale folds are manifest in this area, analysis of stereographic data shows that small-scale folds in this area generally have a fold-axis plunging $03^0 \rightarrow 116^0$.

The bedding orientation in the area of Magaliesberg quartzite on the western side of the Fault between Olifantsnek dam and the synclinal fold axis in Rustenburg Nature Reserve (location 9) is shown in Figure 3.14. This shows overall gentle folding about a fold-axis plunging $03^0 \rightarrow 108^0$.

The bedding geometry from outcrops of Magaliesberg strata further north, between Phokeng and the Pilanesberg Alkaline Complex are shown on Figures 3.15 (west of the Fault zone) and 3.16 (east of the Fault zone). Interpretation of the stereographic data shows that the outcrops on the western side of the Fault zone have more uniformly orientated bedding than those to the east. The western block contains small folds with the average fold axis plunging $05^0 \rightarrow 227^0$ (Figure 3.15), whereas the eastern block contains a wide variety of bedding orientations (Figure 3.16). *SpheriStat* software, however, determined a fold axis of $05^0 \rightarrow 138^0$ in this area. No measurable folds were observed in the field in this area to confirm these plunge directions.

3.1.2.4: Interpretation of stereographic projections:

Interpretation of the stereographic projections must be made in the light of observations made in the field. Field data showed the presence of transitional Type 1-Type 2 interference folds (e.g. locations 3, 4, 5, 6, and 7), with the F_1 fold axial traces trending N.W.-S.E., and the F_2 fold axial traces trending N.E.-S.W. (Section 3.1.2.1). The trend of fold axes presented in preceding stereographic projections are also parallel to one of these two directions. Figures 3.9, 3.10, 3.11,

3.12, 3.13, 3.14 and 3.16 show approximately parallel fold axes, corresponding to the F_1 folds identified from interference patterns. Figure 3.15 shows a fold axial trend corresponding to the F_2 fold axial surfaces identified from the interference patterns. It is possible that the very broad π girdle shown for the F_1 fold axis in Figure 3.16 is due to extreme interference folding, as the F_2 folding direction appears to be well developed in the northern part of the field area (Figure 3.15).

A summary of the trend of axial traces shown on the maps (Appendix and Figure 3.1), and the fold axes presented on the stereographic projections, is given in Table 3.1. As the plunge of the fold axes presented on stereographic projections is generally close to horizontal, their orientations should coincide with the axial traces given on the maps. The average trend of each axial planar trace/fold axis is calculated for each fold set, and maximum compressive directions (σ_1) of 033^0-213^0 and 155^0-335^0 are inferred for F_1 and F_2, respectively.

3.1.2.5: Down plunge projections of large-scale folds:

Down plunge projections of the Olifantspoort and Rustenburg Nature Reserve fold systems were constructed using the method described in section 1.7.3. As both anticlines and synclines are presented together on the same projection, an average fold axis for the Olifantspoort ($07^0 \rightarrow 296^0$) and Rustenburg Nature Reserve ($01^0 \rightarrow 126^0$) areas were calculated. The down-plunge projections of these two areas are shown in Figures 3.17a and 3.18a respectively, and are interpreted in Figures 3.17b and 3.18b. Figures 3.17a and b show that the Olifantspoort anticline is tightened compared to the very open fold of the syncline, and shows cylindrical folding, with approximately upright fold axial planes. This is consistent with observations made in the field (e.g. Figure 3.3). In an idealised cylindrical fold, all planes on a down-plunge projection should be vertical (90^0dip). The variety of dips shown in Figure 3.17a are due to the curved nature of the fold axial surfaces (Appendix, Figures 3.1 and 3.5), which were probably caused by interference folding (Section 3.1.2.1). Figures 3.17 a and b also show steepening of the beds north of the anticline, where shallow dips would be expected on the limbs of a concentric fold. This structure is considered further in section 3.1.3.4.

Figures 3.18 a and b show that Rustenburg Nature Reserve folding also has relatively tight cylindrical folding in the anticline, and relatively open folding on the syncline. The fold axial

planes are approximately upright, also in common with the Olifantspoort fold system. The variability of dips around vertical on Figure 3.18a is again probably due to the curved fold axial surfaces, caused by interference folding.

3.1.3: Faulting in Area 1:

3.1.3.1: The Rustenburg Fault:

The Rustenburg Fault in Area 1 is marked by the presence of a characteristic quartzitic lithology. This Fault quartzite, referred to on the map (Appendix) as 'quartzite within Fault zone', bears a strong resemblance, on a mesoscopic scale, to the Magaliesberg Formation quartzite, except that it lacks primary structures in section and has well developed jointing (e.g. location 10; Figure 3.19). Other than the lack of primary structures, the Fault quartzite can be discriminated from Magaliesberg quartzite by its whiter appearance, as the Fault quartzite generally contains less haematite than the Magaliesberg quartzite (Figures 3.20 and 3.21).

The ability to distinguish between outcrops of Fault quartzite and Magaliesberg quartzite proved to be useful when following the Fault through area 1. The identification of lenses of Fault quartzite amongst the rocks of the Bushveld Complex (e.g. location 11), allowed for the line of the Fault zone to be reconstructed. As shown on the map (Appendix and Figure 3.1), the Fault was found generally to follow a strike of 150^0.

In thin section the Fault quartzite has contrasting characteristics to those in the Magaliesberg Formation quartzite. Comparison of Fault quartzite with Magaliesberg quartzite (Figures 2.15, 2.16, 3.22 and 3.23) shows that the crystal size is generally larger in the Fault quartzite, typically >5 mm, compared to typically <2 mm in Magaliesberg quartzite. Samples of Fault quartzite in thin section usually show the effect of deformation within the crystals, either as undulose extinction (Figure 3.24) or, in higher strain zones, deformation lamellae (Figures 3.22 and 3.25). Unfaulted Magaliesberg quartzite lacks deformation lamellae and rarely contains undulose extinction. Pressure solution at crystal boundaries is common to both types of quartzite.

It is illustrated in Figures 3.24 and 3.25 that neighbouring crystals usually show the same type of deformation. Undulose extinction and deformation lamellae are rarely found together in the same thin section. Thin section analysis of samples from varying localities along the length of the Fault zone showed no systematic spatial relationships between the type of crystal deformation and location on the Fault zone.

Many samples of Fault quartzite showed patches of very fine quartz crystals as inclusions within, or at the edge of larger (5mm sized) crystals, perhaps suggesting a mylonitic or ultracataclasite protolith of the Fault zone which has failed to recrystallise (Sibson, 1977). Examples of these are shown in Figures 3.25 and 3.26.

Whilst the discrimination between Fault quartzite and Magaliesberg quartzite based upon these physical characteristics was useful, areas such as location 9, 15 and 16 proved enigmatic in that all the mesoscopic physical properties of the Fault quartzite are met, with little or no apparent Fault movement (e.g. the southern limb of the Olifantspoort anticline at location 16 shows no discernable displacement- Figure 3.27). Additionally, such areas of Fault quartzite may still contain areas with vague relict bedding planes, showing a geometry concordant with surrounding structures. In thin section, rocks from these areas show many similarities with Fault quartzite, but never show patches of fine grained quartz that failed to recrystallise, associated with the Fault quartzite.

3.1.3.2: Small-scale structures within the Fault quartzite:

Although the appearance of the Fault quartzite is generally massive, in certain places structural features *are* present within this quartzite. These are often in the form of veins in the quartzite, or small fractures and faults of variable orientation. Veins are shown crossing Fault quartzite in Figure 3.28. When viewed in thin section these 'veins' can be seen to have grown in sub-optical continuity to the surrounding crystals (Figure 3.29), and can sometimes be seen to have grown from fractured areas in the crystal (Figure 3.30). These structures suggest that a tectonic event, causing fracturing, and a subsequent thermal event (to cause the annealing) occurred after the recrystallisation of the Fault quartzite.

The micro-faulting shown in Figure 3.30 occurs close to the outcrop shown in Figure 3.31 (location 17), where the Fault quartzite is faulted along a trend of 150^0. The re-lithification of the crush breccia shown in this photograph is analogous to the micro-scaled annealing illustrated in Figures 3.29 and 3.30.

Faulting that led to the brecciation of Fault quartzite can also be seen at location 18, close to where the Rustenburg Fault cuts the western end of the southern limb of the Olifantspoort anticline, and at location 19, the small hill called Gifkoppie, just south of Olifantsnek dam. Here the brecciation is more intense, so that annealing has often failed to recrystallise across the widest brecciated zones. Some areas of brecciated Fault quartzite show no evidence for annealing (Figure 3.32).

Around the lower slopes of Gifkoppie (location 19), the Fault quartzite is more friable, and is dull brown in colour. Thin section analysis showed that this rock was a fine fault breccia, and is comprised of clasts of Magaliesberg quartzite (smaller quartz crystals, lacking much evidence for undulose extinction), surrounded by partially annealed micro-crush-breccia.

At location 20, in a road cut west of Boshoek, a cross-section through the Rustenburg Fault zone can be observed. This section shows large lenses of Magaliesberg quartzite enclosed within a matrix of Fault quartzite (Figures 3.33 and 3.34). Zones of intense jointing are present in the rock adjacent to the interface between the lenses of Magaliesberg Formation quartzite and the Fault quartzite (Figure 3.34). These planes are sometimes visible as shear joints (Shear-joint plane = 200^0 90^0), containing slickensided faces (L_1= $40^0 \rightarrow 200^0$) and patches of breccia (Figure 3.35).

At the western extreme of the Fault zone at location 20, the contact of the Fault quartzite with the Silverton shales can be observed. The sense of movement was difficult to interpret due to the intense weathering and disruption of bedding in the shales.

At location 21, a road cut through the Fault zone just west of Olifantsnek dam, lenses of Silverton shale are found in the Fault quartzite. Lenses of Magaliesberg quartzite incorporated into the Fault zone were also visible elsewhere, e.g. location 22, in Rustenburg Nature Reserve. The apparent long axes of these lenses are always orientated parallel to the trend of the Fault (150^0). It was noted that only lenses of Pretoria Group rocks are included as lenses within the Fault zone.

Outcrops of Bushveld rocks within the Fault zone are conspicuously absent.

Silverton shales are also present at the edge of the Fault zone at location 23, where the Rustenburg Nature Reserve anticline is cut by the Rustenburg Fault. Shales are exposed on a stream bed, and show extreme distortion of laminar bedding (Figures 3.36, 3.37 and 3.38).

3.1.3.3: Smaller-scale faulting and shear-jointing in Area 1:

In addition to the Rustenburg Fault, smaller-scale faults are found throughout Area 1. Many of these are evident from the resultant displacement of the main Rustenburg Fault zone, e.g. at locations 24 and 25 where faults displace the Fault quartzite by around 200 m. Though the fault rocks are not exposed, outcrops of the Fault quartzite do not remain on the trend of the Rustenburg Fault, thus indicating faulting. Similarly at location 26, shown in Figure 3.39, the Fault quartzite is cut and displaced 250 m by two N.E.-striking faults. In both these cases, the classification of the faults is unknown, as the direction and distance of displacement cannot be determined.

At location 27 two faults with perpendicular strikes can be seen. The first fault, with a strike of 120^0, is cut by a later fault with a strike of 030^0 . The first fault was found to contain Fault quartzite along its zone, whilst no evidence for Fault quartzite could be found in the second fault. The displacement on the second fault is about 30m of sinistral movement, as shown by the displaced outcrop of the vertically dipping Fault quartzite.

Shear jointing in the Magaliesberg quartzite is shown in Figure 3.40, and on the northern limb of the Olifantspoort anticline in Figure 3.41. The direction of displacement of the shear jointing shown in Figure 3.41 suggests that it may have been imposed as conjugate faulting to post-Bushveld movement on the Rustenburg Fault (Chapter 4).

Similarly small-scale faults were observed on the limbs of the Rustenburg Nature Reserve anticline, sub-parallel (strike = 350^0) to the strike of the Rustenburg Fault, and showing apparent dextral movement (location 30), inferred from the displacement of southwards dipping beds. On the

northern limb of the Rustenburg Nature Reserve anticline at location 31, some reverse faulting along a plane 160^0 70^0 N.E. was recorded, as shown in Figure 3.42. This suggests that E.-W.-directed compression created this structure.

3.1.3.4: Thrust faulting in Area 1:

At location 32 (Figure 3.43) an area of anomalously thick Magaliesberg quartzite can be observed (Appendix, Figure 3.1 and Figure 3.5). This area contains Magaliesberg quartzite approximately 700 m thicker than the strata in the neighbouring areas of the Magaliesberg Formation. This feature is also illustrated in the down-plunge projection shown in Figure 3.17.

This phenomenon could have been formed either by (a) creation of a second-order basin by synsedimentary normal faulting of the Rustenburg Fault, with downthrow to the east, causing deepening of the first-order sedimentary basin, or (b) by thickening due to thrusting. It is important to note that the Bushveld Complex may have assimilated large volumes of Magaliesberg Formation strata in this area. Therefore the true thickness of the Magaliesberg Formation, and the true thickness and extent of the thickened portion cannot be determined accurately.

The contact between the top of the Magaliesberg Formation proper (as defined by the area adjacent to this thicker portion) and the base of the thickened portion, is marked by a cliff, about 10 m high (Figures 3.43 and 3.45). At the base of the cliff, strongly recrystallised quartzites show remains of a planar fabric, shown in Figure 3.44. The orientation of this fabric is parallel to the bedding both above and below the contact. Thin section analysis failed to discriminate whether this fabric is recrystallised convolute bedding in sandstone, which would suggest that the thickening in this location was due to tectonic second-order basin formation, or is a recrystallised tectonic foliation, which would suggest thickening due to thrust stacking.

However, the anastomosing nature of the relict fabric shown in Figure 3.44 suggests that it is not convolute bedding, and it therefore suggests a recrystallised secondary structure. Additionally, synsedimentary downthrow to the east is hard to reconcile with the synsedimentary westerly downthrow seen in the Daspoort Formation (Section 4.1).

Aerial photographs (section 1.7.1) show that joints do not pass northwards into the thickened section, indicating that the 'hanging wall' had been tectonically juxtaposed by low angled thrusting, after the joint set had been locally imposed in the footwall. This argument is strengthened by evidence shown in Figure 3.45, which shows contrasting haematite staining in the hanging wall (red) and footwall (white), indicating that they were lithified in different diagenetic environments.

Therefore the evidence suggests that the localised thickening of the Magaliesberg Formation at location 32 is due to bedding parallel thrusting. However, due to the destruction of kinematic indicators during recrystallisation, the precise direction from which thrusting occurred cannot be determined.

3.2: Structural data from Area 2 (Olifantspoort to 26^{0}S):

Area 2 contains the lower formations of the Pretoria Group, and is of generally poor outcrop quality compared to area 1. Outcrop of argillaceous and volcanic formations is particularly poor. A detailed geological map of the area is given in Figure 3.46.

3.2.1: Structures in the Silverton Formation:

Where the Rustenburg Fault passes through the Silverton shale and encompassed sills in the northern part of Area 2 (Appendix), the Fault could only be traced using aerial photographs. Outcrop is very poor, though the River Hex appears to follow the trend of the Fault. Faulting in the Silverton shale could, however, be traced by displaced sills (Appendix). The exact age of these sills is unknown, and may be pre-, syn- or post-Bushveld in age (Cawthorn et al., 1981). Displacement of these sills is therefore a poor indicator of the history of the Fault zone.

At locations 33 and 34, N.E.-trending streams also indicate the presence of an underlying structural weakness. The outcrop of gabbroic sills was found to terminate abruptly at the stream at location 33, indicating that the streams at locations 33 and 34 may occupy a fault line, which has subsequently been displaced by the Rustenburg Fault. However, these two structures need not necessarily be the same fault, and cannot conclusively be used to indicate the displacement of the Rustenburg Fault.

3.2.2: Structures in the Daspoort Formation:

Better outcrop is found where the Fault cuts the Daspoort Formation. Here, the Fault was inferred to diverge, creating a lens of Daspoort sandstone, between two sub-parallel branches of the Rustenburg Fault. There is no evidence for the continuity of the eastern branch of the Rustenburg Fault south of the Daspoort Formation (Appendix and Figures 3.1 and 3.46).

Although outcrop of fault rock in Area 2 is generally rare, a good outcrop can be seen at location 35. This is a dull brown incohesive quartz-based rock, and comprises protocataclasite and cataclasite (as defined by Sibson, 1977) (Figure 3.47). The quartzitic composition of the cataclasite suggests the Daspoort Formation quartzose sandstone as the protolith of this fault rock.

3.2.3: Structures in the Timeball Hill Formation:

3.2.3.1: Folding, faulting and foliation in the Timeball Hill Formation:

At locations 36, 37 and 38, a dull brown rock possessing a well developed planar fabric (S_1) of average orientation 170^0 59^0 W (Figures 3.48 and 3.49) can be found. In thin section this planar fabric resembles slaty cleavage (Figure 3.50), and at locations 37 and 38, this fabric forms an axial planar cleavage in folded shales (Figures 3.51 and 3.52 for two specific examples).

However the cleavage planes were only found in the immediate vicinity of the Fault zone, suggesting that their development are somehow related to Fault movement. The cleavage plane and axial surfaces of the small-scale folding (Figures 3.50 and 3.51) suggest that these structures were imposed as a result of E.-W. compression, the interpretation of which cannot which cannot be reconciled with structural data from the Fault zone in Area 1 (Table 3.1), or with the proposed direction of movement of the Rustenburg Fault (Chapter 4). The orientation of these structures therefore shows that they were unlikely to have been related to the Rustenburg Fault, though the coincidence between the presence of these structures and the projected strike of the Fault zone may suggest that the cleavage is somehow related to development of "mylonitic fabric", especially as in some areas (e.g. location 36) bedding is not preserved in areas of cleavage development. the cause of this planar fabric therefore remains enigmatic.

Commonly, the Timeball Hill Formation rocks along the Fault zone which posses the planar fabric described above, contain quartz veins, often 1-2 m wide and 10-15 m long, orientated parallel to the Fault zone, probably reflecting exploitation of fissility of the planar fabric within the Fault zone by circulating fluids. Close to location 37, there is evidence for small prospecting pits, which have been dug into the rock to expose the side walls of these veins. There is no evidence for mineralisation within these veins, as shown by the abandonment of these prospecting pits at an early stage.

3.2.3.2: Thrust faulting in the Timeball Hill Formation:

At location 39 in the road cutting on the R509 between Magaliesberg and Koster, where a railway bridge crosses the road (Appendix and Figure 3.46), a good outcrop of tectonised Timeball Hill shales can be found. Along the length of the road cutting, two distinct layers are visible, separated by a 10 cm-wide undulating, sub-horizontal zone filled with fault gouge. The lower level, beneath the gouge, contains an almost constant bedding surface (S_0) of 263^0 31^0S in less disturbed areas at the centre of the cutting. This shale is cross-cut by a set of quartz veins of orientation $357^0 57^0$ E (Figure 3.53).

This relatively undisturbed geometric relationship is in contrast to the layer above the fault gouge, which shows a much greater degree of tectonic disturbance, and appears to have been thrusted over the lower layer, with vergence to the S.W. (Figure 3.53). In the upper layer, on the northern side of the cutting, west of the railway bridge, a wide range in bedding orientation were recorded (Figure 3.54), though only occasionally are folds evident, due to the complexity of the deformation. However, when plotted stereographically, the orientation of collected bedding data suggests that folding is imposed along a fold axis with a plunge direction of $22^0 \rightarrow 110^0$ (Figure 3.54). This fold axis generally corresponds with the plunges of axial traces recorded elsewhere in the upper layer of the outcrop (Figure 3.54).

The orientation of the fold axis suggest that the thrusting shown in Figure 3.53 has occurred as a result of N.N.E.- S.S.W. directed compression (perpendicular to the strike of the fold axis). However, compression in this direction cannot be reconciled with the compression required to produce the proposed displacement on the Rustenburg Fault (Chapter 4), and it seems, therefore

that thrusting from this direction may be related to F_1 folding (Section 3.1.2.3) and may, perhaps, also be related to bedding-parallel thrusting in the Magaliesberg Formation (Section 3.1.3.4).

3.3: A summary of structural geological features inherent to the Rustenburg Fault zone:

The Rustenburg Fault zone and its adjacent areas, contain a variety of structures rarely encountered elsewhere in Pretoria Group strata around the edge of the Bushveld Complex. The strike of the Fault zone through the Magaliesberg Formation quartzite can be traced by the presence of Fault quartzite, a generally massive lithology which is otherwise difficult to distinguish from Magaliesberg quartzite. Later faults cross-cutting the Fault zone can be traced by the resultant displacement of the Fault quartzite.

The adjacent areas to the Fault zone are characterised by interference folding, resulting from N.E.-S.W. compression, followed by S.E.-N.W. compression. These deformational events may also have caused thrust faulting in the vicinity of Fault zone.

GEOLOGICAL MAP OF THE RUSTENBURG FAULT

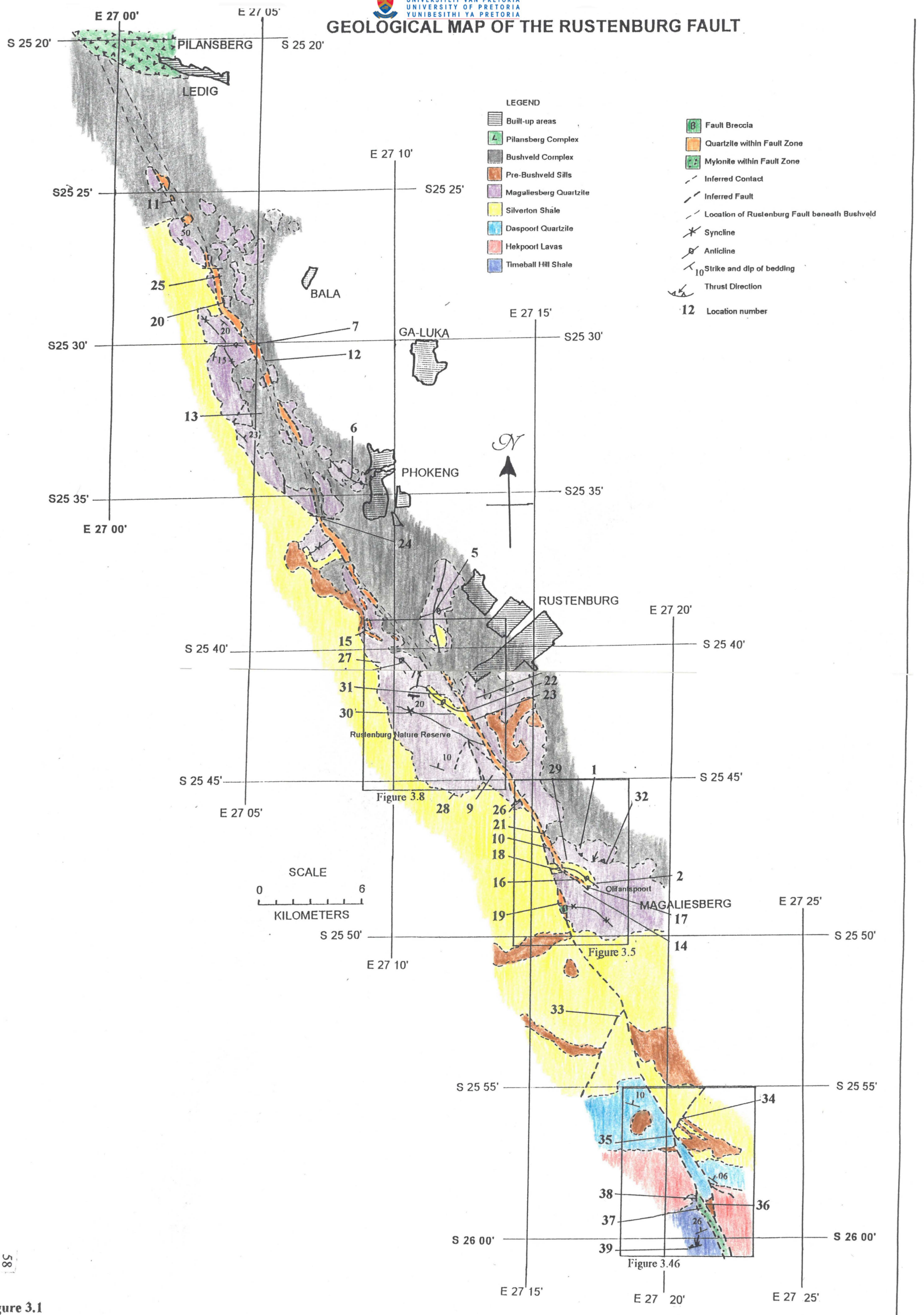

Figure 3.1

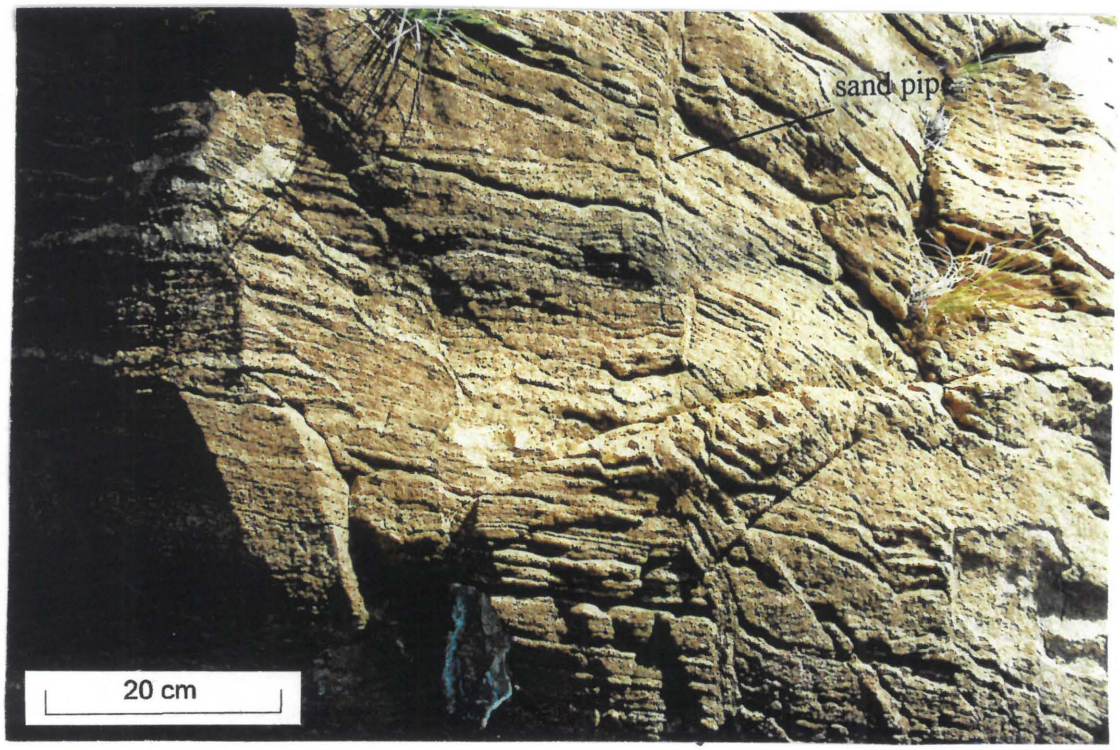

Figure 3.2: Soft-sedimentary deformation in the Magaliesberg Formation at location 1, showing disrupted bedding and a 1 cm wide sand pipe, probably caused by flow of water from high to low pressure areas during sediment loading.

Figure 3.3: The Olifantspoort anticline, showing upright fold axial plane and symmetrical, open folding. Photograph is taken looking S.E., to where the hinge zone of the anticline has not been eroded.

a

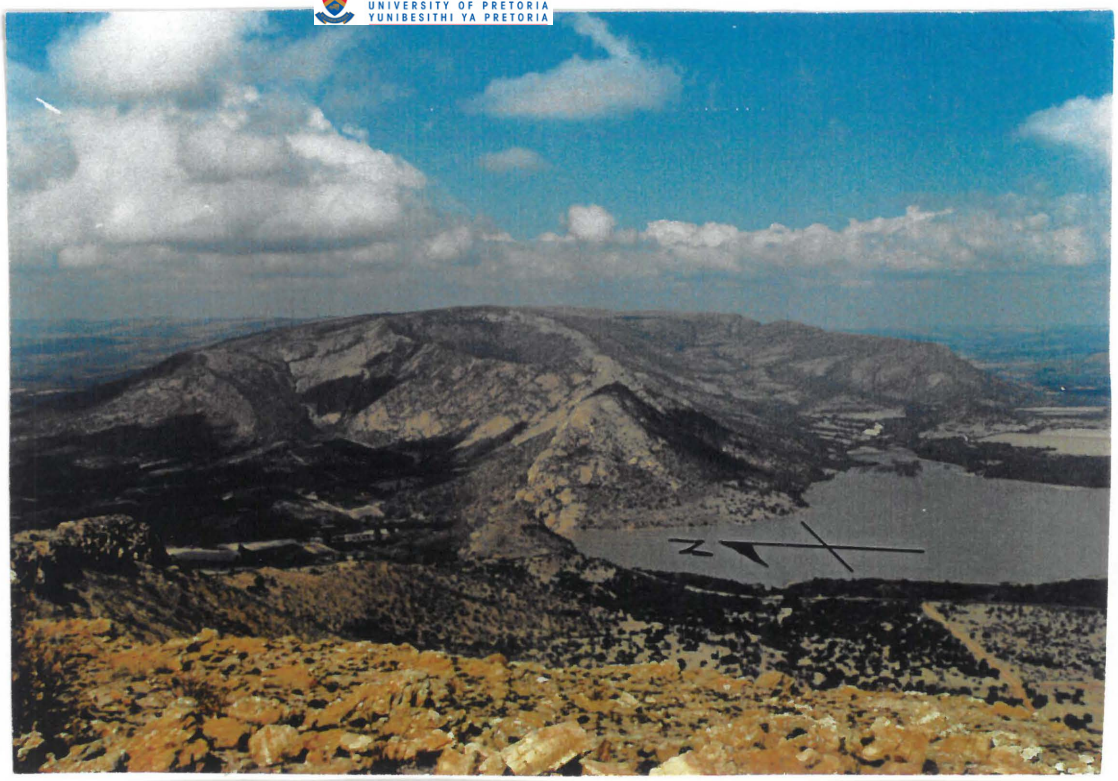

b

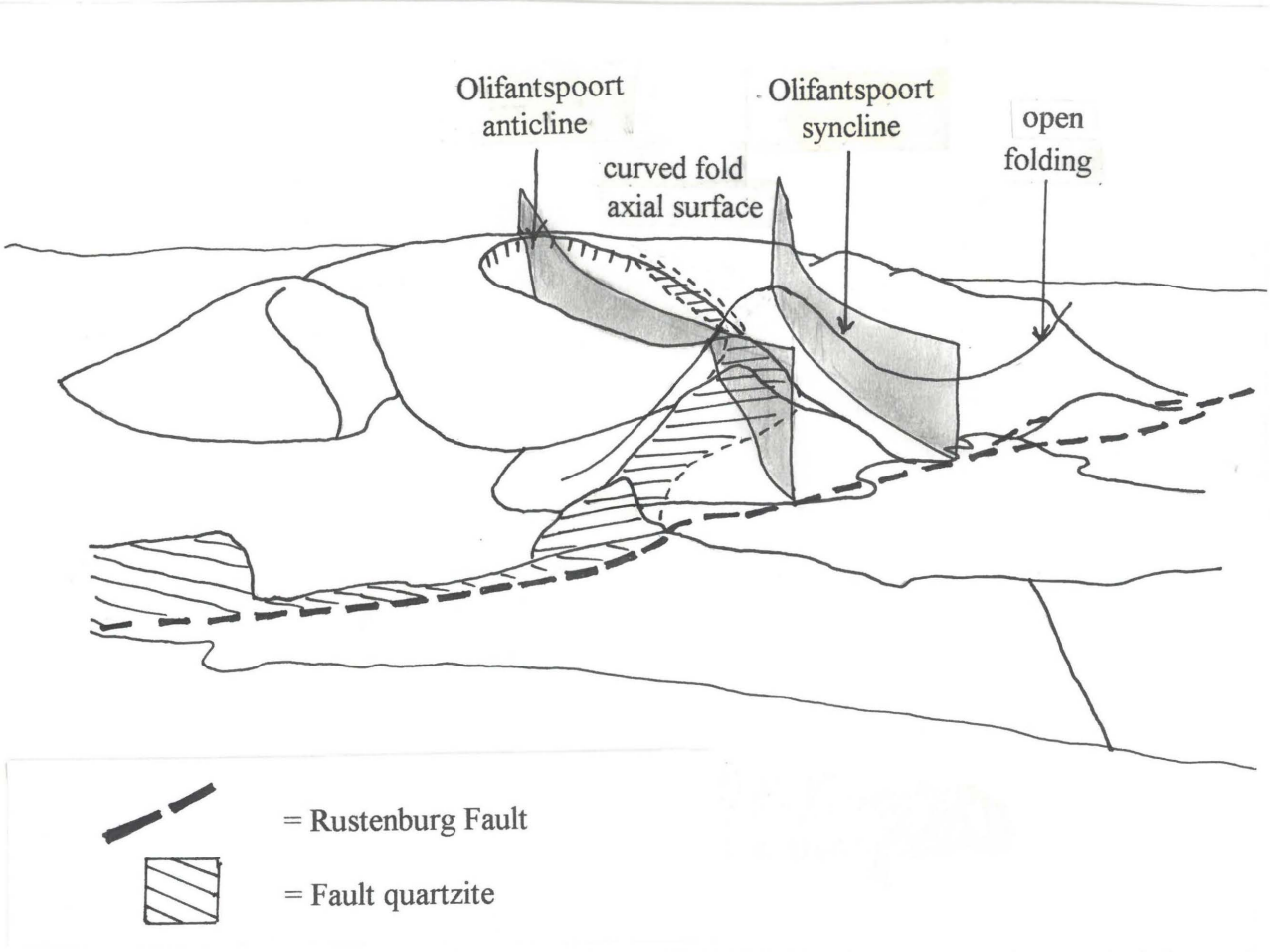

Figure 3.4: Folding at Olifantspoort. Photograph (a) is taken looking S.E., with Olifantsnek dam in the foreground. The anticline is to the north, syncline to the south. The Rustenburg Fault crosses the area between the dam and Olifantspoort (b). b. shows the inferred shape of the folding, with upright, curved fold axial surfaces and open folding.

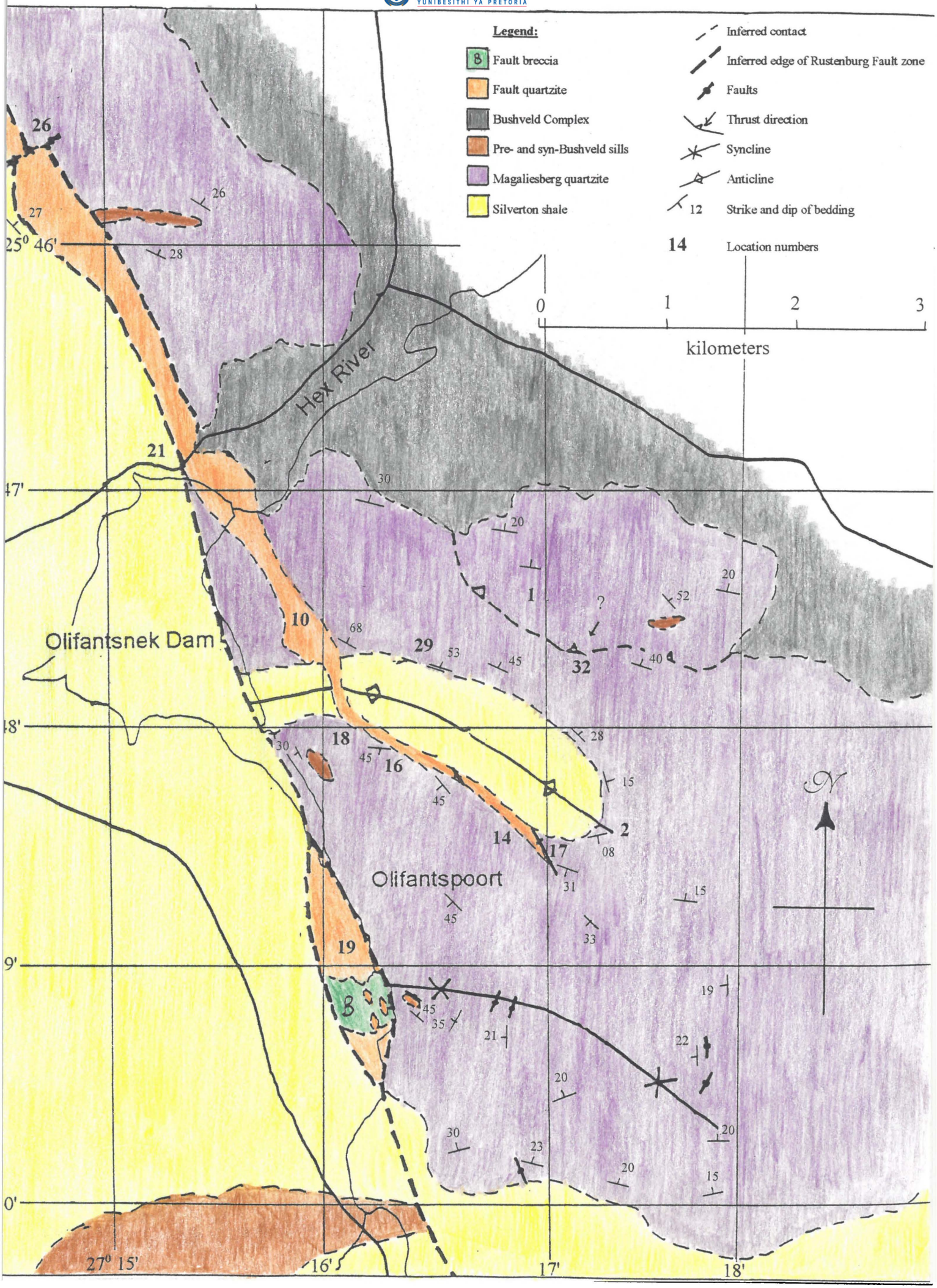

igure 3.5: Detailed geological map of the Olifantspoort area, showing curved fold axial races, and tightened folding on the anticline

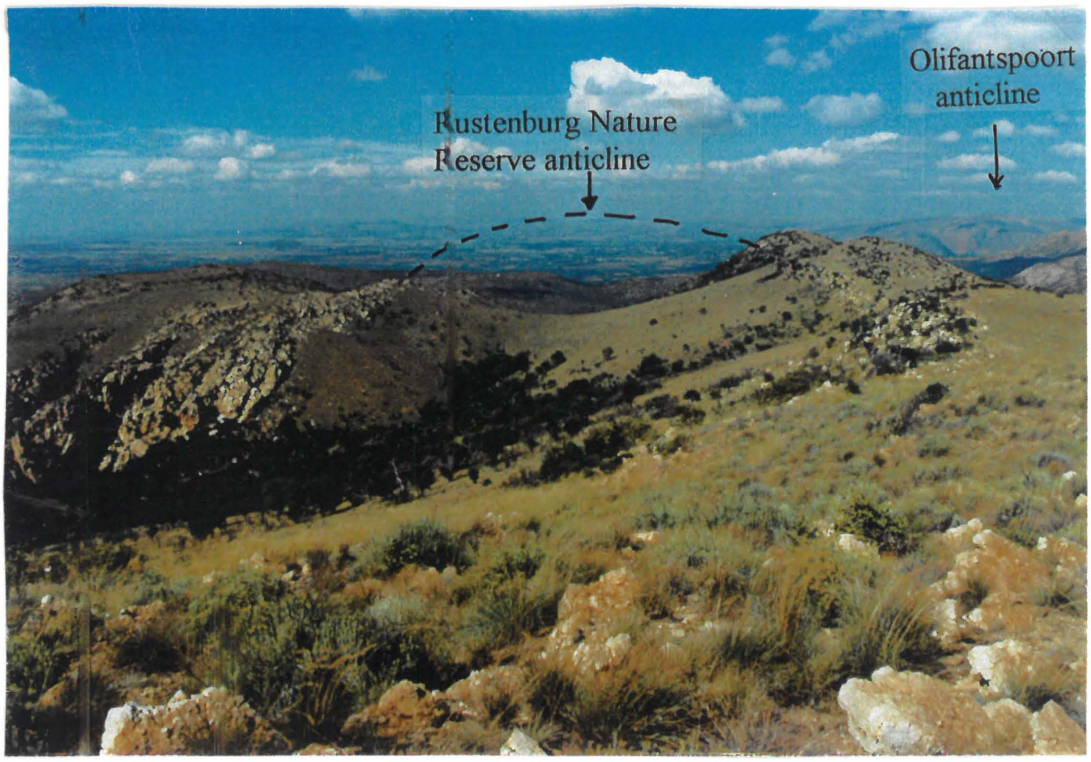

Figure 3.6: The Rustenburg Nature Reserve anticline, showing open folding with an approximately upright fold axial surface. The photograph is taken looking eastwards. Note Olifantspoort anticline just visible in the distance to the S.E..

Figure 3:7: Parasitic open folds on the southern limb of the Rustenburg Nature Reserve syncline. The fold axial trace trends 160^0 (dotted line), which is of similar trend to the main fold axis at Rustenburg Nature Reserve. The open shape of the folding is indicated by the solid line.

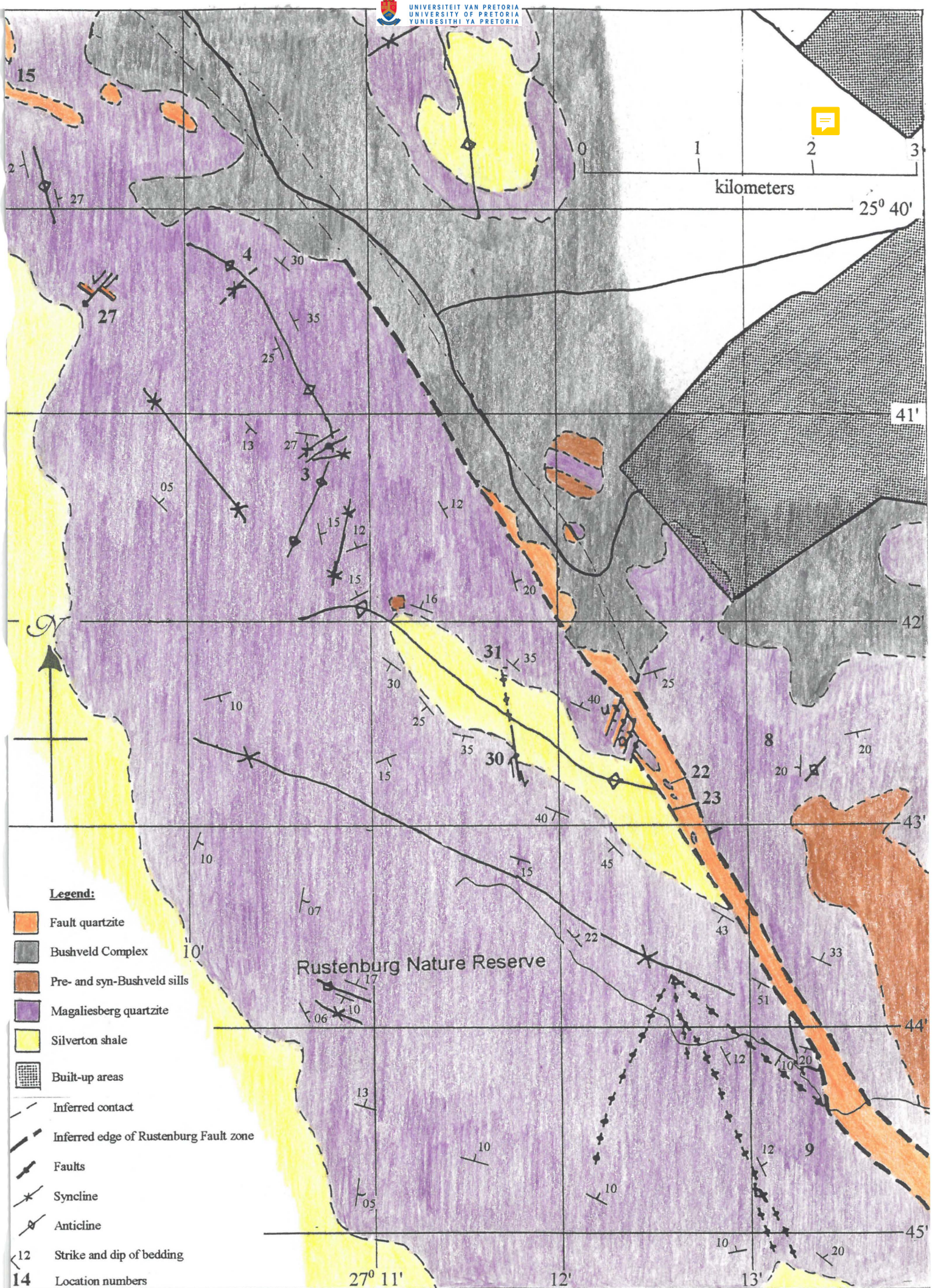

Figure 3.8: Detailed geological map of the Rustenburg Nature Reserve area, showing curved fold axial traces, and tightened folding on the anticline

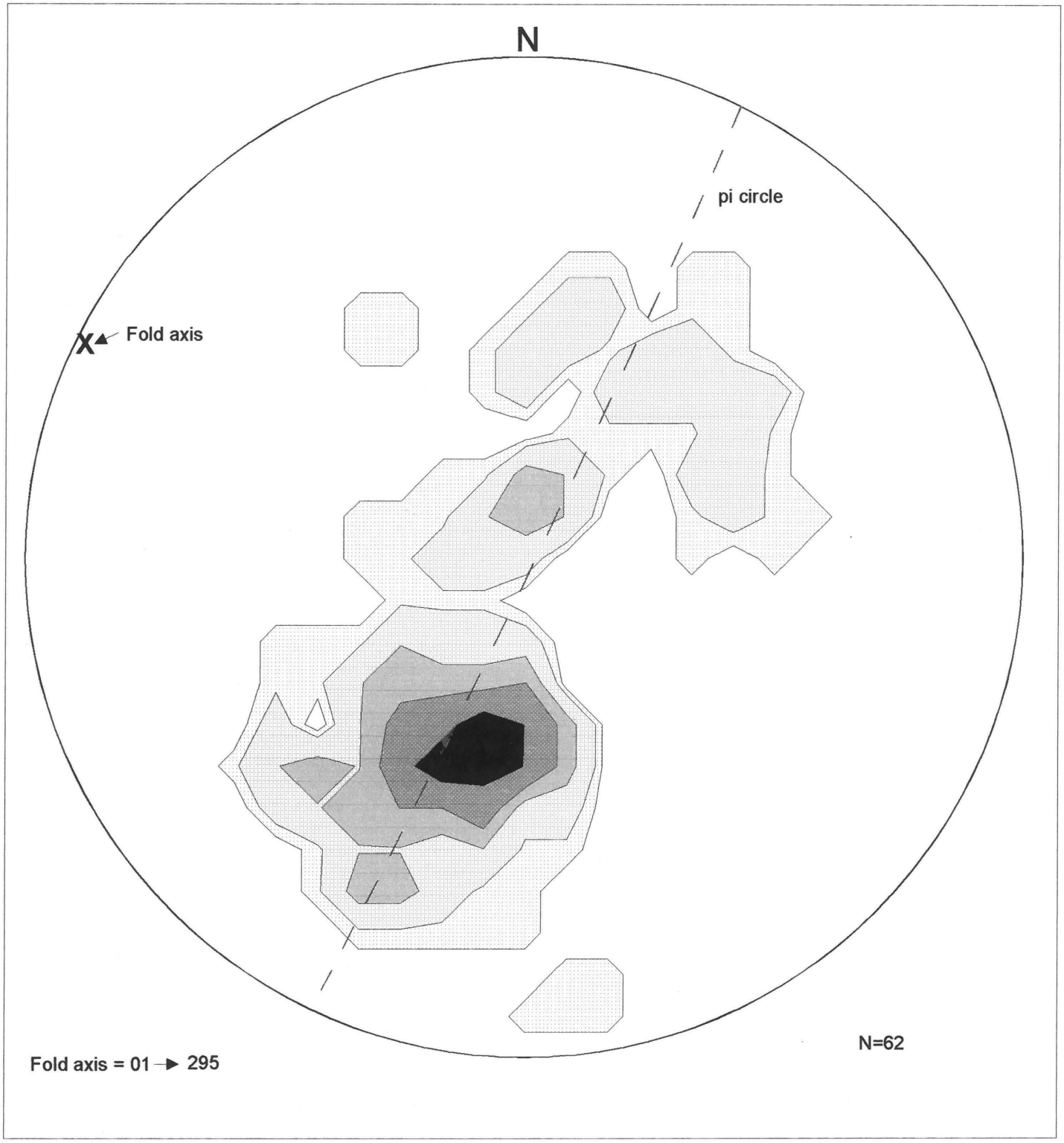

Figure 3.9: Stereographic projection of the density distribution of poles to bedding in the Olifantspoort anticline. Fold axis plunges 01→ 295.

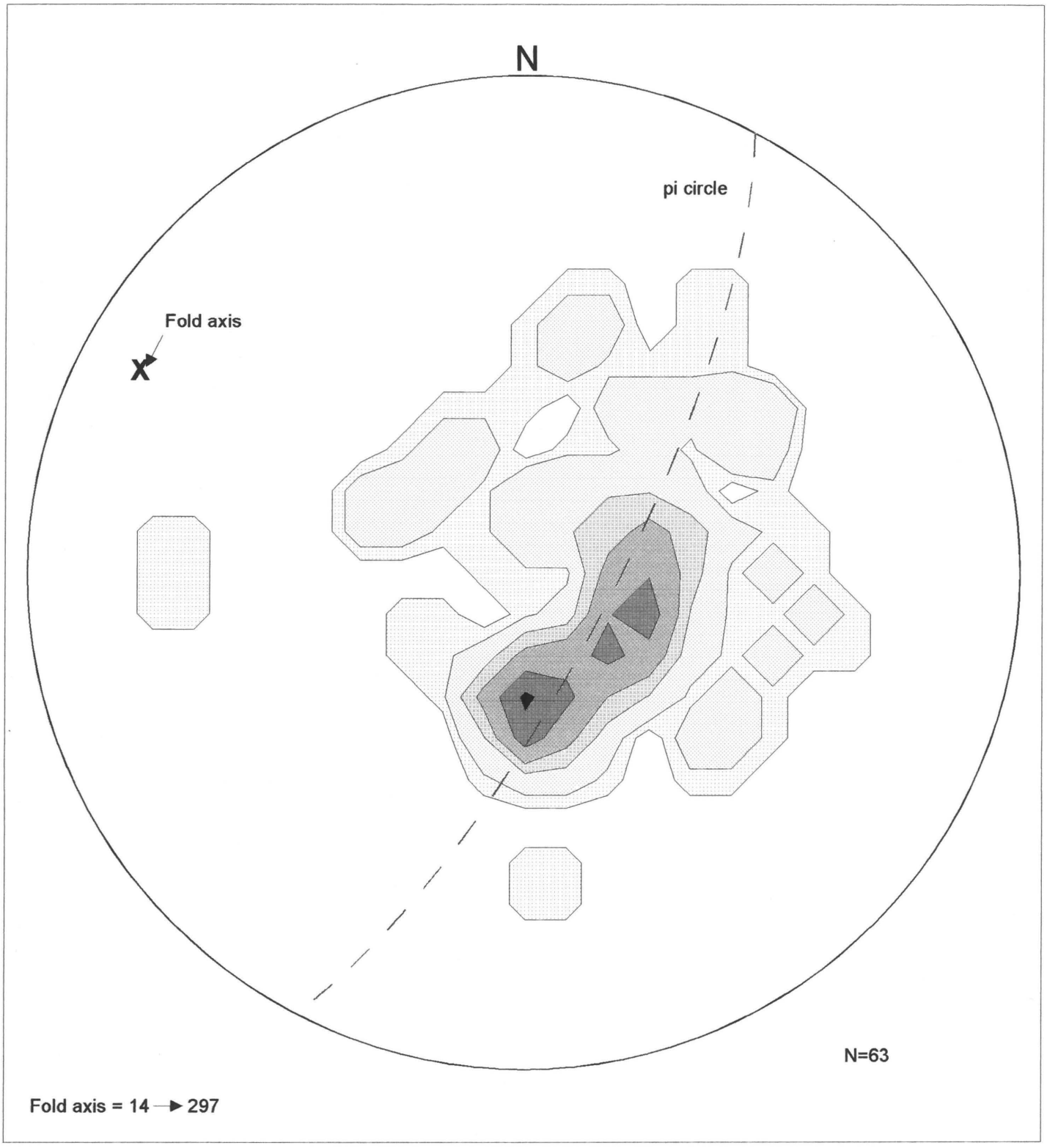

Figure 3.10: Stereographic Projection of the density distribution of poles to bedding in the Olifantspoort syncline. Fold axis plunges 14 → 297.

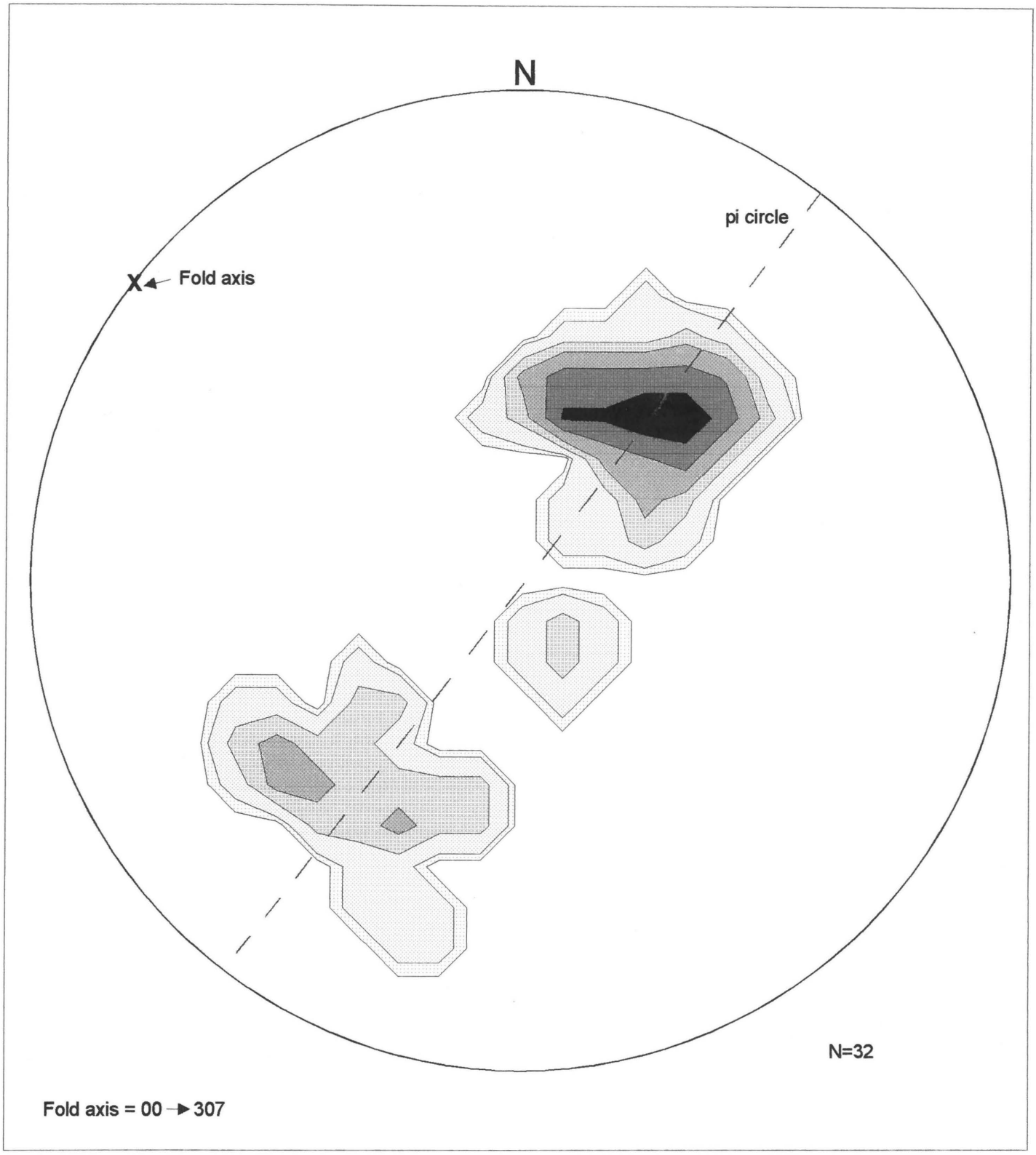

Figure 3.11: Stereographic projection of the density distribution of poles to bedding in the Rustenburg Nature Reserve anticline. Fold axis plunges 00→307.

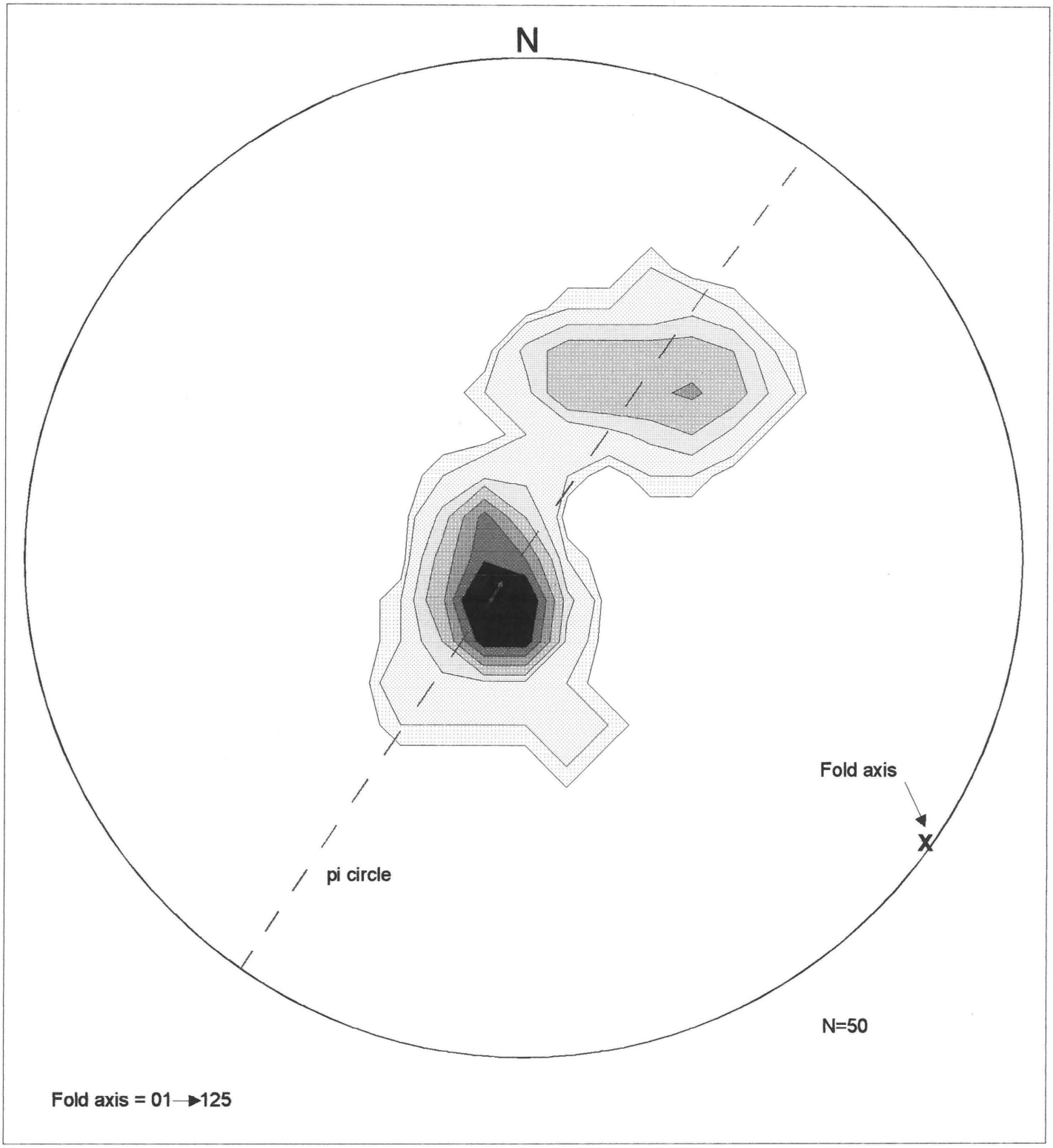

Figure 3.12: Stereographic projection of the density distribtution of poles to bedding in the Rustenburg Nature Reserve syncline. Fold axis plunges 01 → 125.

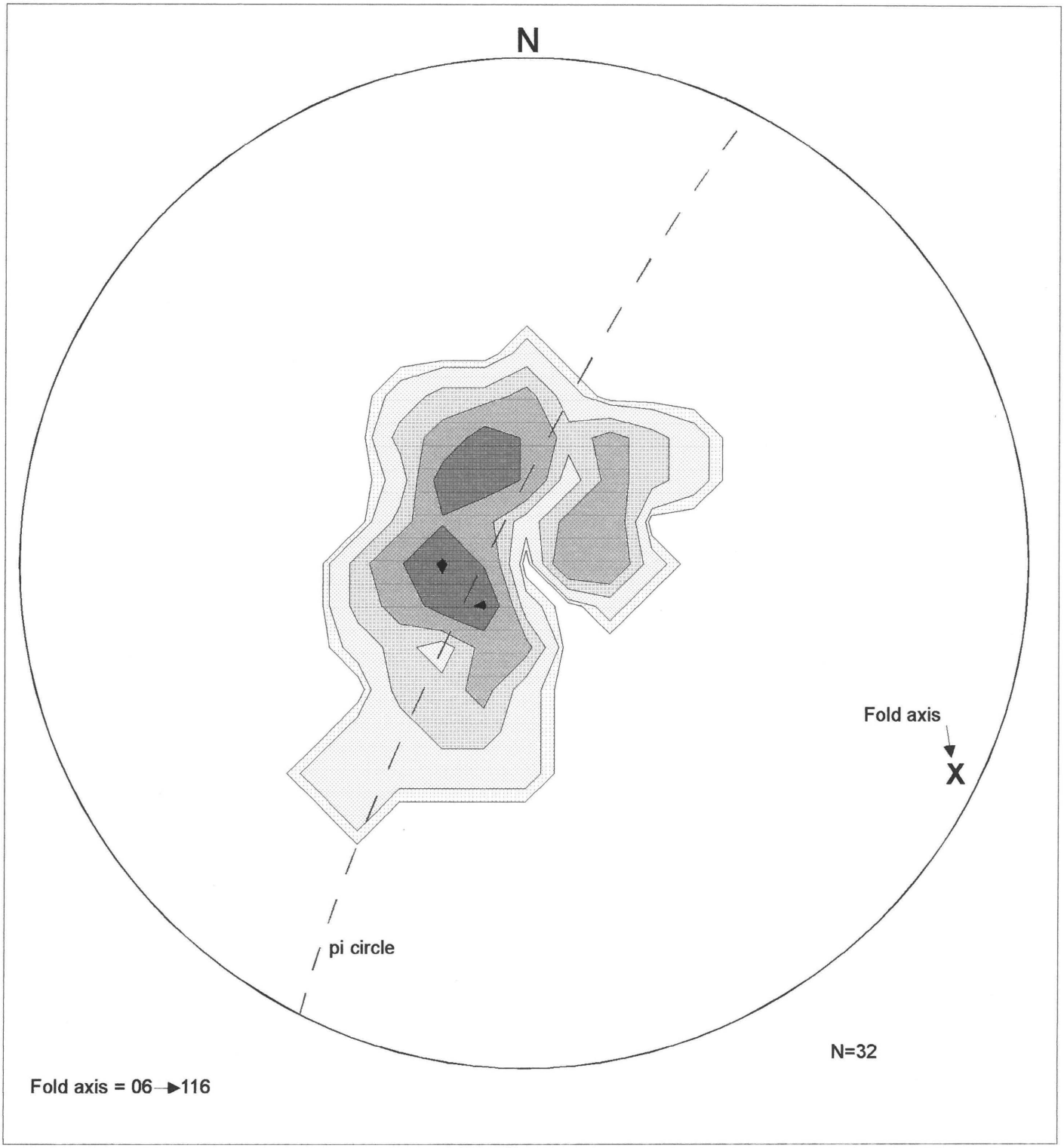

Figure 3.13: Stereographic projection of the density distribution of poles to bedding in the area east of the Rustenburg Fault (location 8) in Rustenburg Nature Reserve. Fold axis plunges 06→116.

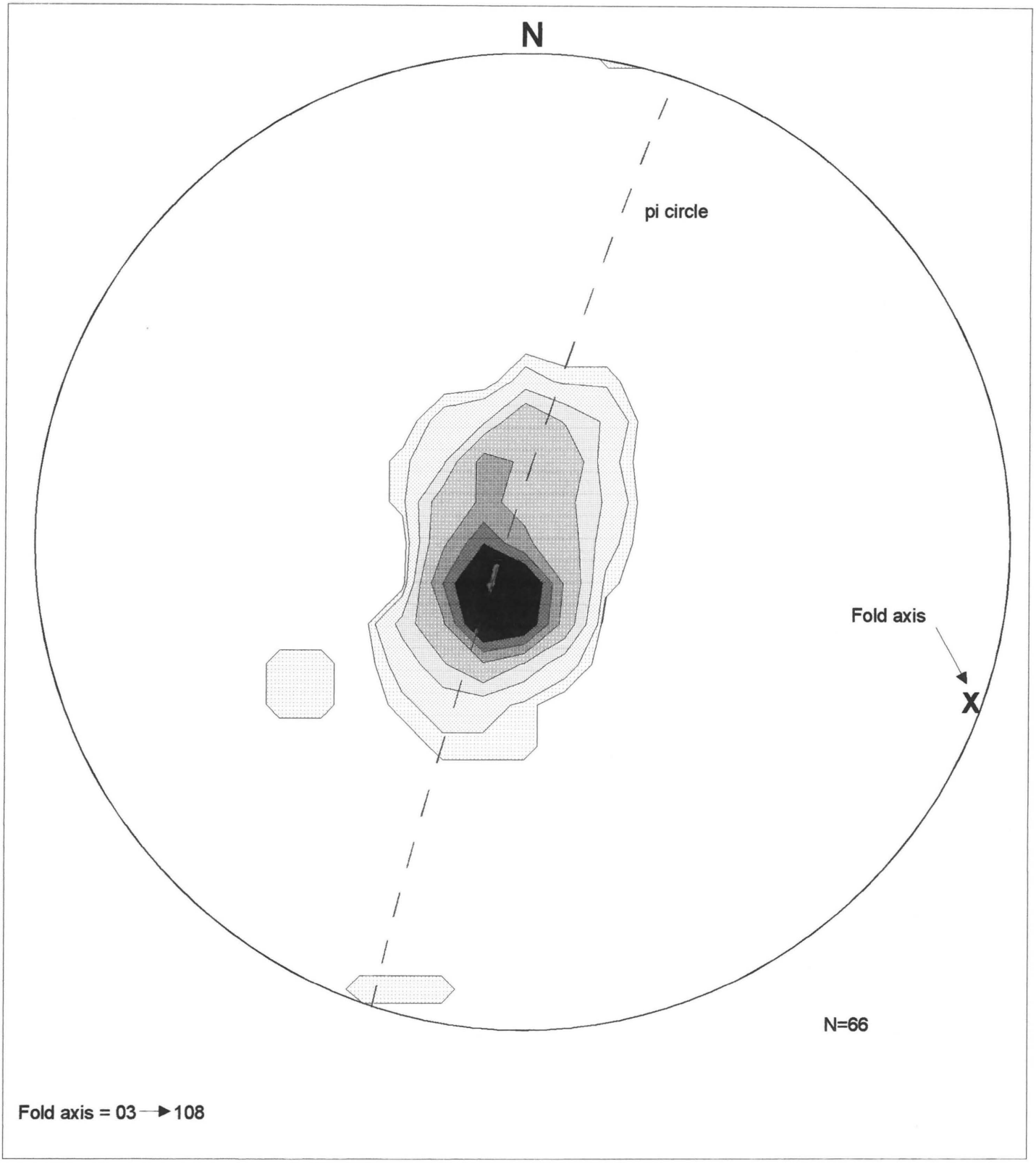

Figure 3.14: Stereographic projection of the density distribution of poles to bedding in the Magaliesberg quartzite in the partially fault-bounded area between Olifantsnek dam and the synclinal fold axis (location 9) in Rustenburg Nature Reserve.
Fold axis plunges 03→108.

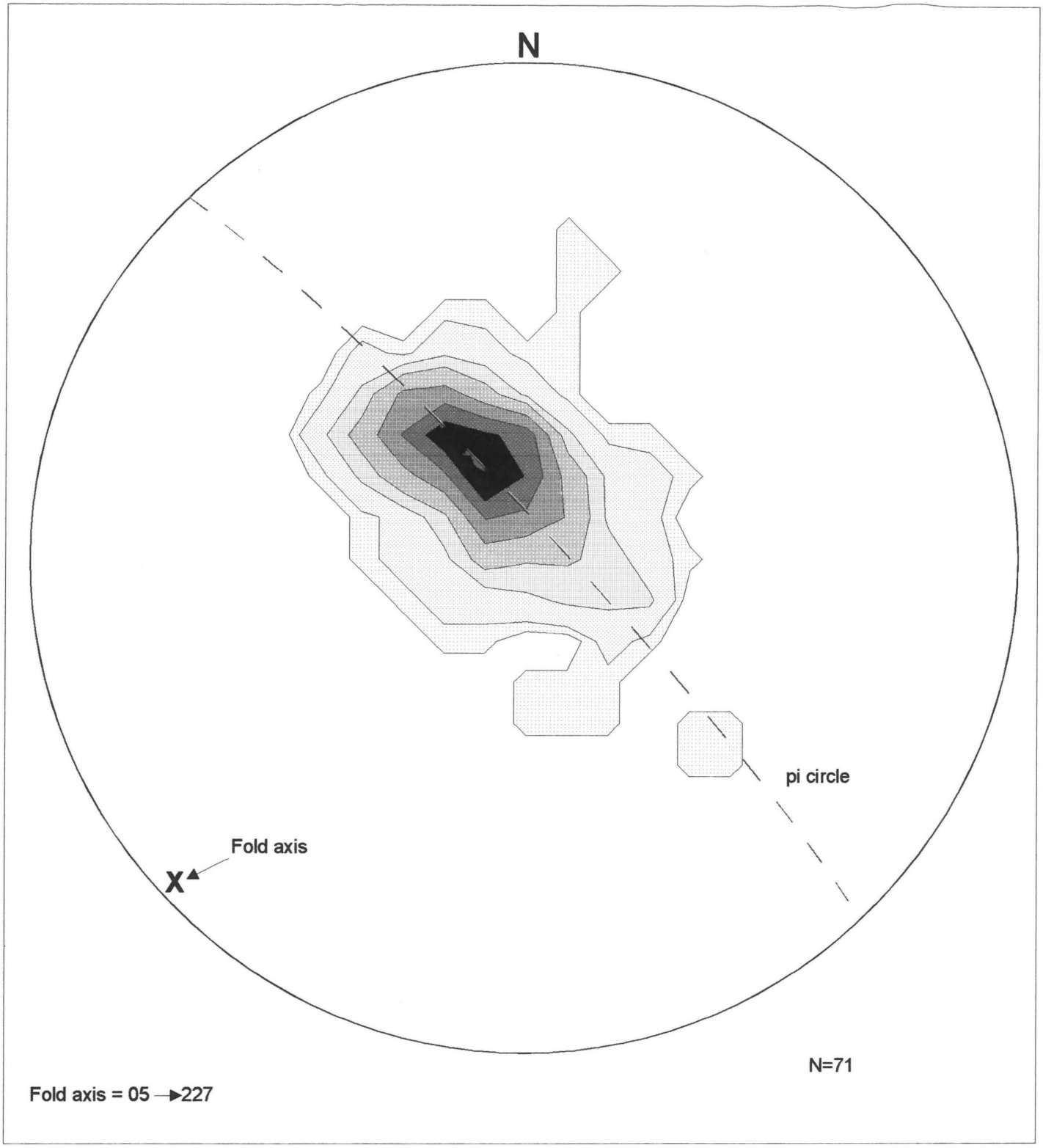

Figure 3.15: Stereographic projection of the density distribution of poles to bedding in the Magaliesberg quartzite in the area from Phokeng to Pilanesberg, west of the Rustenburg Fault. Fold axis plunges 05→227.

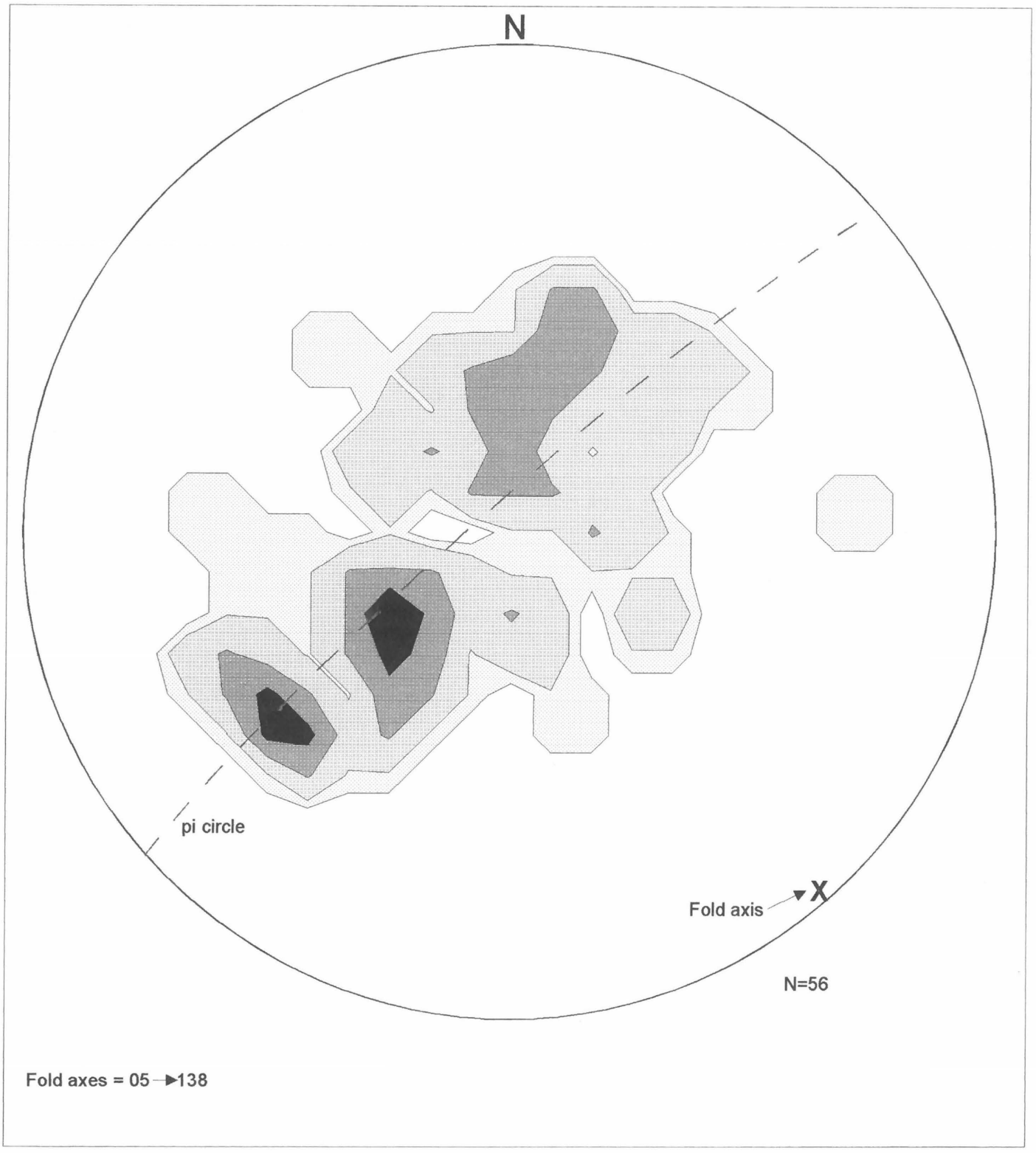

Figure 3.16: Stereographic projection of the density distribution of poles to bedding in the Magaliesberg quartzite in the area from Phokeng to Pilanesberg, east of the Rustenburg Fault, showing that variable bedding orientation may have resulted from interference folding around two fold axes.

DATA SOURCE	FOLD SET 1 (F_1)	FOLD SET 2 (F_2)
Trend of axial traces presented on maps	113, 123, 130, 135, 115, 140	30, 30, 55, 45, 45, 55, 65, 70, 70, 90
Trend of fold axes presented on stereographic projections	115, 117, 127, 125, 116, 108, 138	47, 48
Average	**123^0**	**65^0**
Inferred maximum compressive direction (σ_1)	**033^0-213^0**	**155^0 -335^0**

Table 3.1: Summary of the trend of fold axial traces shown on maps, and the fold axes presented on the stereographic projections. The average trend for each fold set, and the maximum compressive direction (σ_1) required to produce that fold set is also given.

Figure 3.17: a.: Down-plunge projection of the Olifantspoort folds. The variable nature of the dips around vertical results from the curved fold axial surfaces.

b.: Interpretation of the down-plunge projection, showing concentric folding in a relatively tightened anticline, with open folding on the syncline. Parasitic folds are inferred on the southern limb of the anticline.

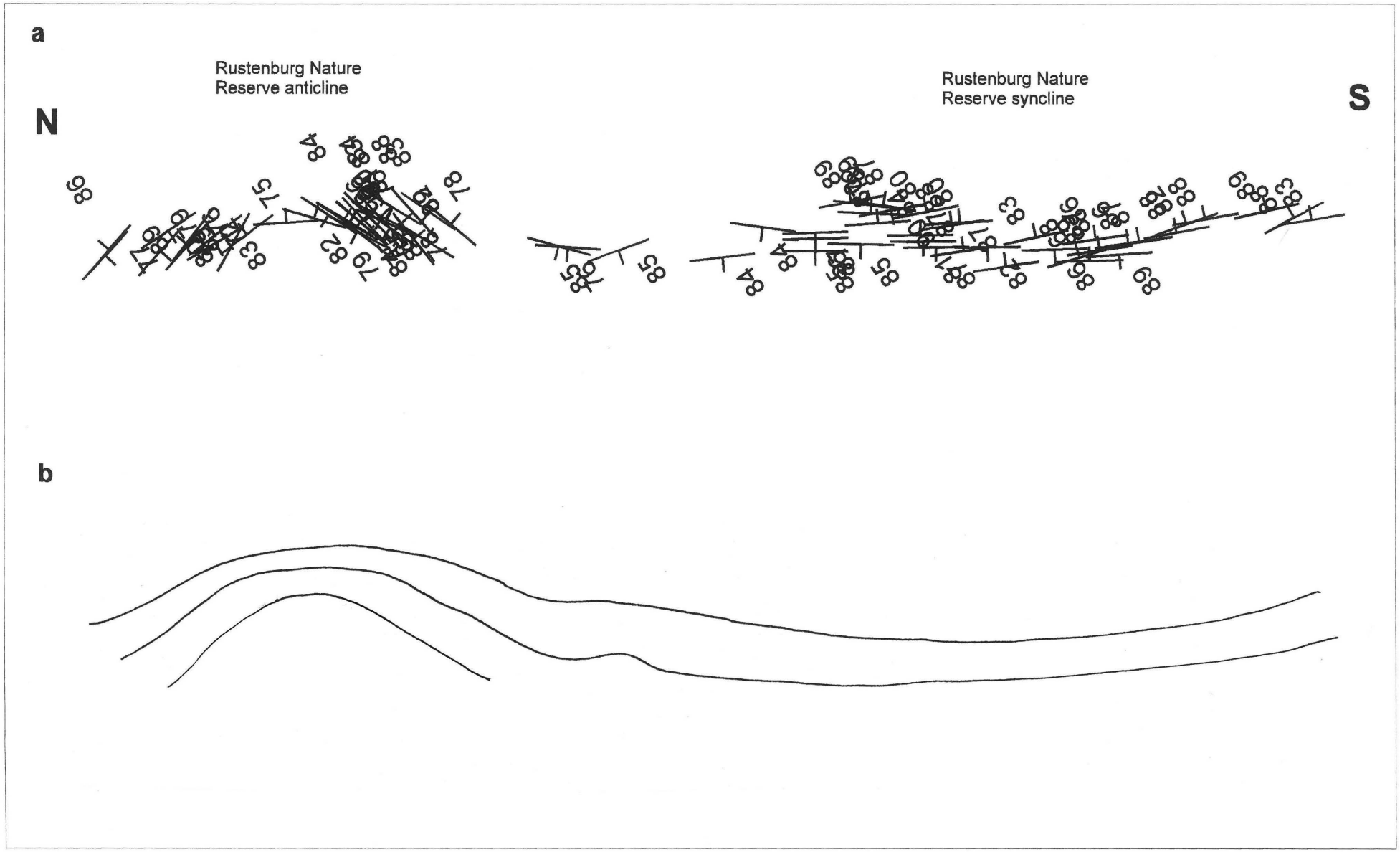

Figure 3.18: a.: Down-plunge projection of the Rustenburg Nature Reserve folds. The variable nature of the dips around vertical results from the curved fold axial surfaces.

b.: Interpretation of the down-plunge projection, showing concentric folding in a relatively tightened anticline, with open folding on the syncline.

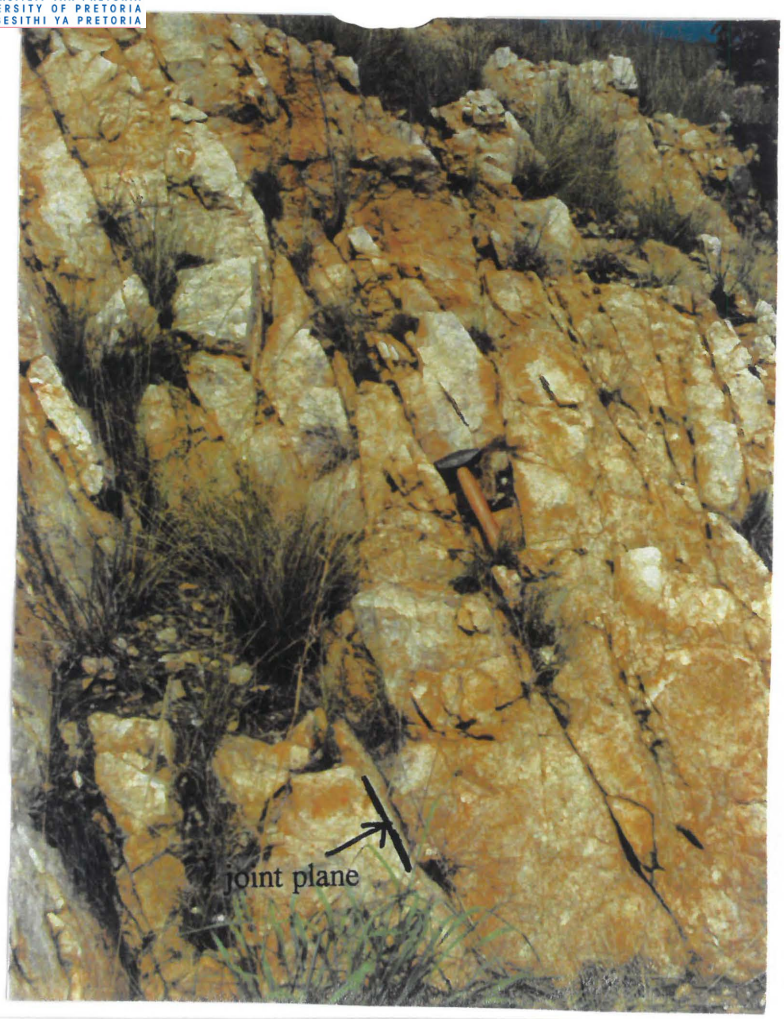

Figure 3.19: Fault quartzite at location 10, showing apparently massive character, and a joint plane of 132^0 70^0 S.W..

Figure 3.20: The edge of the Rustenburg Fault Zone at location 9. Bedded Magaliesberg quartzite to the west (right hand side) is cut by non-bedded Fault quartzite with whiter appearance when weathered.

Figure 3.21: Rustenburg Fault Zone at location 10. Bedded Magaliesberg quartzite to the east (left hand side) is cut by a small cliff of Fault quartzite of whiter appearence when weathered.

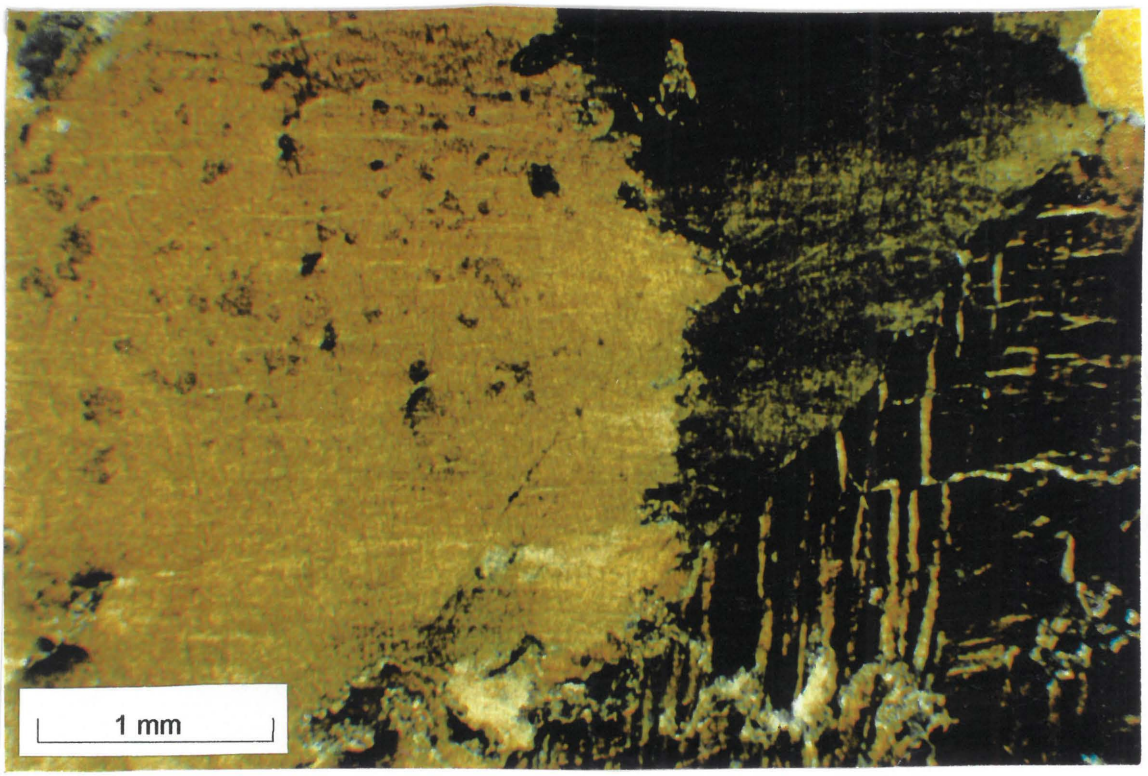

Figure 3.22: Photomicrograph of Fault quartzite from location 12 showing undulose extinction and deformation lamellae (at bottom right) and very large crystal size (about 5mm).

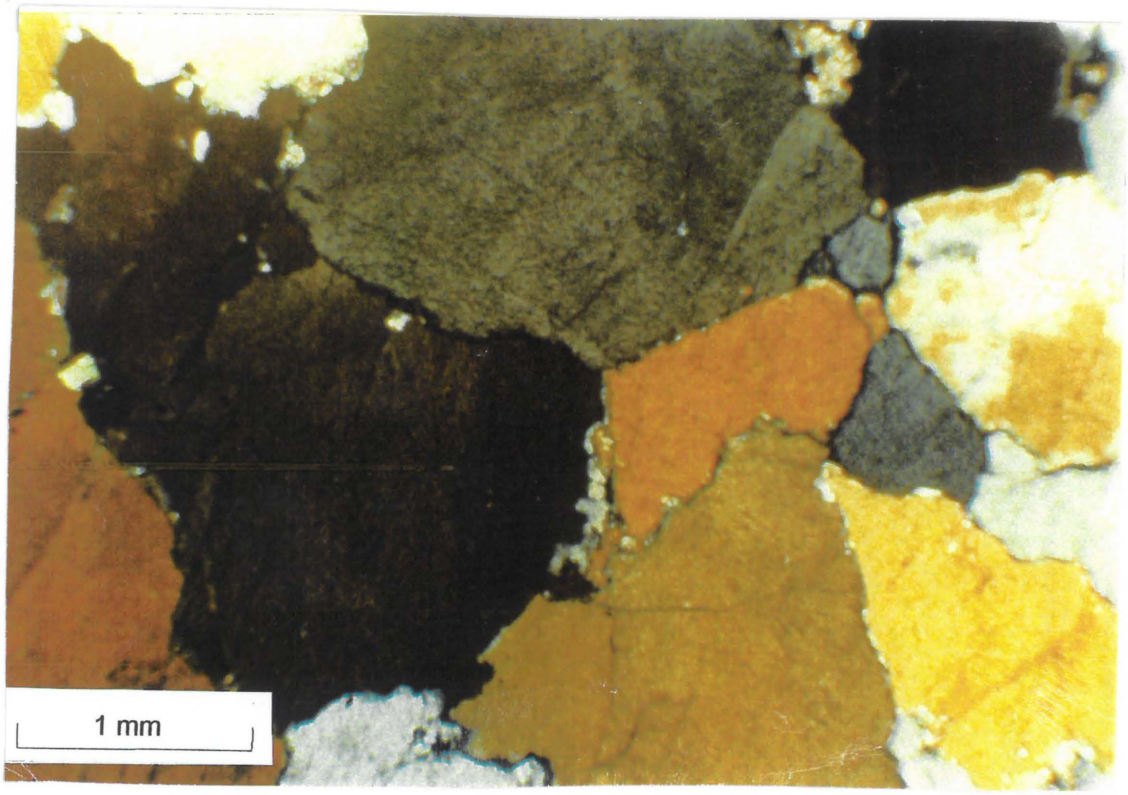

Figure 3.23: Photomicrograph of Magaliesberg quartzite at location 13, showing an average crystal size of 2mm, slight undulose extinction and pressure solution at grain boundaries.

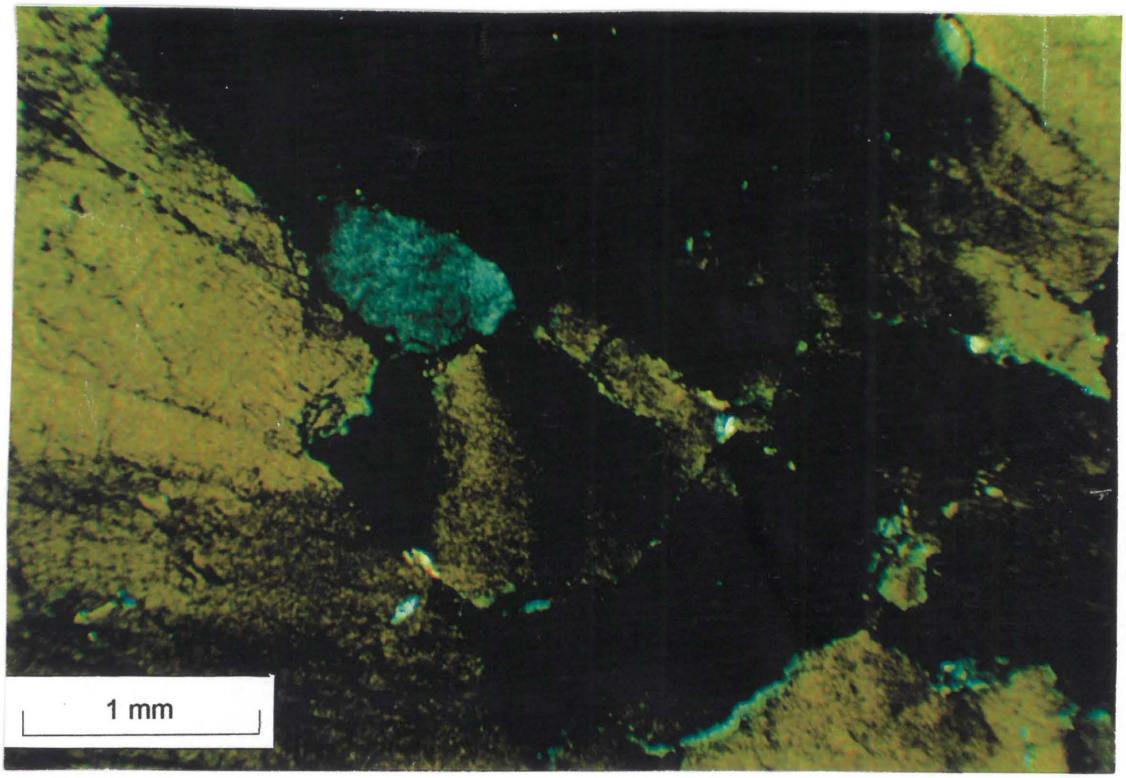

Figure 3.24: Photomicrograph showing undulose extinction in Fault quartzite from location 14.

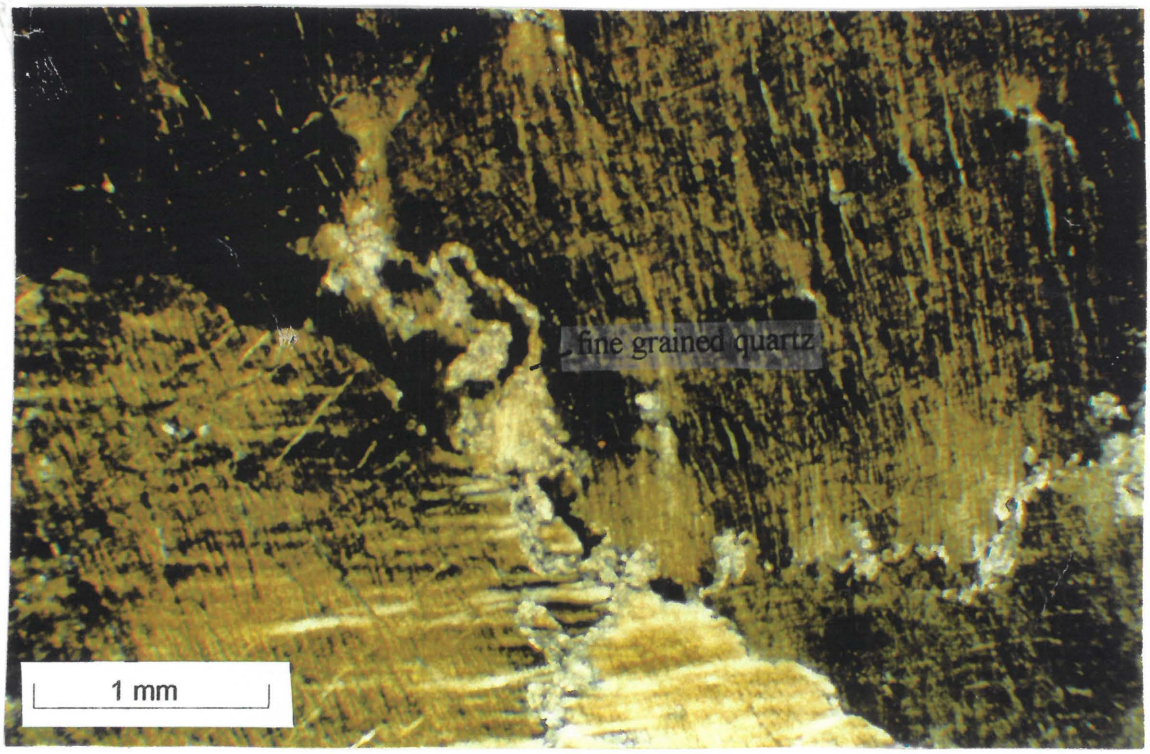

Figure 3.25: Photomicrograph showing deformation lamellae in Fault quartzite from location 12. Note that all crystals possess the same type of deformation within each photomicrograph (also figure 3.24). Extremely fine-grained quartz can be seen along the large crystal boundaries.

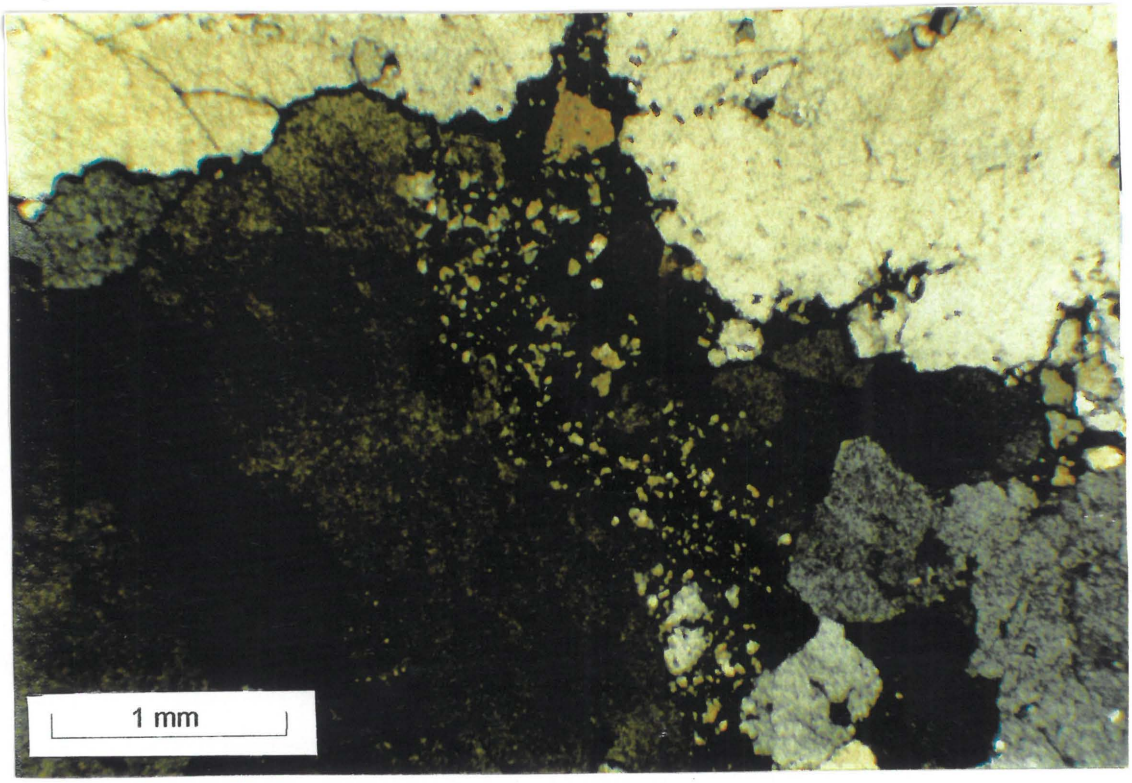

Figure 3.26: Photomicrograph from location 15, showing fine-grained quartz crystals within Fault quartzite which have failed to be recrystallised.

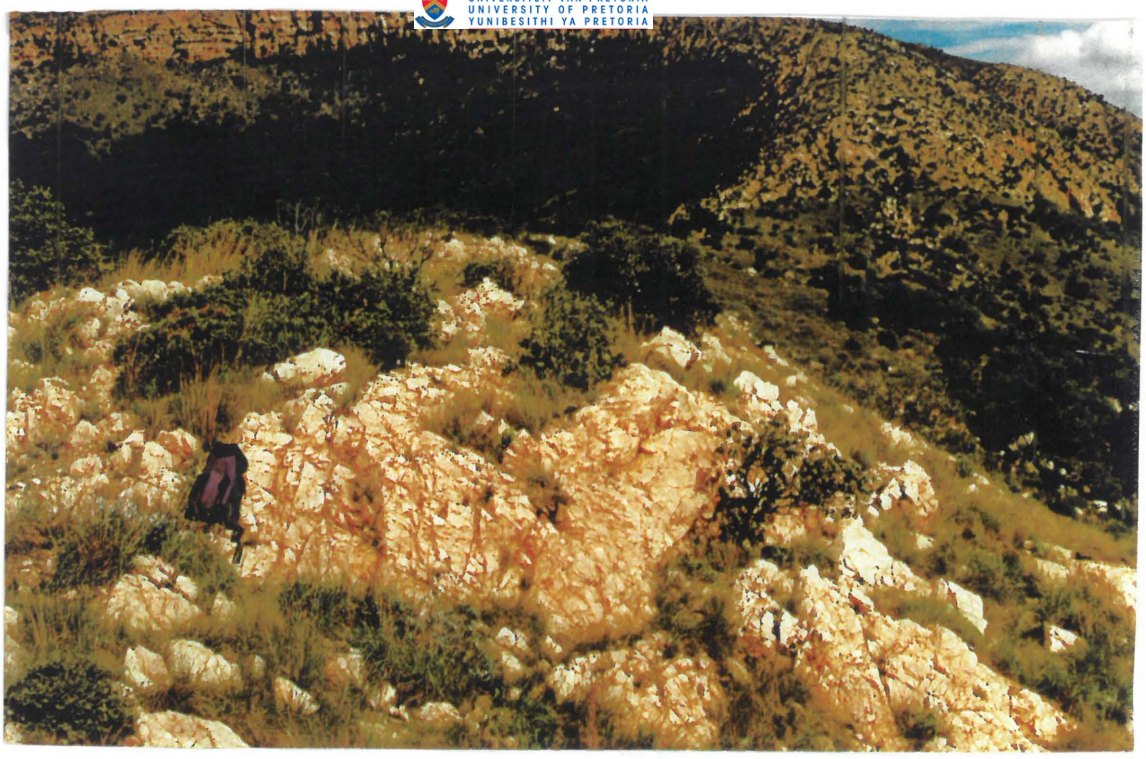

Figure 3.27: Location 16 at Olifantspoort. White Fault quartzite can be seen in the foreground, in contrast to the reddish Magaliesberg quartzites of the Olifantspoort anticline behind. Note the visible, but poorly defined, relict bedding planes in the 'Fault quartzite' which match the geometry of the antiform, indicating no movement of the Fault in this area, despite the diagnostic lithology.

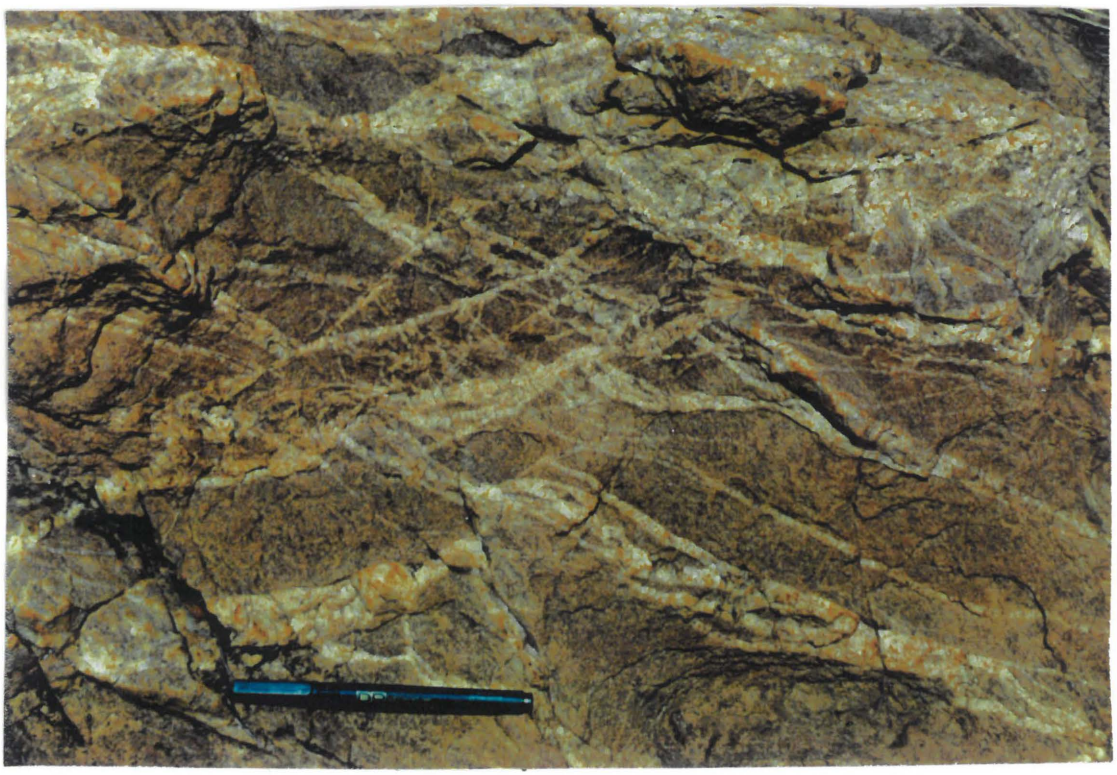

Figure 3.28: Veins cross cutting Fault quartzite at location 12. The haematite staining is untypical of Fault quartzite. Note that at least two sets of veins are present (from top right to bottom left, and top left to bottom right). Pen is 13 cm long.

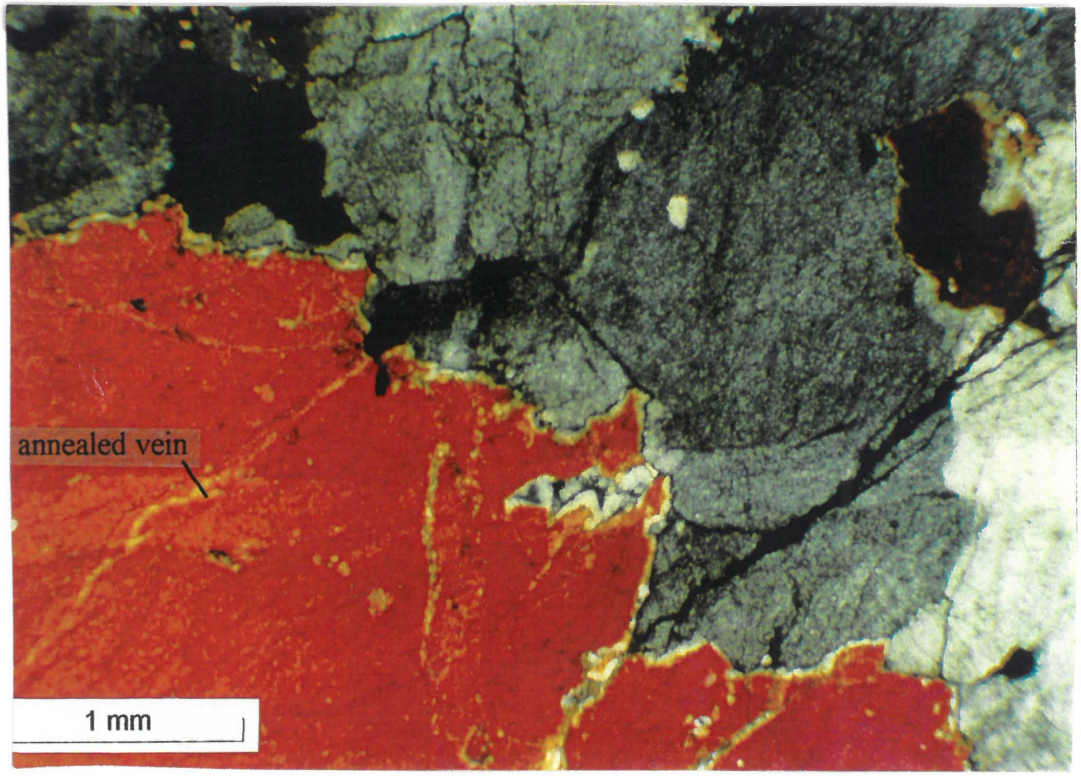

Figure 3.29: Photomicrograph from location 12, showing annealed veins grown in sub-optical continuity across quartz in crystals in Fault quartzite (thick section).

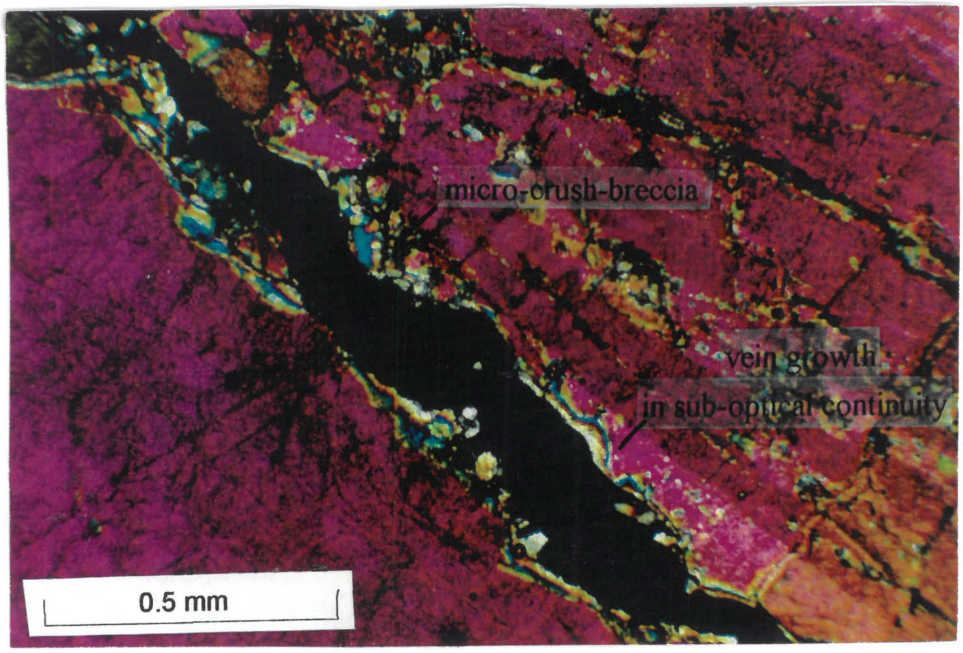

Figure 3.30: Photomicrograph showing annealing halted in progress at location 17. Vein growth in sub-optical continuity is occurring across a micro-fault filled with a micro-crush-breccia (as defined by Sibson, 1977) (thick section).

Figure 3.31: Faulting of Fault quartzite at location 17. Note that the 'crush breccia' left of the compass has been welded back into a cohesive rock. Faulting has occurred along a trend of 150^0 (compass is orientated N.-S.). Compass is 8 cm wide.

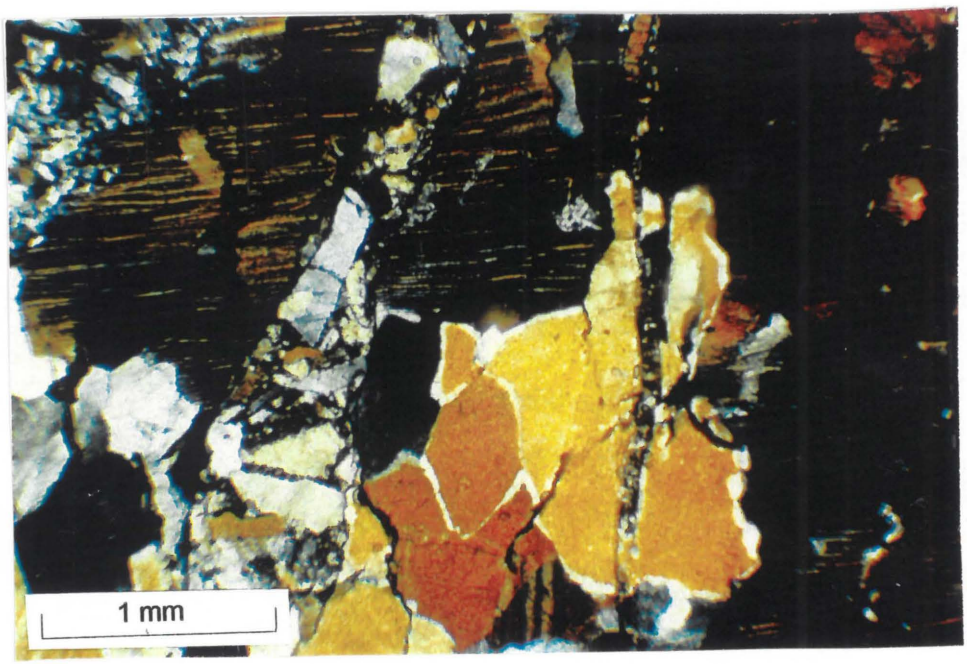

Figure 3.32: Photomicrograph showing brecciation of Fault quartzite (from location 19).

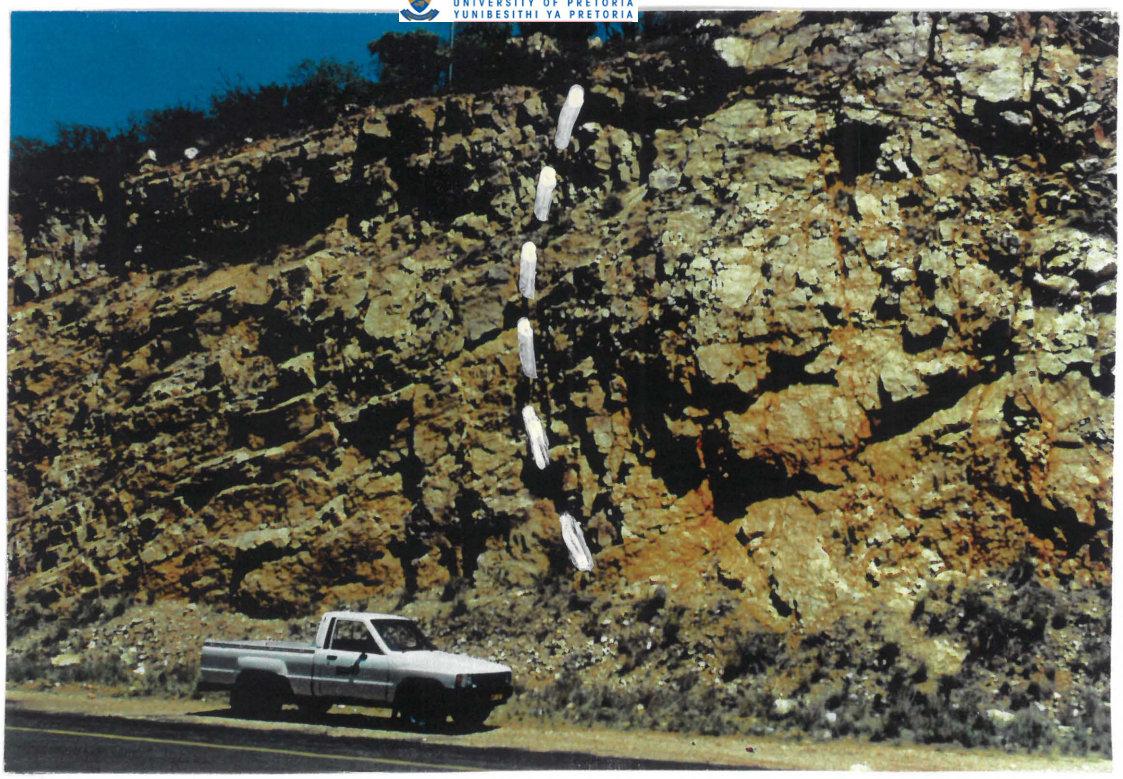

Figure 3.33: Rustenburg Fault zone at location 20. Photograph is taken looking southwards. A 20m diameter block of Magaliesberg quartzite (note bedding planes on the left) is enclosed within a matrix of Fault quartzite to the right. The edge of the Magaliesberg block is marked by a dashed white line. Note the intense jointing at the interface between these two lithologies (also Figure 3.34).

Figure 3.34: Strongly jointed zone, marked by dashed black lines, at the interface between lenses of Magaliesberg Formation quartzite and Fault quartzite in the Rustenburg Fault zone at location 20. Photograph is taken looking southwards.

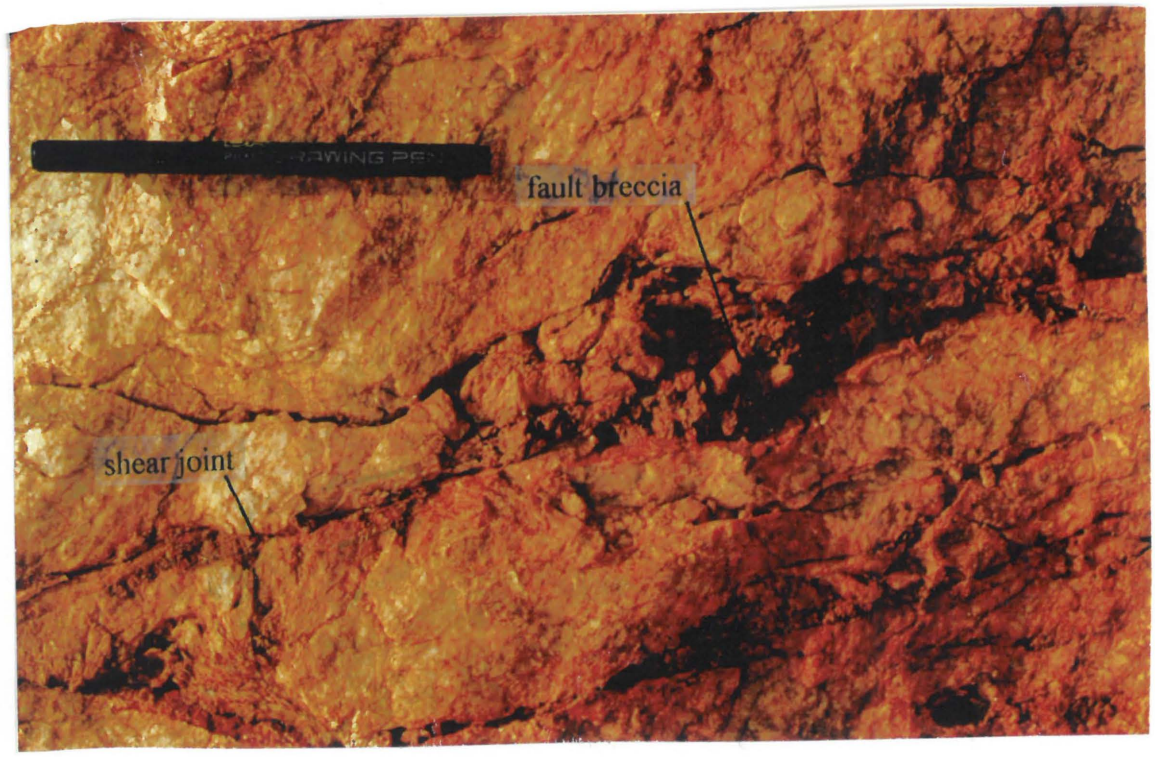

Figure 3.35: Fault breccia produced by shear jointing in Fault quartzite at location 20. Pen is 13 cm long.

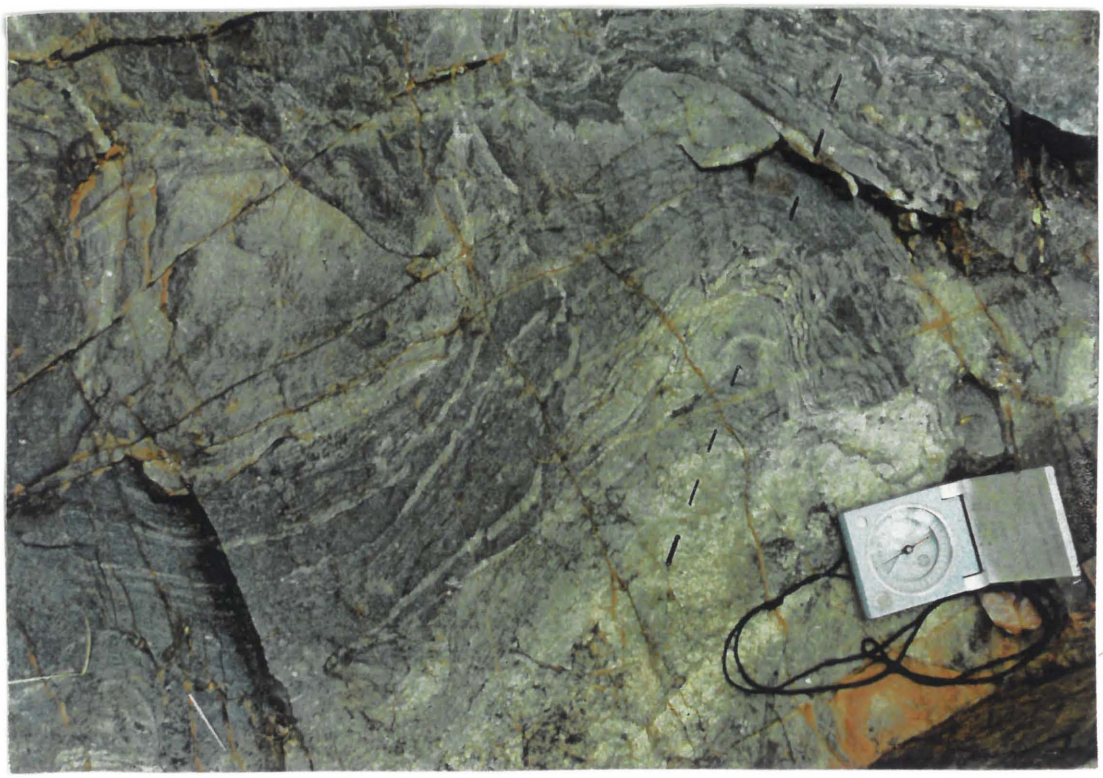

Figure 3.36: Folding of psammitic and pelitic laminations in Silverton shale at location 23. The indicated fold axial trace has a trend of 120^0 (note north arrow on compass). Parasitic folds of the same orientation are also visible on the fold limbs. It was not possible to measure the plunge or fold axial plane on this outcrop. Note that the trend of this fold axial trace is parallel to the F_1 folds identified in section 3.1.2.3. Compass is 8 cm wide.

Figure 3.37: Small scale folding of Silverton shale at location 23. Trend of fold axial trace = 050^0. It was not possible to measure the fold axial plane or the plunge at this outcrop. Note that the trend of this fold axial trace is parallel to F_2 folds identified in section 3.1.2.3. Pen top is 3 cm long.

Figure 3.38: Folding and faulting of laminations in Silverton shale at location 24. Sinistral movement has occurred along a fault of strike 025^0, possibly as a Riedal shear within the Fault zone. Lens cap is 6 cm wide.

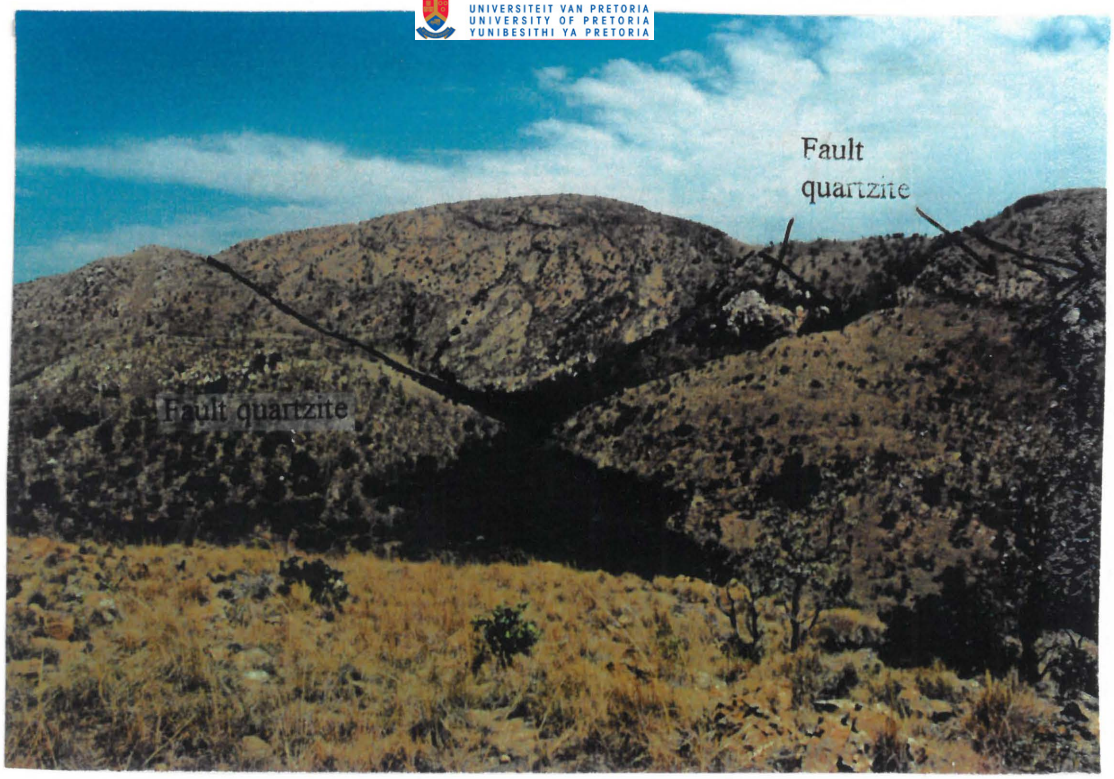

Figure 3.39: Disruption of the Rustenburg Fault zone at location 26 by later faults. The western edge of the steeply N.E.-dipping Rustenburg Fault zone (i.e. the contact of the Fault quartzite with The Magaliesberg Formation quartzite) is shown by the solid line, and the cross-cutting N.E.-striking faults are shown by dashed lines.

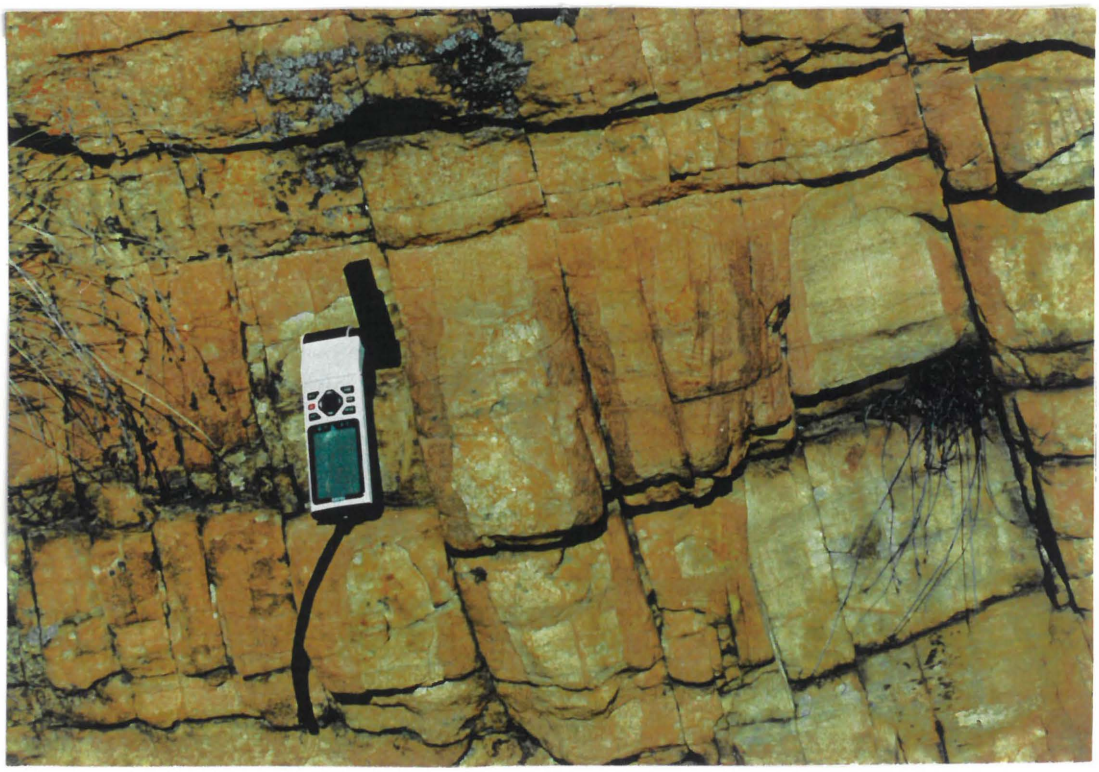

Figure 3.40: Shearing and fluid transport along joints at location 28, showing 2 cm of normal displacement, with downthrow to the S.W.. The joints have also acted as fluid conduits, with each joint showing a 3cm wide band of strong haematite staining on each side. G.P.S. receiver is 15 cm tall.

Figure 3.41: Photograph from location 29 on the northern limb of the Olifantspoort antiform. North-south striking minor faults display a generally sinistral movement of 25cm, as shown by the horizontal displacement of steeply dipping beds with contrasting degrees of recrystalisation.

Figure 3.42: Reverse faulting and drag folding at location 31.This photograph shows folded Magaliesberg quartzite on either side of a 20 cm wide fault zone filled with gouge. The dip of the fault decreases to the right (listric), indicating that this may be a thrust, with fault-propagation folding of the adjacent bedding Displacement cannot be judged, but drag folding/fault propagation folding indicates movement direction.

Figure 3.43: Well bedded Magaliesberg quartzite at location 32 is shown dipping to the north, with a cliff line, about 10m high, parallel to bedding. This cliff line can be seen on the map to mark the base of a greater preserved thickness of quartzite in this area.

Figure 3.44: Planar fabric in Magaliesberg Formation quartzite at location 32.

Figure 3.45: Contrasting haematite content in the hangingwall and footwall of the thrust at location 32.

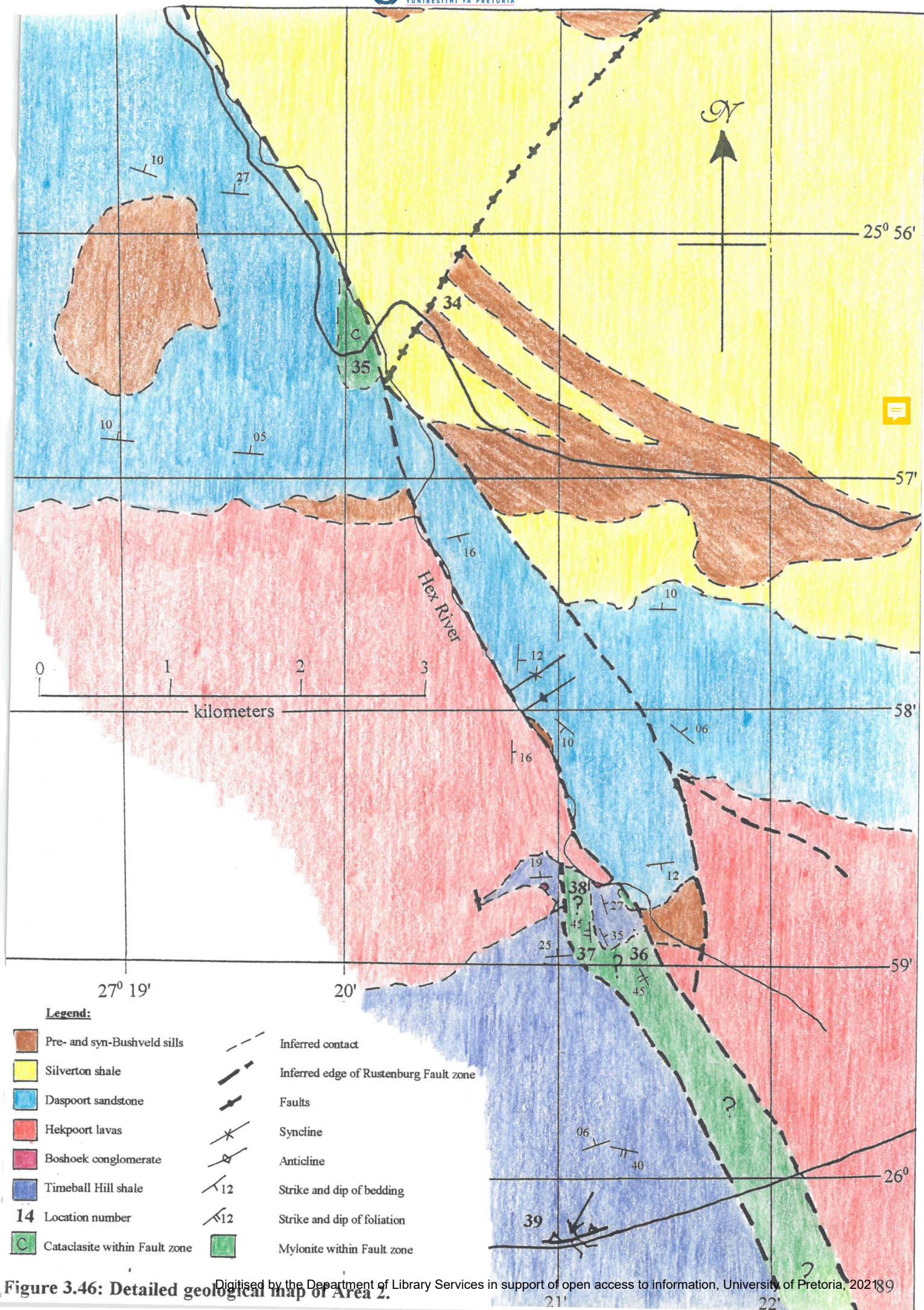

Figure 3.46: Detailed geological map of Area 2.

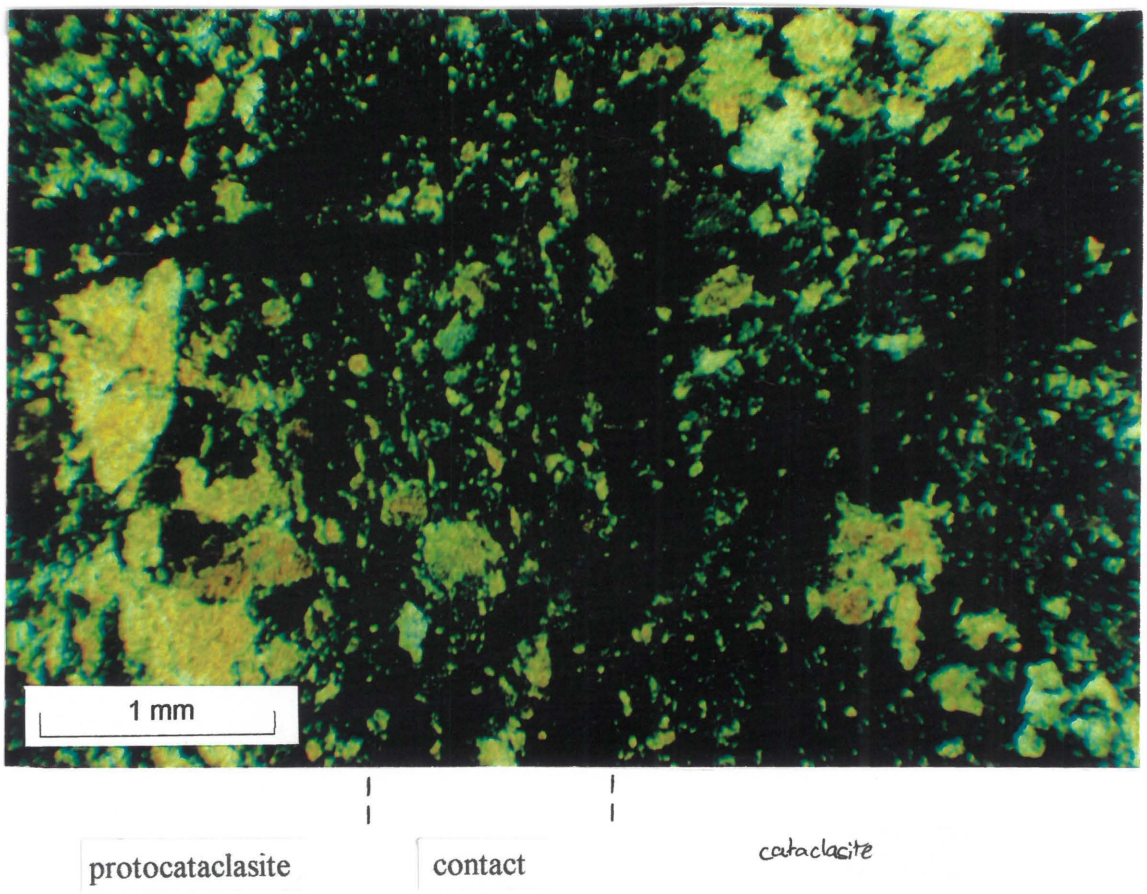

Figure 3.47: Photomicrograph of protocataclasite from location 36, showing larger quartz grains in protocataclasite, grading into cataclasite in the centre.

Figure 3.48: Timeball Hill shale at location 36 containing a foliation, S_1 = 160^0 50^0 W. Compass is 8 cm wide.

Figure 3.49: Lineation at location 37, caused by intersection of bedding and foliation in "mylonite". S_0 = 170⁰ 30⁰ W (30 ⁰→260 ⁰) and S_1 (160 ⁰ 45 ⁰ W) intersect to form L_1 (08 ⁰ →330⁰). Pen top is 3 cm long.

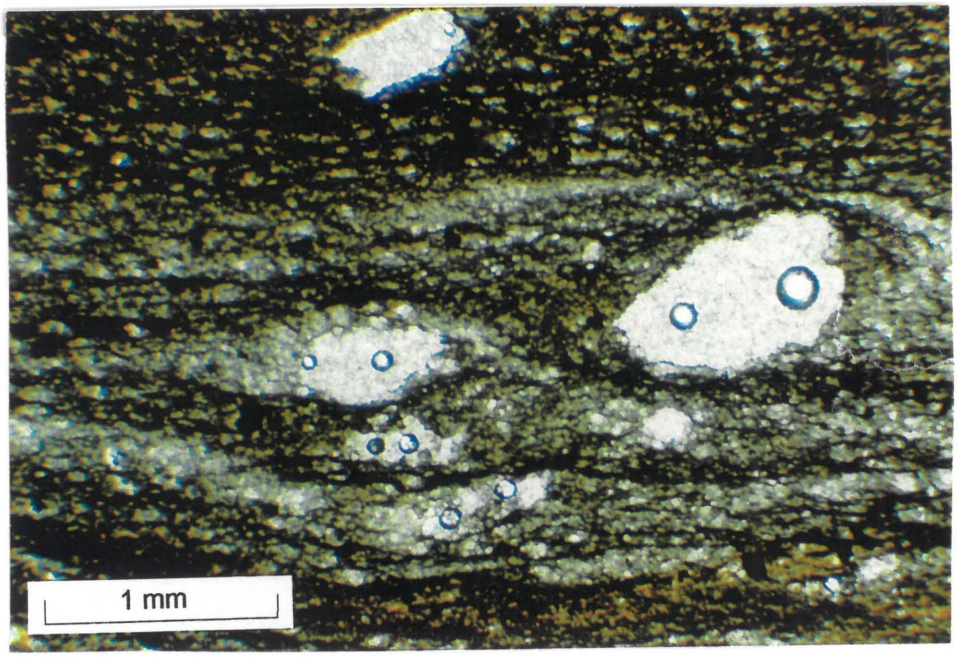

Figure 3.50: Photomicrograph from location 37. Slaty cleavage has developed, with mica-rich domains typically anastomosing around either silt lenses or lenticular metamorphic minerals, which have now weathered out (voids are filled with Canada balsam during section preparation). The lenses have developed quartz overgrowths, and are alligned parallel to the orientation of the cleavage plane.

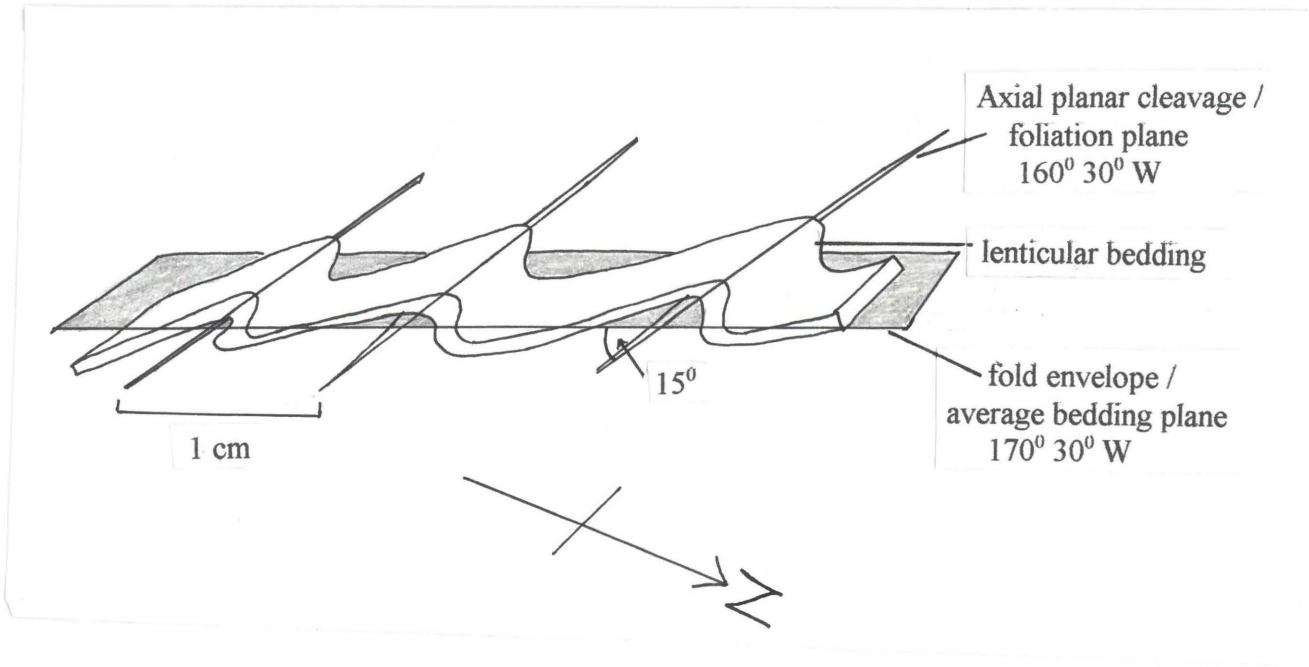

Figure 3.51: Sketch showing folding of lenticular laminations, with foliation present as axial planar cleavage, developed in Timeball Hill shales at location 37.

Figure 3.52: Axial planar cleavage (S_1) 163⁰ 55⁰ W developed in Timeball Hill shales on small (30cm amplitude) moderately inclined open folds (location 38). Compass is 8 cm wide. Photograph is taken looking north.

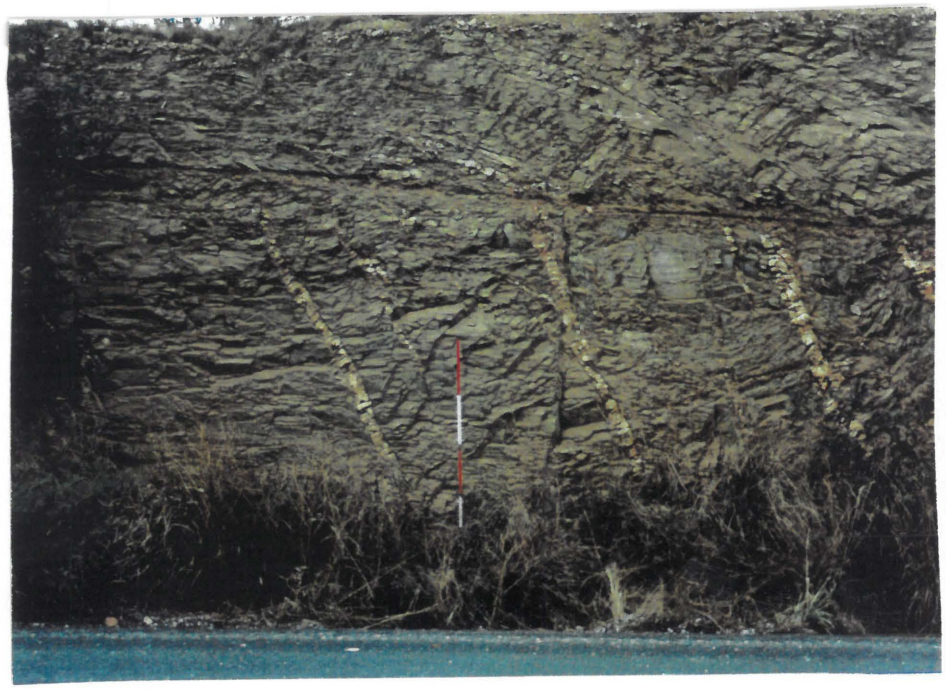

Figure 3.53: Location 39. Southward dipping shales beneath a fault gouge are intruded by c.10cm wide quartz-filled veins. Neither bedding direction nor veins continue above the fault gouge zone. This indicates that the upper layer has been thrust over the lower layer. Photograph is taken looking north. (Scale bar is 2 m long.)

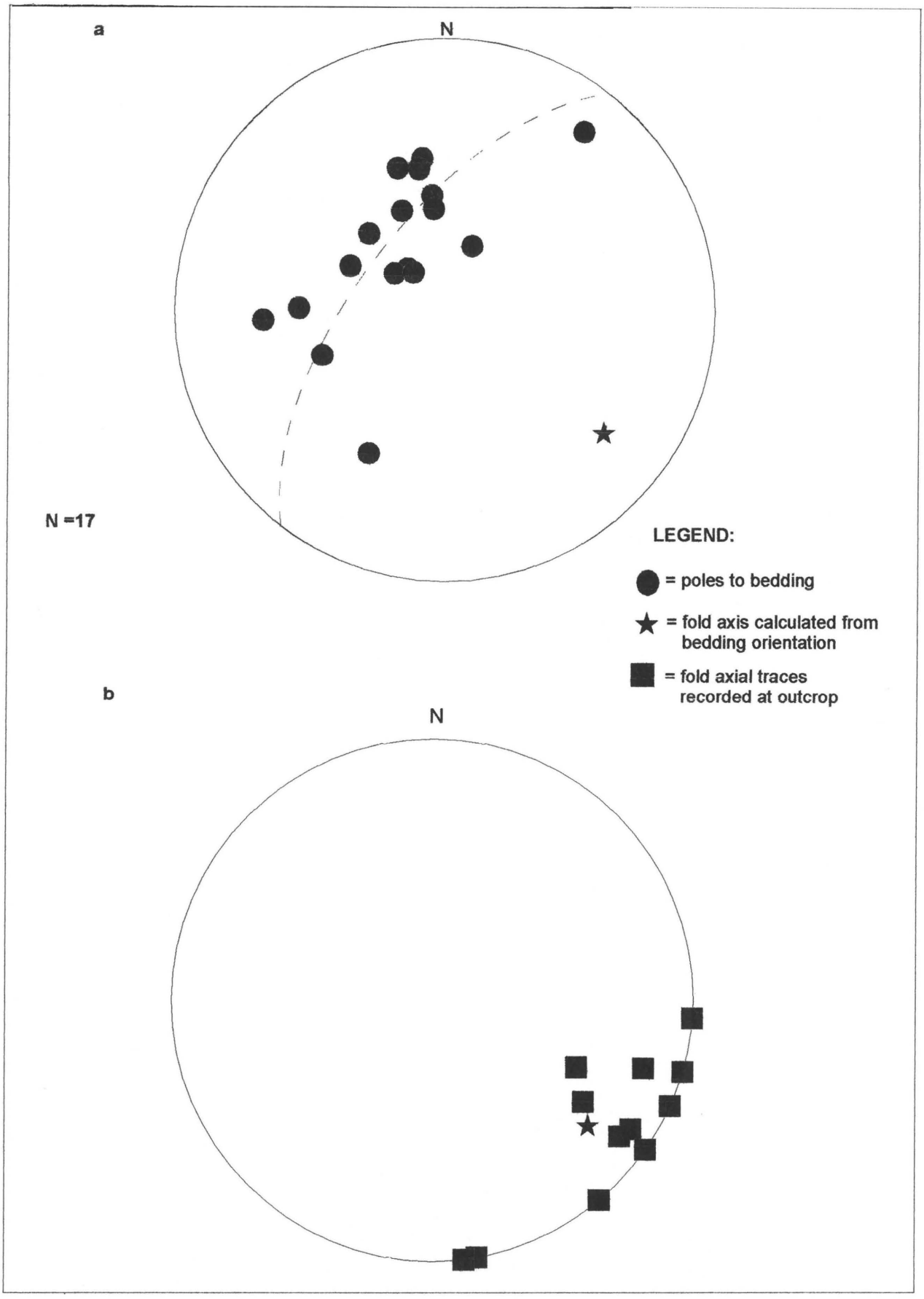

Figure 3.54: Stereographic projections of poles to bedding and fold axes at location 39.
a. shows the orientation of poles to bedding, the best fit pi circle, and the fold axis.
b. shows the orientation of fold axial traces recorded throughout the outcrop, which are of similar orientation to the fold axis predicted in a.

4: STRUCTURAL ANALYSIS.

In this chapter the lithological and structural data presented in Chapters 2 and 3 will be interpreted to produce a model for the evolution of the Rustenburg Fault. The shortcomings of the model in explaining structural phenomena in the field area will then be examined. Finally, the proposed model will be compared to other tectonic models established by workers in this part of the Kaapvaal Craton, and a regional-scale model contributing to the tectonic evolution of the area will be put forward.

4.1: Discussion of data:

Data collected in the field area can only be used to provide evidence for the history of the Fault from syn-depositional (i.e Pretoria Group) times onwards. It is possible that the history of the Rustenburg Fault is far older than that chronicled in the surface outcrops. The Transvaal Supergroup in the field area is underlain locally by Ventersdorp Supergroup lavas (Burke et al., 1985) which are, in turn, underlain by the basement granite-greenstone of the Kaapvaal craton and other units (Section 1.5.1). The two principal trends of weakness, illustrated by the orientation of greenstone belts, were imposed by the lateral accretion of oceanic mafic rocks during assembly of the Kaapvaal Craton. These trends are E.N.E.-W.S.W and N.N.W.-S.S.E (Stanistreet & McCarthy, 1991, and Section 1.5.1). The Rustenburg Fault and neighbouring structures (e.g. the Swartruggens fault and post-Bushveld Brits graben) have the latter trend (Figure 4.1), indicating that the Rustenburg Fault follows a trend of fundamental craton-wide basement structures. It is therefore proposed that the Pretoria Group sediments in the vicinity of the Rustenburg Fault were deposited over an area with a 150^0 trending basement weakness that was pre-susceptible to tectonic disturbance, and these sedimentary rocks exhibit marked thickness variations on either side of the Fault (Eriksson & Reczko, 1995; Reczko et al., in press).

Evidence for synsedimentary movement of the Rustenburg Fault is slight, though comparison of thickness differences of formations in the present field area on opposite sides of the Fault (Appendix), shows a good indication of synsedimentary fault activity. The Daspoort Formation shows considerable thickening west of the Fault, where the sandstones are nearly 3½ times thicker than on the east. This suggests a syn-Daspoort downthrow of 600m to the west, thus creating a

deep localised second-order basin (the Pretoria Group basin being the first-order basin; Reczko et al., in print). The presence of intense soft-sediment deformation in the Magaliesburg Formation sandstone at location 1 is perhaps indicative of shock-induced slumping and dewatering, caused by earthquakes as the adjacent Fault moved in syn-Magaliesberg times.

Evidence for establishing the post-Pretoria Group tectonic history of the field area is more voluminous, due to the excellent outcrop afforded by the Magaliesberg quartzite. The fold sequences with N.E.-S.W. trending fold axes seen at Olifantspoort and Rustenburg Nature Reserve are all cut by the Fault without closure of the folds. The sub-parallel fold axes of these fold sequences indicate that they are the opposite ends of the same F_1 fold structure (Figures 3.9, 3.10, 3.11 and 3.12). The close similarity in the geometry of the folds, shown in the down plunge projections from these two areas (Figures 3.17 and 3.18), confirms that the Olifantspoort and Rustenburg Nature Reserve Folds are opposite ends of the same structure. The present position of the two displaced ends of the fold system provides a useful marker from which the displacement of the Rustenburg Fault can be determined. The outcrop of Magaliesberg Formation quartzite in this area (Appendix) could have resulted either from normal movement on the Rustenburg Fault, with downthrow to the east, or from dextral strike-slip movement on the Rustenburg Fault. The occurrence of the same fold system on opposite sides of the Fault, and the lack of vertical displacement between hinge points (Figures 4.2 and 4.3) indicates that no vertical displacement has occurred. Therefore classification of the Rustenburg Fault, as recorded by the displacement of the Magaliesberg Formation quartzite is a dextral strike-slip (right lateral) fault.

N. to N.N.E. striking sinistral faulting and shear joints at locations 23 and 29 (Figures 3.38 and 3.41, respectively) can be interpreted as conjugate faults to the main dextral Fault movement (Figure 4.5). Other small-scale structures seen at location 23, such as folds with axial traces trending S.E. (Figure 3.36) and N.E. (Figure 3.37) can be interpreted in terms of F_1 and F_2 folding.

The displacement of the Fault can be accurately calculated by measuring the distance between the projected corresponding fold axial traces of the Olifantspoort and Rustenburg Nature Reserve folds. The horizontal displacement of the Rustenburg Fault is 10.6 km. A reconstructed map, showing the pre-Fault location of strata is shown in Figure 4.4.

Section 3.1.2.4 identified a number of folds with parallel orientation to the Rustenburg Nature Reserve-Olifantspoort folding (F_1 in Section 3.1.2.4). The average trend of the fold axial traces and fold axis of F_1 folds is 123^0, suggesting that the maximum compressive direction (σ_1) required to produce this folding is 033^0-213^0 (Table 3.1). Figure 4.5 shows that it is not possible for the F_1 folds to be created as *en-échelon* structures in the strain ellipse related to the faulting, as the average trend of the F_1 fold axis is at least 33^0 greater than the maximum compressive direction (σ_1) required to produce strike-slip movement on the Fault (Figure 4.5).

Therefore the F_1 folding and dextral movement of the Rustenburg Fault cannot be reconciled by the same maximum compressional direction (σ_1), but rather require two independent compressional events, with the event producing the F_1 folding pre-dating the faulting event, as F_1 folds are cut by the Fault. The first deformation (D_1), to produce the F_1 folding, requires compression in the direction 033^0- 213^0 (Table 3.1). The second event (D_2), to produce strike-slip movement on the Rustenburg Fault, requires a theoretical compressional direction 30^0 from the trend of the Fault. This orientates σ_1 in a N.-S. direction, as the Fault trends 150^0. However, as previously described, a pre-existing zone of weakness existed along the trend of the Fault, so any compressional direction oriented within c.30^0 of the trend of this zone of weakness could have reactivated the Fault by strike-slip movement.

The F_2 folds identified in section 3.1.2.4 (which post-date the F_1 folds), have an average fold axial trend of 65^0, suggesting a σ_1 directed at 335^0 -155^0 (Table 3.1). As described above, the Rustenburg Fault could have been reactivated by any compressional direction within c. 30^0 of its strike. F_2 folds are also cut by the Rustenburg Fault (e.g. location 7), suggesting that these folds may have formed as an early response to N.W.-S.E. directed compression that culminated in strike-slip displacement of the Rustenburg Fault. It is also possible that a third deformational event (D_3) was responsible for the reactivation of the Rustenburg Fault, so that dextral strike-slip movement was unrelated to the N.W.-directed σ_1 of the D_2event . The σ_1 of D_3 could have been directed from the north at 30^0 from the strike of the Fault. However, a simpler two stage deformational model (D_1 and D_2) is more favourable to account for both the F_1 and F_2 folds, and the displacement of the Rustenburg Fault. It is therefore likely that a single second deformational event (D_2) was responsible for both F_2 folding (producing interference folding with F_1 folds) and causing dextral displacement on the Rustenburg Fault. The two locations at which thrusting was

identified in the field area (locations 32 and 39), may have been thrusted from the N.E. to the S.W.. This suggests that the thrusting occurred as a response to D_1 compression, and is not related to the Rustenburg Fault.

The movement of the Rustenburg Fault seems to have produced a mylonitic-type fault rock, unrecrystallised patches of which can be seen in Figures 3.25 and 3.26. It is difficult to reconcile mylonitisation under ductile conditions in the Magaliesberg Formation. Previous workers (e.g. Nell, 1985) calculated that the Bushveld Complex was intruded at a depth of 5 km (at the top of the Magaliesberg Formation), suggesting that the pre-Bushveld depth of upper Pretoria Group rocks of the field area was from 5 to10 km, which is usually insufficient to raise temperatures to the heat required to cause ductile deformation (Davis & Reynolds, 1996). The rising geotherms associated with the imminent arrival of the Bushveld magmas would, however, have created temperatures as high as 750^{0}C at depths as shallow as 5 km (Nell, 1985). It is therefore not unlikely that ductile deformation would occur at such shallow crustal levels. Brittle deformation along the Fault zone (Figures 3.35 and 3.47) is most likely due to subsequent reactivation of the Fault, after the cooling of the Bushveld.

It can be seen from the map (Appendix and Figure 3.1) that the displacement of the Daspoort Formation is considerably less than the displacement of the Magaliesberg Formation (6.1 km compared to 10.6 km). This is probably due to accommodation of strain by folding or thrusting in the unexposed and less competent Silverton Formation shales.

The data suggest that both the D_1 and most of the D_2 activity was completed before the beginning of the intrusion of the Bushveld Complex (thereby constraining both of the deformational events to between the time of Pretoria group lithification and c.2050 Ma. (Harmer & Von Gruenewaldt, 1991). The evidence for this pre-Bushveld timing is considerable. Firstly, there is a lack of topographical expression where the Fault zone passes into areas occupied by the Bushveld Complex. In older lithologies, the Fault zone is accompanied by abrupt changes in relief, or by rivers occupying the Fault. However the topography remains planar in Bushveld lithologies, as can be seen by stereoscopic viewing of aerial photographs. As illustrated in Figure 3.33, Bushveld rocks are absent from the Fault zone, despite their present day proximity, indicating that they were not present during the D_2 event. Finally, as shown in Figures 3.25 and 3.26, the recrystallisation

leading to production of the Fault quartzite and the Magaliesberg quartzite appears to have occurred after faulting, as the original Fault mylonite is visible where discrete patches have escaped recrystallisation. Note that grain size in the Magaliesberg quartzite is generally smaller than that in the Fault quartzite (e.g. compare Figures 3.22 and 3.23). If faulting had occurred *after* the Bushveld metamorphism, it would be expected to see grain size reduction of Magaliesberg quartzite crystals along the Fault zone.

Metamorphism may have begun due to geothermal heat associated with the impingement of the Bushveld Complex at shallow crustal levels. Geothermal heating may have led to increased circulation of crustal fluids through adjacent permeable rocks. The larger crystal size in the recrystallised Fault quartzite is a function of fluid availability and protolith purity, as the presence of other minerals impedes quartz crystal growth (e.g. Figure 2.15). The relative lack of haematite staining in the Fault quartzite is apparent, whereas it might have been present in the protolithic mylonite. This suggests that the Fault zone acted as a fluid conduit for the siliceous fluids responsible for the recrystallisation of the surrounding rocks. The fluids may have dissolved and flushed out any haematite present in the Fault zone, allowing for free growth of quartz, with an abundant supply of silica. The suggestion of the Fault zone behaving as a fluid conduit, or mega-vein, is supported by the outcrop at location 16, where 'Fault' quartzite is present, with no apparent displacement of surrounding structures. In the case of location 16, a small kink in the Fault plane at Olifantspoort has not been exploited by the intruding fluids, and the fluid continued along the same trend, exploiting bedding-parallel weaknesses on the southern limb of the Olifantspoort anticline, rather than the Fault zone. Analogous flushing of haematite and free growth of quartz occurred at this location, leading to a lithology comparable to true Fault quartzite, except that patches of mylonite are never present, as that protolith never existed at this location.

The contact between the top of the Magaliesberg Formation and whatever lithology overlay (possibly the Rayton Formation, or rocks of the Rooiberg Felsite Group) was generally exploited by the intruding Bushveld magmas. The undulating base of the complex in the field area (Appendix) can best be explained either by intrusion into the underlying Pretoria Group at a variety of levels in the stratigraphy, or by assimilation of the Pretoria Group by the Bushveld magmas. South of Rustenburg, the Bushveld Complex is in contact close to the top of the Magaliesberg Formation. South of the Pilanesberg mountains, Magaliesberg quartzite is usually absent, and the

magmas appear to have intruded or assimilated their way down through the entire Magaliesberg Formation and into the Silverton Formation shale beneath. Varying thicknesses of quartzite have been lifted or assimilated in the intervening areas.

Localised lenses of Fault quartzite (e.g. location 11) and the abutment of the Bushveld Complex against the Fault zone west of Rustenburg, indicates that this lithology was not readily assimilated into the Bushveld Complex. The newly recrystallised Fault zone seems to have acted as an impediment, preventing the consuming Bushveld magmas from incorporating large volumes of Pretoria Group rocks. The domal structures produced by interference folding also appear to have had the Bushveld magmas pond against them, whilst adjacent basins were intruded by the magma. Burial of the Fault zone and Pretoria Group sedimentary rocks beneath the Bushveld Complex led to compaction and pressure solution at the new quartz crystal boundaries. Pressure solution seems to have occurred regionally (thin sections of Daspoort, Magaliesberg and Fault quartzites all show evidence for pressure solution).

It is probable that a D_3 compressive event, in the same orientation as the D_2, became active again, after the intrusion and cooling of the Bushveld Complex. Evidence for post-Bushveld tectonic activity is present in thin sections of Fault quartzite, and in post-Bushveld displacement of Masgaliesberg quartzite and Fault quartzite (Figure 4.6). Evidence for D_3 stress can be found in the Fault zone, south of Olifantsnek dam where a S.S.W. direction can be inferred for post-Bushveld faulting. (see below and Figure 4.6). In thin section, all Fault quartzites can be seen to possess undulose extinction (Figure 3.24), or even deformation lamellae (Figure 3.25) where strain was particularly intense. This undulose extinction is not well developed in neighbouring Magaliesberg quartzite (e.g. Figure 3.23). The undulose extinction must have been imposed after pressure solution, as crystal deformation is constant within each thin section, indicating no intercrystal movement during or after the straining event. Despite such intense deformation of the quartz crystals, only occasionally can fracturing be seen to have occurred, and is usually annealed (Figures 3.29 and 3.30), perhaps by still-circulating Bushveld fluids, or any subsequent thermal event. In the areas adjacent to the Bushveld Complex, such post-Bushveld fracturing is rare. This raises the question as to why the Fault generally failed to reactivate during post-Bushveld times (when D_2-directed compression was resumed), as is evident by the largely unbroken trend of the Fault quartzite.

The answer to this may lie in the fact that the Bushveld magmas had solidified across the Fault zone, thus locking the fault blocks together. Post-Bushveld D_2-type activity created insufficient stress to fault the Bushveld Complex, so strain was partially accommodated by deformation within the quartz crystals.

However, evidence for post-Bushveld reactivation of the Rustenburg Fault is stronger away from the Bushveld Complex. Locations 17, 18 and 19, which are stratigraphically well below the Bushveld Complex, show intense fracturing of deformed Fault quartzite (e.g. Figures 3.31 and 3.32). Figure 3.32 shows that undulose extinction was imposed before brecciation of the Fault quartzite. Both of these deformations must have been imposed after recrystallisation by the Bushveld Complex. It is therefore probable that deformation of quartz crystals (undulose extinction and deformation lamellae), fracturing and annealing are more or less coeval, due to the same post-Bushveld deformational event. The small hill 'Gifkoppie' (location 19) south of Olifantsnek dam shows thin section evidence for being a post-Bushveld fault block, entirely consisting of a breccia of refaulted Fault quartzite (Figure 3.32) and a fault breccia of Magaliesberg quartzite (appendix and Figure 3.8). It appears that this may have been displaced from the N.W. by two or three kilometres, from the most southerly source area for the Fault quartzite at Olifantsnek dam. The fact that the Fault quartzite at Olifantsnek Dam is not displaced by this post-Bushveld faulting is difficult to reconcile, but may stem from post-Bushveld movement along the Silverton-Magaliesberg interface beneath the Bushveld Complex (Figure 4.6).

The final major tectonic event to have affected the field area is the thermal collapse, associated with cooling of the Bushveld Complex. Bedding direction in unfolded areas gives an indication of the geometry of this collapse. The estimated upright orientation of the fold axial surfaces at Olifantspoort and Rustenburg Nature Reserve suggest that these locations, occurring at a sharp bend in the rim of the Bushveld basin, failed to be accommodated into this collapse. This is schematically shown in Figure 4.7.

4.2: Model for the evolution of the Rustenburg Fault:

Some movement along the line of the Rustenburg Fault probably occurred before Pretoria Group sedimentation, and the structures observed in the field all represent reactivation of this original Fault. During Pretoria Group sedimentation, occasional synsedimentary movement involving vertical displacement led to the production of second-order depositional basins on the downthrown side of the Fault.

Between the lithification of the Pretoria Group and the intrusion of the Bushveld Complex, a considerable tectonic history is indicated from the field area. Firstly, a N.E.-S.W.-directed compressive event (D_1) caused F_1 folding, with generally upright open folds with an axial planar trace trending N.W.-S.E.. D_1 faulting was subordinate to folding, though some bedding parallel thrusting occurred. Following this, a second compressive direction (D_2) was imposed, orientated N.W.-S.E.. This event caused some folding with a E.-W. to N.E.-S.W. trending fold axis, but is particularly manifest in its reactivation of the Rustenburg Fault. The faulting caused up to 11km of dextral (right-lateral) displacement of the Pretoria Group sedimentary rocks, and produced a Fault zone several hundred metres wide.

The Bushveld intrusion followed the D_2 event. Contact metamorphism led to circulation of quartz-rich fluids along lines of pre-existing weakness, and causing intense recrystallisation in more permeable areas. The permeable fault rocks of the Rustenburg Fault were particularly susceptible to exploitation as a fluid conduit, and were readily flushed of soluble impurities. The fault rock recrystallised as a quartz-rich coarse quartzite.

The intrusion of the Bushveld magmas into the country rocks was accommodated by either by lifting of upper Pretoria Group strata or by considerable assimilation of the wall of the magma chamber. The quartzite along the Fault zone proved resistant to intrusion, often acting as a barrier against which the magma ponded. In other places, the Bushveld magmas seem to have assimilated through the Fault zone and preferentially consumed the Pretoria Group rocks there. Where the Pretoria Group rocks on the Bushveld side of the Fault withstood the assimilation process, the quartzite in the Fault zone remained intact. Areas of Pretoria Group sediments with strong interference folding often created structures against which the Bushveld magmas abutted.

In post-Bushveld times, a D_3 compressional event, orientated parallel to D_2, occurred, though by this stage the Rustenburg Fault had been considerably strengthened by having had the Bushveld magmas pond and solidify over its Fault zone, effectively locking both fault blocks in position. Though the area occupied by the Bushveld Complex was highly stressed, movement did not occur. However, post-Bushveld movement did occur in areas such as the southern part of the field area, which are further removed stratigraphically from the solidified Bushveld intrusion.

Thermal collapse of the Bushveld Complex and loading of the floor rocks caused a dipping of the Pretoria Group sedimentary rocks into the centre of the Complex. Flat lying bedding was tilted up to 30^0 towards the centre of the intrusion, though areas at corners in the Bushveld basin could not be accommodated into this collapse.

Though the model presented in this section can account for much of the recorded data, several anomalies and questions still remain unanswered. Some of these are considered in the next section.

4.3 Problems with the model:

Some of the structural data observed in the field remain enigmatic, and do not easily fit the model given above. In some cases the model can be modified, and speculative reasons given to explain phenomena. Sometimes no explanation can be offered to account for anomalous data.

One question that can be asked is why does the Fault quartzite fail to penetrate into the rest of the lower Pretoria Group, other than the Magaliesberg quartzite? There is a strong coincidence between the presence of the Magaliesberg quartzite and the presence of Fault quartzite. The growth of Fault quartzite in the Bushveld aureole may have been dependant on a quartzitic mylonite/cataclasite protolith, and the fault rock in other Pretoria Group lithologies may have been insufficiently porous to fluids, and chemically too diverse for seeding quartz growth.

At location 27, the D_1-D_2 relationship seems reversed: Fault quartzite with a D_2 trend is cut (in post-Bushveld times) by a D_1 trending fault, which lacks recrystallisation. This can be best accounted for by Hartzer's (1995) work in the Pretoria Group inliers of the Bushveld Complex. Here he found evidence for slight D_1 directed compression in post-Bushveld times, due to

necessary accommodation of the Bushveld intrusion. Hartzer's model will be considered in more detail in section 4.4.2.

Another problem concerns the lack of development of undulose extinction in Magaliesberg quartzite. If post-Bushveld stress is shown only by undulose extinction and deformation lamellae in Fault quartzite, with no large-scale movement along the Fault, then it would be expected that some of the stress would be accommodated, not only by plastic deformation in Fault quartzite, but also by deformation in Magaliesberg quartzite. Though undulose extinction is present in Magaliesberg quartzite, it is poorly developed, irrespective of distance from the Fault zone.

Another problem associated with the undulose extinction is that it often co-exists with post-Bushveld fracturing and faulting. According to the model, both undulose extinction / deformation lamellae and post-Bushveld faulting are due to the same tectonic event (late-stage D_2). It would therefore be expected that, where post-Bushveld movement could occur readily, strain would be accommodated by faulting instead of deformation within quartz crystals. It is possible that the faulting observed at Gifkoppie and on the southern limb of the Olifantspoort anticline is unconnected to the post-Bushveld event causing undulose extinction. This fault movement may represent a separate, later tectonic event.

A final problem is why, in an otherwise undistorted basin, should the upper Pretoria Group show signs for such complex deformation along such a narrow zone parallel to the Fault? Why should there be a coincidence in the manifestation of two separate deformational events in such a localised area, when effects of these events are subordinate elsewhere? Why are the effects of D_1 and D_2 not evident in other parts of the Transvaal basin?

The coincidence of both D_1 and D_2 structures co-existing only along the Fault zone can be explained by the presence of fundamental structural weakness in the basement beneath. The area of the Rustenburg Fault zone may have been pre-susceptible to deformation, and was easily exploited along its trend by any stresses imposed on the region.

Section 4.5 will show that there *is* some evidence for similar tectonic events in the Pretoria Group inliers elsewhere in the basin, and in section 4.6, a regional tectonic model will be presented which

shows basin-scale structures which may have resulted from these same deformational events.

4.4: Comparison of the proposed model to other models for movement of the Rustenburg Fault:

The variety of models which have been proposed by workers for the Rustenburg Fault over the last forty years was outlined in section 1.5. To summarise, post-Bushveld faulting with a normal sense of displacement (downthrow to the east) has been proposed (Coertze, 1962; Vermaak, 1970; Du Plessis and Walraven , 1990). Friese et al. (1995) suggested Kibaran-aged sinistral (left-lateral) movement of the Fault. These models bear little resemblance to that proposed in Section 4.2.

Only the work of Bloy (1986) suggested dextral displacement, a conclusion reached from aerial photographic interpretation and the measurement of slickencrysts (accretionary growth fibres), quartz vein orientation and 'breccia planes' at Olifantsnek dam. These structures were not observed in the present study. No time constraint was offered for the movement of the Fault. Bloy (1986) suggested that the [F_1] folding at Olifantspoort and Rustenburg Nature Reserve was created as a result of en-échelon structures evolving in the strain ellipse during simple shear (Figure 4.5).

Whilst this model of Bloy (1986) accurately predicts creation of normal faults (e.g. at location 23), and accounts for shear jointing as conjugate faults at location 29, the predicted fold-axis would trend at 90^0-270^0, whereas the Olifantspoort - Rustenburg Nature Reserve fold axis trends at 127^0. It is therefore considered that the observed folding and dextral strike-slip faulting cannot be easily reconciled by the same tectonic event.

The suggestion of Friese et al. (1995), that the Rustenburg Fault was reactivated due to N.W. directed compression during the Kibaran (1200-1000 Ma) orogeny, suggesting considerable post-Bushveld faulting with a sinistral sense of movement, is clearly at variance with the proposed model. The evidence upon which this model of Friese et al. (1995) was based was the apparent sinistral displacement of two Pilanesberg-aged (1250 Ma: Lurie, 1986) dykes north of Carletonville (A.E.W. Friese, pers. comm., 1997). However, these same dykes have been interpreted by Meadon (1973) as being intruded after the Rustenburg Fault, as he could trace the dykes as

exploiting the pre-existing fault plane (Figure 4.8), rather than being cut by it. The surrounding country rocks exhibit no indications for sinistral movement, but rather show evidence for slight dextral displacement (Map sheet 2626, Wes Rand).

Coertze (1962) proposed that movement on the Rustenburg Fault was post-Bushveld on account of small-scale faulting of Bushveld chromitite, S.W. of the Pilanesberg Complex. In discussing the paper, Cousins (1962) suggested that this displacement was due to movement along localised Pilanesberg-aged faults of 080^0 trend, and not to post-Bushveld movement of the Rustenburg Fault. Coertze also suggested an easterly downthrow of the Fault, on the rather scant data afforded by the outcrop locations of the same chromitite seams. However, according to Cousins, this indicates Pilanesberg-aged normal faulting, but cannot be applied to the Rustenburg Fault. Coertze's contention that the areas of Magaliesberg quartzite surrounded by Bushveld rocks are xenoliths, cannot be reconciled with the predictability of deformation directions observed in these inliers. If they were xenoliths in the Bushveld Complex, then a certain degree of rotation of fold-axes could be expected. The trend of the Fault rarely alters whether or not it passes through the inliers, suggesting that these structures are attached to the floor of the Complex. These are often apparent in outcrop as floor domes caused by interference folding (F_1 and F_2), rather than as xenoliths.

Vermaak (1970), working west of the Pilanesberg, agreed with this suggestion that the inliers of Magaliesberg quartzite are folded floor projections. He also distinguished two folding events in the area west of Pilanesberg, each equivalent to the F_1 and F_2 described in the model above. However both these folding events were interpreted by Vermaak as being syn-Bushveld in age, deformation occurring to create space for the intrusion. Vermaak (1970) agreed with Coertze (1962), that the Rustenburg Fault was downthrown to the east in post-Bushveld times.

Du Plessis and Walraven (1990) took the movement direction of the Rustenburg Fault established by Coertze (1962) and Vermaak (1970) and attempted to account for its pre-supposed post-Bushveld normal sense of movement (downthrow to the east), by considering the Fault as a feature of the strain ellipse of the Thabazimbi-Murchison Lineament (T.M.L.). In Pre-Bushveld times they proposed a N.W.-S.E.-directed compression, causing dextral movement on the T.M.L.. They showed that, according to the strain ellipse, such compression would create extension along the

Rustenburg Fault, as shown in Figure 4.9a. By post-Bushveld times, they show a reorientation of the stress field having taken place, producing N.E.-S.W. compression (Figure 4.9b), as shown by sinistral movement on the T.M.L..

However, the post-Bushveld strain ellipse does not allow for the extension along the Fault zone required for the proposed post-Bushveld normal faulting, as the σ_1 is orientated perpendicular to the Fault. Du Plessis and Walraven suggest that extension *could* occur in a compressional environment if the Fault plane pre-existed, though this seems an unlikely explanation. If the post-Bushveld strain-ellipse of Du Plessis and Walraven (1990) is correct, then it cannot be used in conjunction with post-Bushveld normal movement on the Rustenburg Fault.

Though the stress directions from the model of Du Plessis and Walraven (1990) do not support Coertze's (1962) and Vermaak's (1970) model of fault movement particularly well, they can be interpreted to support the model proposed here. The pre-Bushveld strain ellipse (Figure 4.9a) shows σ_1 as coincident to the D_2 direction of the model proposed here (both involve S.E-N.W. directed compression), and indicates the possibility that the Rustenburg Fault may have been activated as a Riedel shear within the stress field. The post-Bushveld σ_1 direction shown in Figure 4.9b can account for the general lack of post-Bushveld movement of the Fault. However, no equivalent of D_1 is suggested in pre-Bushveld times, and the continued post-Bushveld D_2 stress direction proposed in the model cannot be reconciled in these strain ellipses.

Earlier interpretations regarding the movement direction of the Rustenburg Fault (e.g. Coertze, 1962; Vermaak, 1970) were based upon data from west of the Pilanesberg Complex. As implied by Cousins (1962), this area is unsuitable as an indicator for movement and timing indicators of the Fault because of the presence of a suite of Pilanesberg-aged faults cross-cutting the Rustenburg Fault, making the Liliput Fault (the displaced northern extension of the Rustenburg Fault after its interruption by the Pilanesberg suite of faults) a structurally separate unit from the main Rustenburg Fault. It is therefore inadvisable to apply whatever timing constraint and movement direction was invoked on the Liliput Fault by earlier workers, to the main part of the Rustenburg Fault.

4.5: Comparison of the proposed model to other models for regional-scale deformation:

Results of this study very closely resembles those proposed by Hartzer (1995), working in the larger Pretoria-Group inliers in the Bushveld. He found that the Crocodile River, Marble Hall and Dennilton domes are floor projections resulting from pre-Bushveld interference folding of F_1 (= N.W.-S.E. trending fold axis) and F_2 (= E.N.E.-W.S.W trending fold axis). Hartzer's F_1 and F_2 structures were produced by exactly the same compression directions proposed for the D_1 and D_2 in this model. Hartzer proposed that these structures acted as physical barriers against which the mafic rocks of the Bushveld Complex ponded, in a similar fashion to the process proposed for the edges of the Fault zone and interference folds in this model. Hartzer (1995) presented evidence for a third (post-Bushveld) folding event (F_3) which caused tightening of the old F_1 direction. Evidence in the present field area for post-Bushveld compression in this direction is slight, though rare relationships, such as at location 27, where a post-Bushveld dextral fault strikes 030^0 are easily explained by invoking Hartzer's D_3 direction. The evidence for post-Bushveld timing of this and other small faults along the Fault zone, is given by the fact that the Fault quartzite (which was created by during recrystallisation by the Bushveld Complex) is cut by faults which do not contain this lithology.

A summary of the contrasts and similarities between the models of Du Plessis and Walraven (1990) (Section 4.4) and Hartzer (1995) and the model proposed here is presented in Table 4.1.

Therefore the model produced by this work fits well into the latest regional-scale model of Hartzer (1995), though it fails to agree with previous suggestions for movement direction and timing of the Rustenburg Fault. The reaffirmation of Hartzer's regional scale model shown by this work allows for speculation in other parts of the Bushveld basin, which show evidence for being affected by the same tectonic directions. This larger-scale model is presented in the next section.

4.6: Regional-scale model resulting from the proposed tectonic history of the Rustenburg Fault:

A reconstruction of the geological map after removal of the proposed displacement by the Rustenburg Fault (Figure 4.4) still leaves a considerable kink in the Pretoria Group sediments

around the rim of the Bushveld. This 'kink' is caused by large E.N.E-W.S.W. trending folds west of the field area (Figure 4.10). Similar gentle folding can be seen in the outcrop pattern north of Pilanesberg. The direction of this fold axis indicates that it is F_2 folding, related to the D_2 event which culminated in dextral displacement along the Rustenburg Fault zone. It seems that failure along the Rustenburg Fault accommodated some of the D_2 compressive stress, preventing the propagation of the F_2 folds eastwards (Figure 4.10). Ultimately, this F_2 folding has led to the creation of an synclinorium through the far western Transvaal basin, the present ground surface largely occupied by folded Woodlands sediments (Eriksson et al., under review) (Figure 4.10).

F_2 folding of such a large scale implies pre-Bushveld basin inversion of the far western Transvaal basin (Eriksson et al., under review). The failure of the Bushveld to intrude the far western basin (except the small Nietverdiend intrusion) is easily explained by this regional model: The N.N.W-S.S.E.-directed compressional regime operating in pre-Bushveld times in this part of the basin could not accommodate significant volume expansion due to intrusion. Intrusion of the Bushveld Complex was therefore much greater in the other lobes of the Bushveld where the F_2 anticlinoria were not developed, as shown by the lack of D_2-related structures in more easterly parts of the basin.

The pre-Bushveld Rustenburg Fault can therefore be thought of as a flexure zone accommodating stress differences between the compressed western side, and the non-compressed eastern side in the pre-Bushveld Transvaal basin inversion.

This regionally-extended model implies that D_2 was a large-scale tectonic event, capable of inverting the entire far western Transvaal basin. If such a model is to be taken seriously, then a mechanism for such a significant D_2 event is required. It is postulated here that earliest accretion terranes in the Kheis belt in central Botswana at the beginning of the Eburnian orogeny, may provide the necessary tectonic direction and compression to create such an inversion, though the estimated dates of Eburnian orogenesis are rather too young (maximum age of 1.9-2.0 Ga; Thomas et al., 1993). However, Coward et al., (1995) propose a similar model for the creation of the 2023 Ma. Vredefort Dome (interpreting it as a pop-up structure rather than the widely held astrobleme model), resulting from Eburnian-aged S.E.-directed compression resulting from collision along the Kheis belt in Botswana.

This model questions the proposal of Eriksson et al. (1995) that continental rift-related extension during the Pretoria Group deposition continued in post-Pretoria Group times, and culminated in the intrusion of the Bushveld Complex. This proposal cannot be reconciled with two compression events in the post-Pretoria Group pre-Bushveld time period, proposed in this model.

Potgieter (1992) suggested that the unconformity between the Chuniespoort- and Pretoria Groups (Section 1.5.2) was caused by basin inversion due to N.-S.-directed compression. Though Potgieter reached no firm conclusions regarding the cause of this compression, it seems that this event, which caused the end of Chuniespoort Group sedimentation, is analogous to the regional-scale model proposed here, which seems to have inverted part of the Pretoria Group basin, in a similarly directed stress field, albeit around 200 Ma. after the Chuniespoort basin inversion.

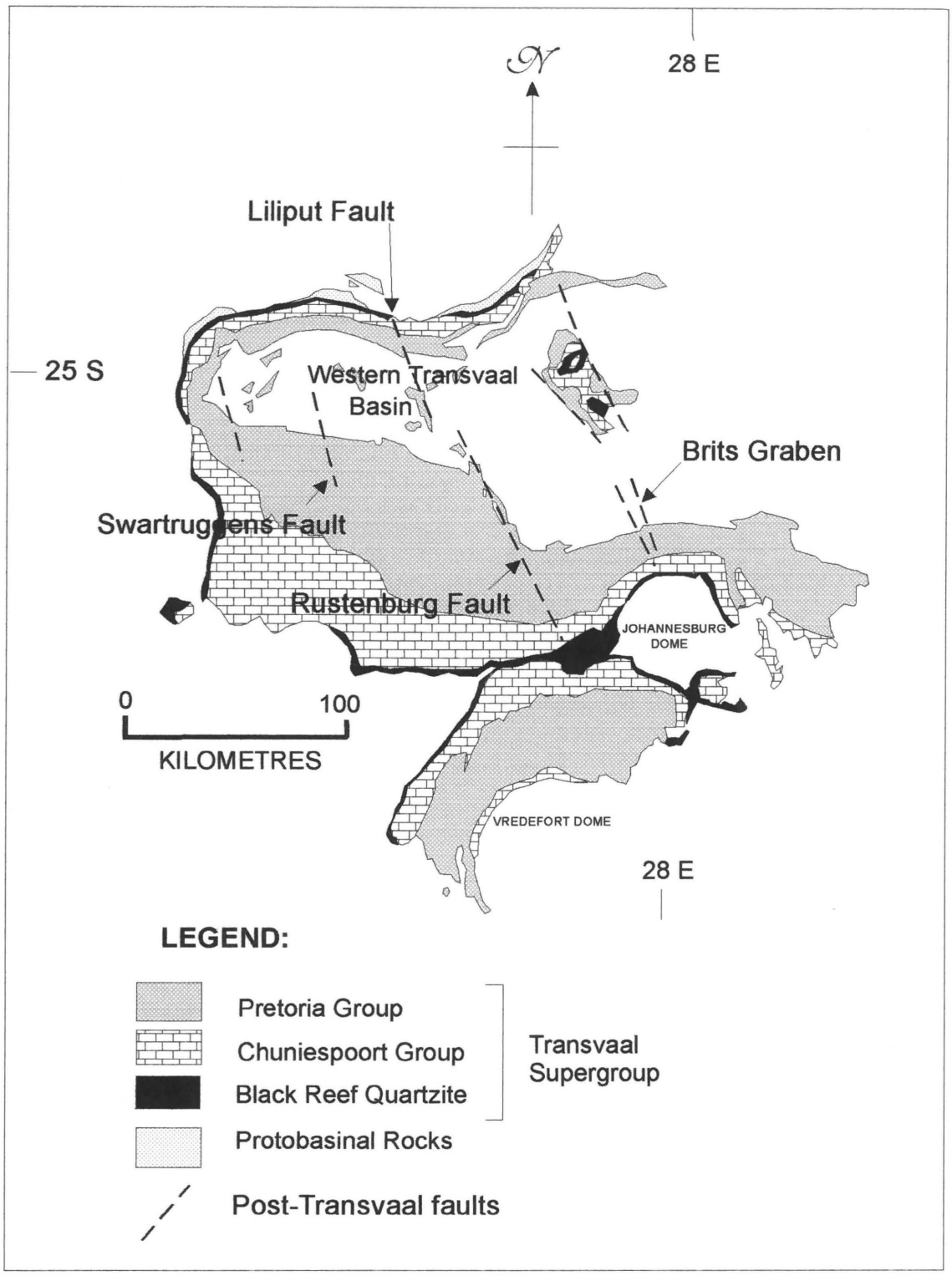

Figure 4.1: Parallel post-Transvaal Supergroup faults in the western Transvaal basin (after Dietvorst, 1991).

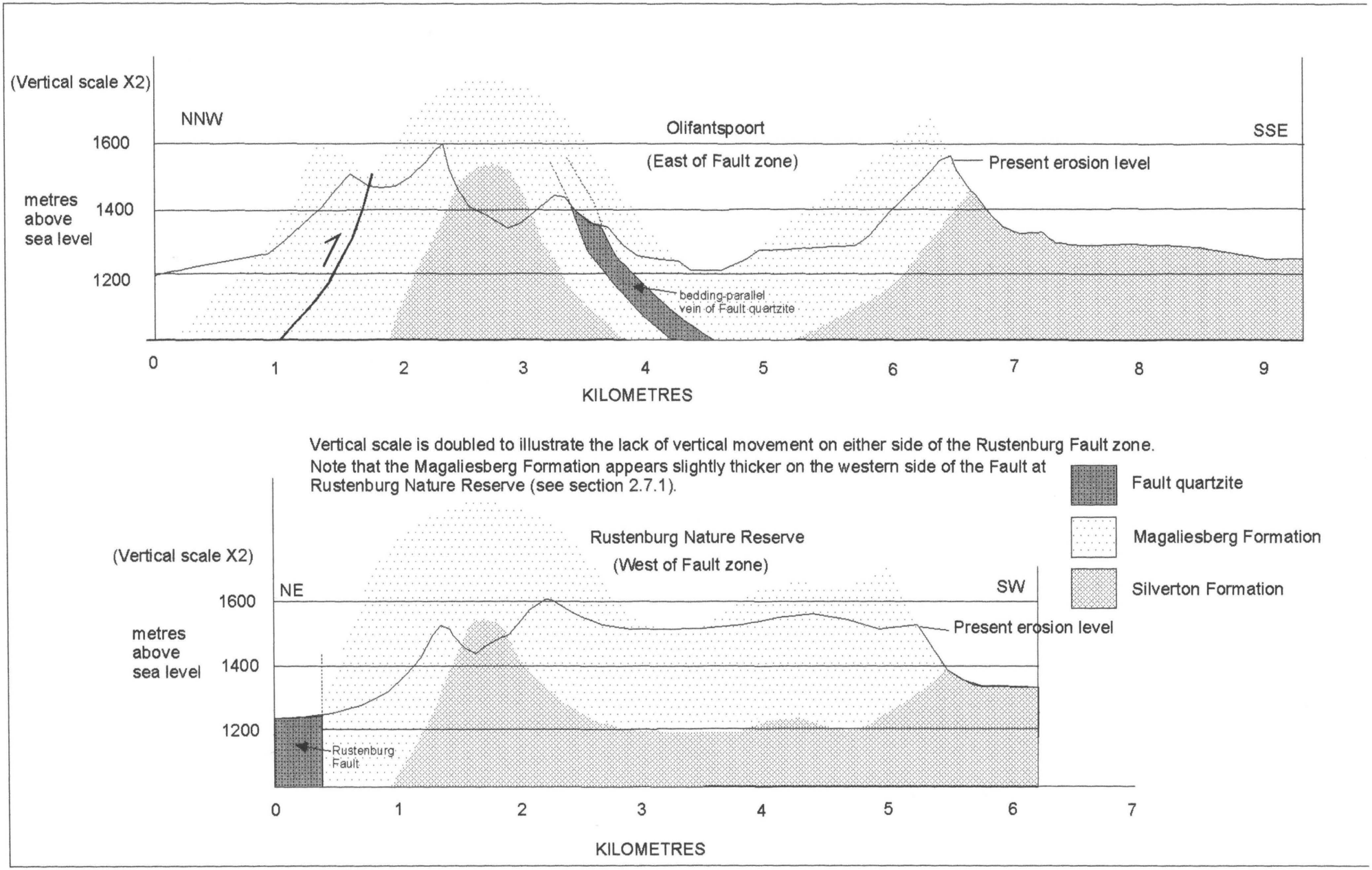

Figure 4.2: Cross sections through the Olifantspoort and Rustenburg Nature Reserve folds, showing little vertical displacement, as shown by the corresponding altitude of the projected crests of the anticline in both areas.

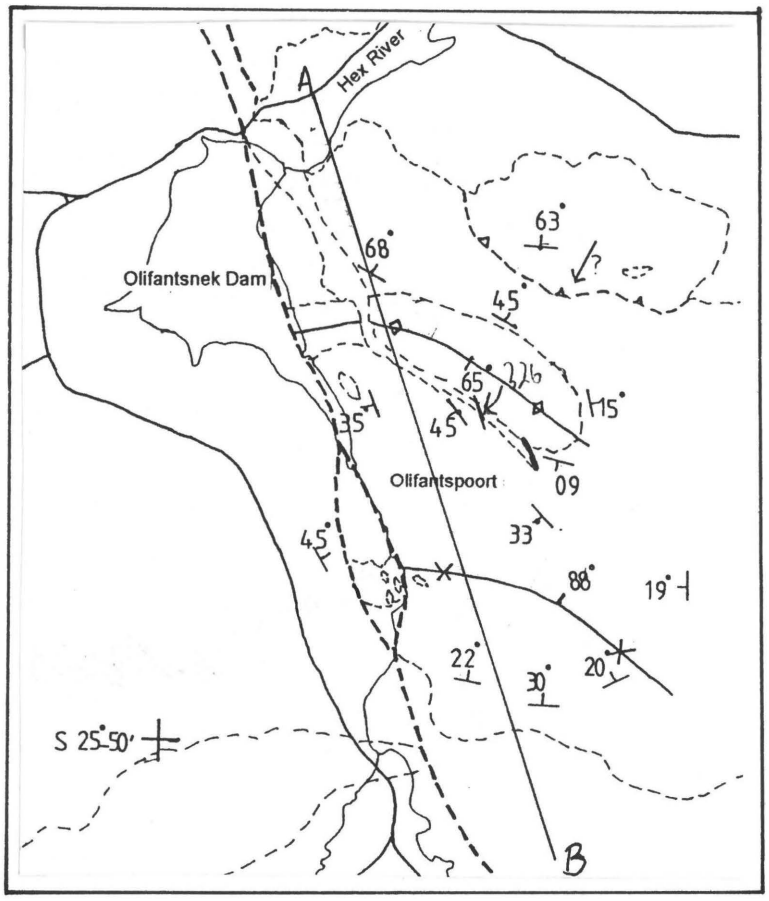

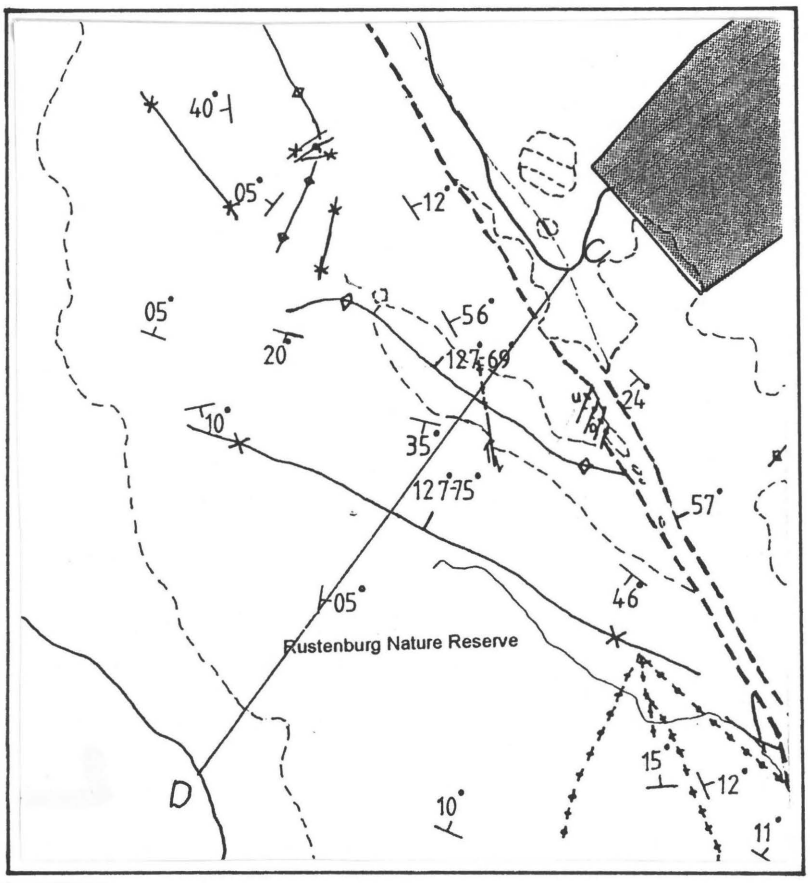

Figure 4.3: Locations of cross-sections constructed in Figure 4.2.

Figure 4.4: Reconstructed geological map of the strata in the field area, prior to dextral strike-slip displacement along the Rustenburg Fault.
Insert shows that reconstruction of the field area does not remove 'kinks' from the southern edge of the western Transvaal basin.

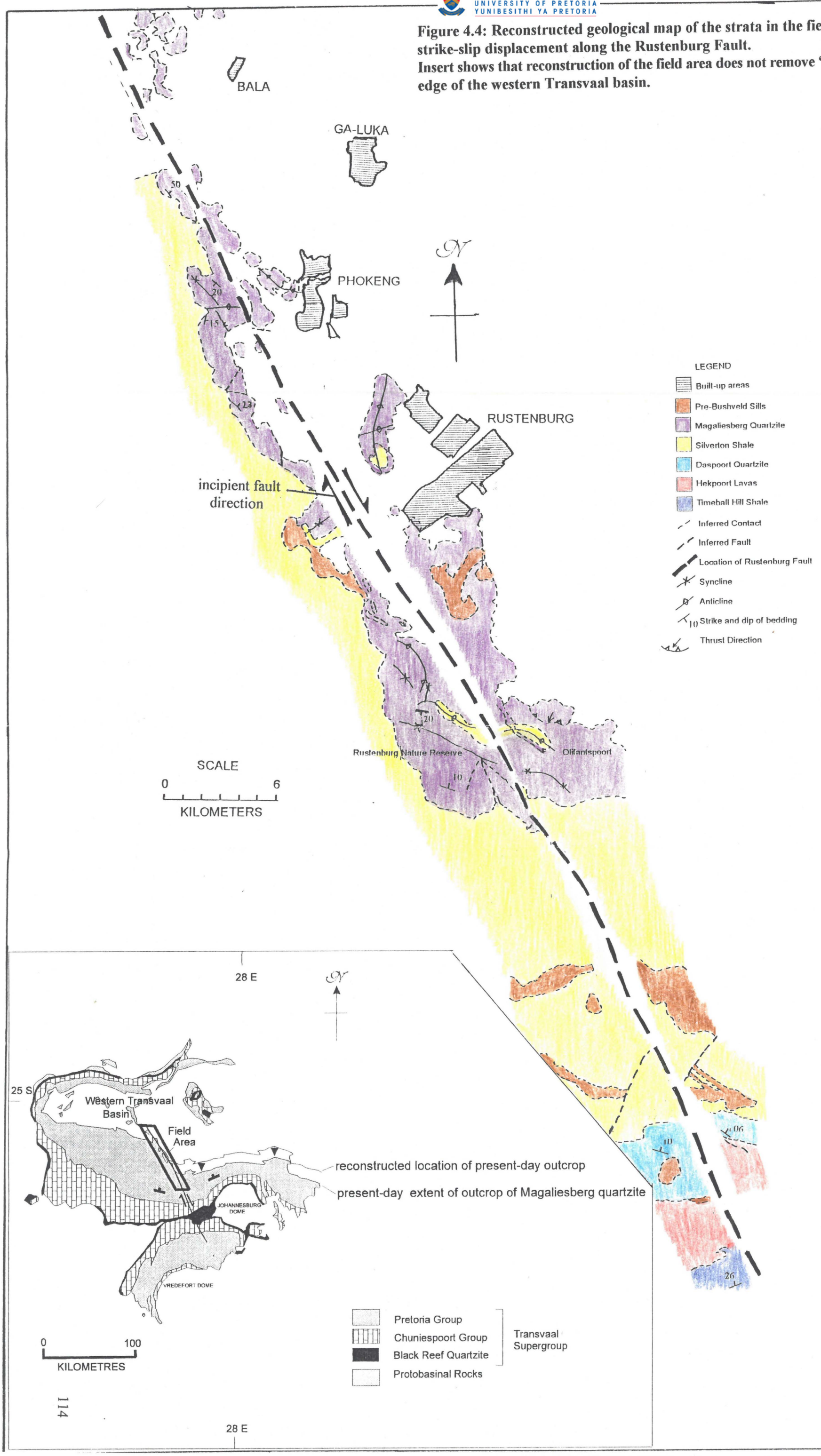

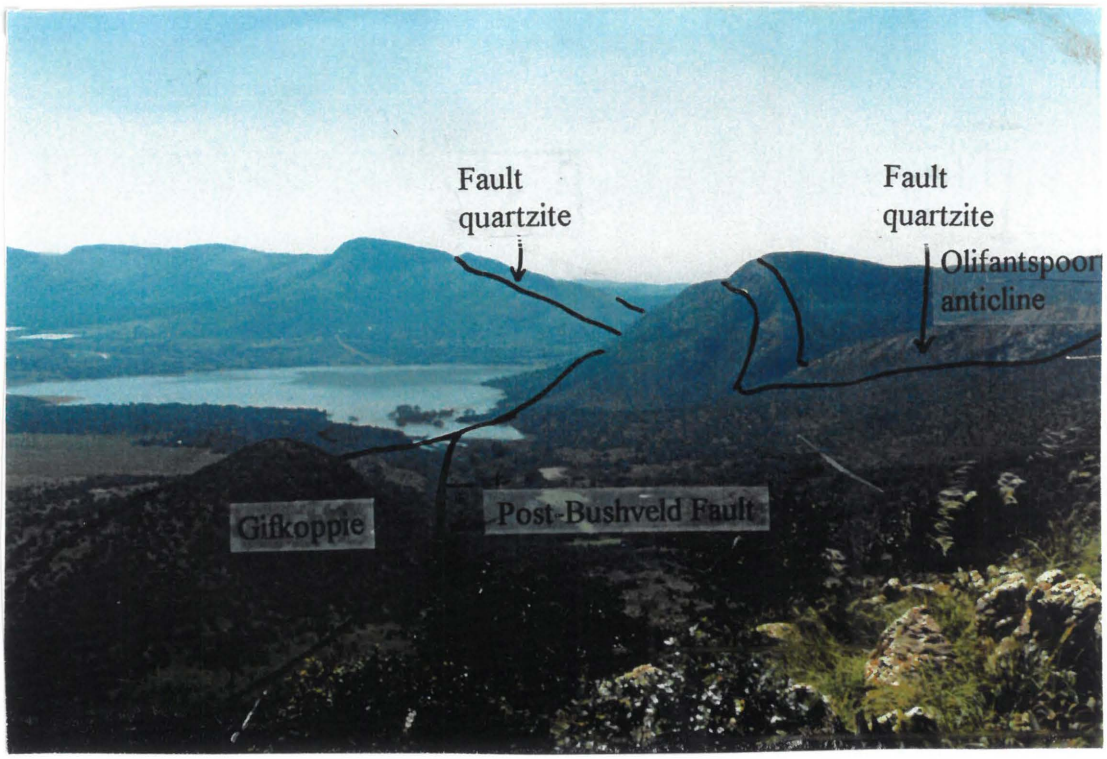

Figure 4.6: Inferred fault geometry at location 19, looking northwards. The unbroken line of Fault quartzite passes from left to right across the top of the photograph. Gifkoppie may have been faulted from beneath Olifantnek dam and dragged southwards to its present location, without disturbing the trend of the Fault quartzite above.

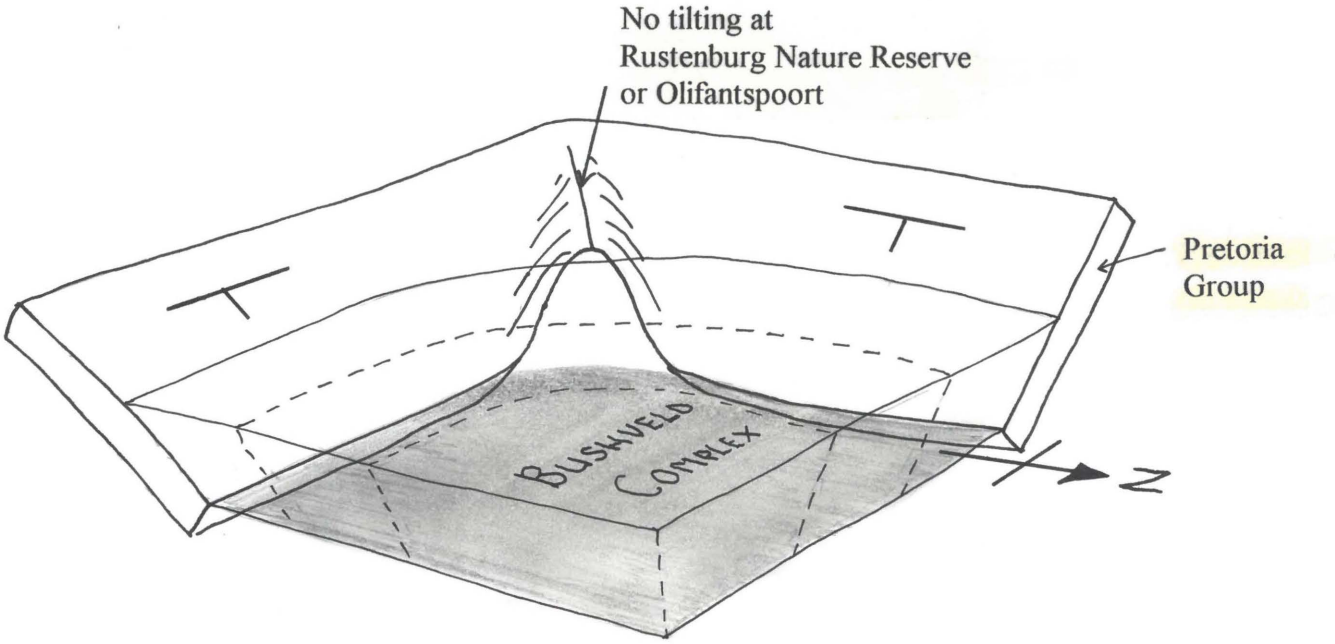

Figure 4.7: Schematic drawing showing why areas at corners of the Transvaal basin may fail to be accommodated during thermal collapse of the Bushveld Complex.

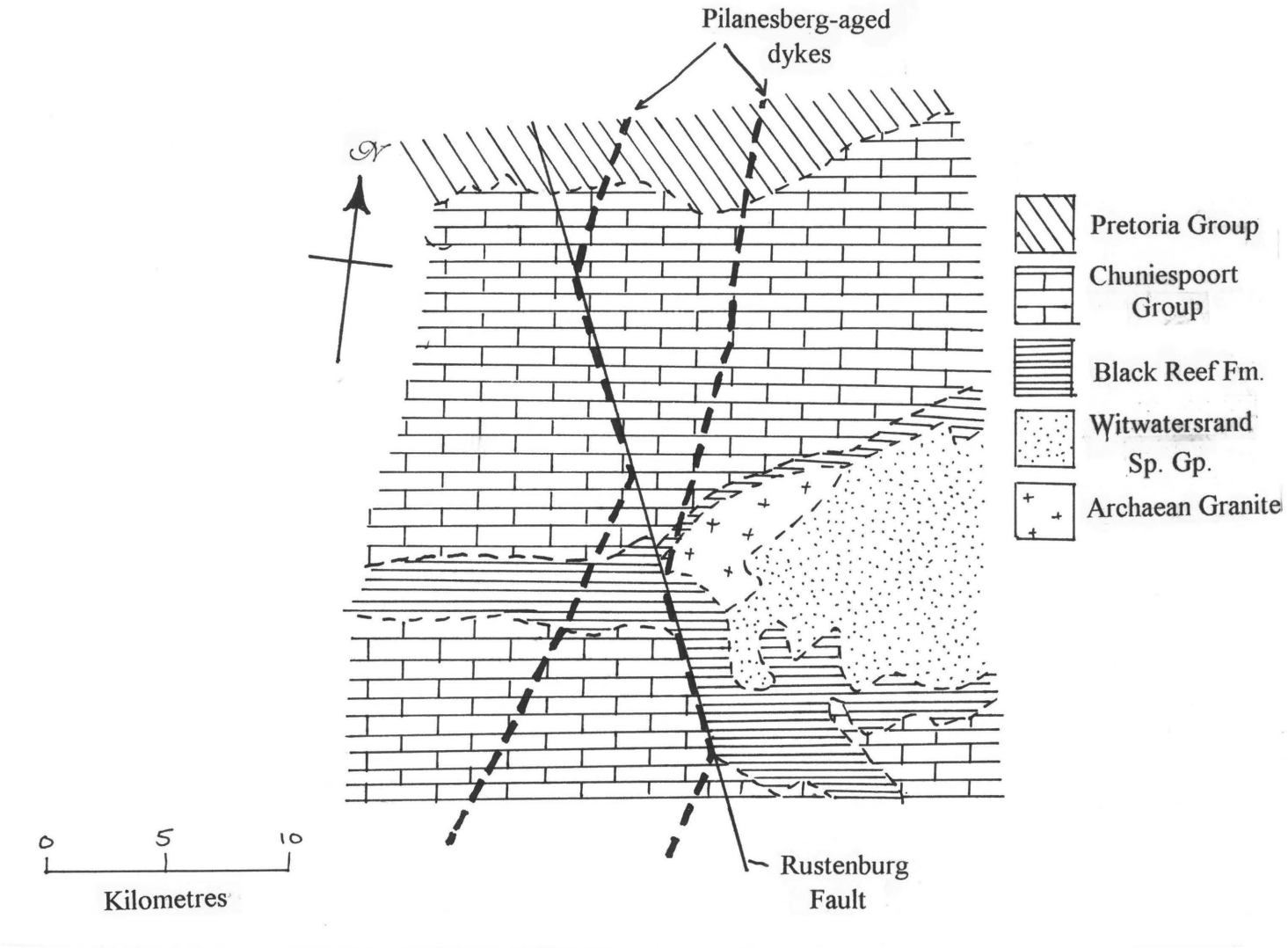

Figure 4.8: Exploitation of the Rustenburg Fault by Pilanesberg-aged dykes, rather than displacement (after Meadon, 1973).

a. Pre-Bushveld strain ellipse (2200 Ma.)

b. Post-Bushveld strain ellipse (2050 Ma.)

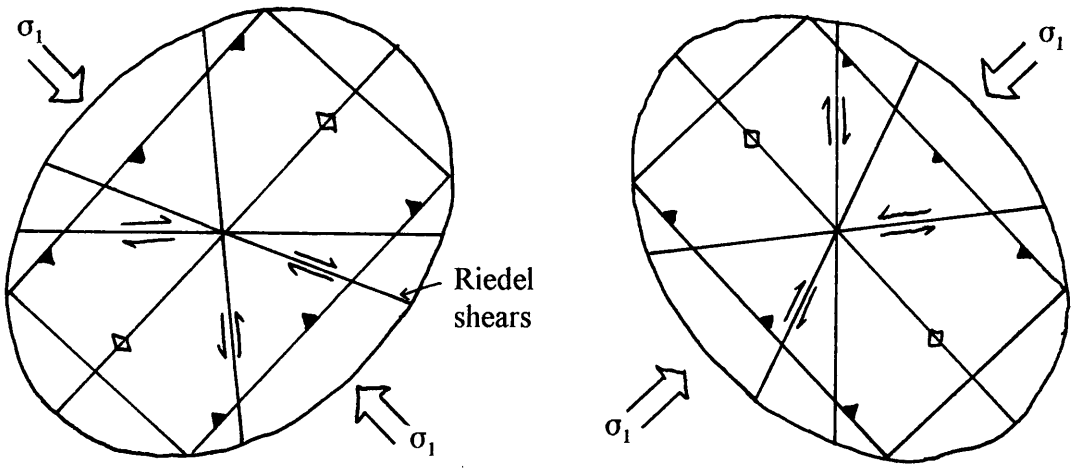

Figure 4.9: Strain ellipses on the T.M.L. proposed by Du Plessis and Walraven at 2200 Ma. and 2050 Ma., showing pre-Bushveld dextral movement on the T.M.L. and normal movement on the Rustenburg Fault, followed by post-Bushveld folding along N.W.-S.E. trending fold axes.

Tectonic Event	σ_1 direction	Trend of fold-axis	Strike of inferred extensional faults	Timing
D_1	N.W.-S.E.	F_1 = E.N.E.-W.S.W.	N.W.-S.E.	Pre-Bushveld
D_2	N.E.-S.W.	F_2 = N.W.-S.E.	N.W.-S.E. continued	Syn- and Post-Bushveld (long-lived)

Du Plessis and Walraven (1990).

Tectonic Event	σ_1 direction	Trend of fold-axis	Timing
D_1	N.E.-S.W.	F_1 = N.W. to S.E.	Pre-Bushveld
D_2	N.N.W.-S.S.E.	F_2 = E.N.E. to W.S.W.	Pre-Bushveld
D_3	N.E.-S.W.	F_3 = N.W. to S.E. F_1 tightened and Bushveld folded	Post-Bushveld

Hartzer (1995).

Tectonic event	σ_1 direction	Trend of fold axis and orientation of faults	Timing and regional events
D_1	N.E.-S.W.	F_1 = N.W. to S.E.	Pre-Bushveld
D_2	N.W.-S.E.	F_2 = between E.N.E. to W.S.W. and N.E. to S.W. Culminates in dextral displacement on Rustenburg Fault.	Pre-Bushveld (inversion of far western Transvaal basin)
D_3?	N.W.-S.E.	Some reactivation of Rustenburg Fault	Post-Bushveld

This model.

Table 4.1: Comparison of proposed model to other models for regional deformation in the western Transvaal Basin.

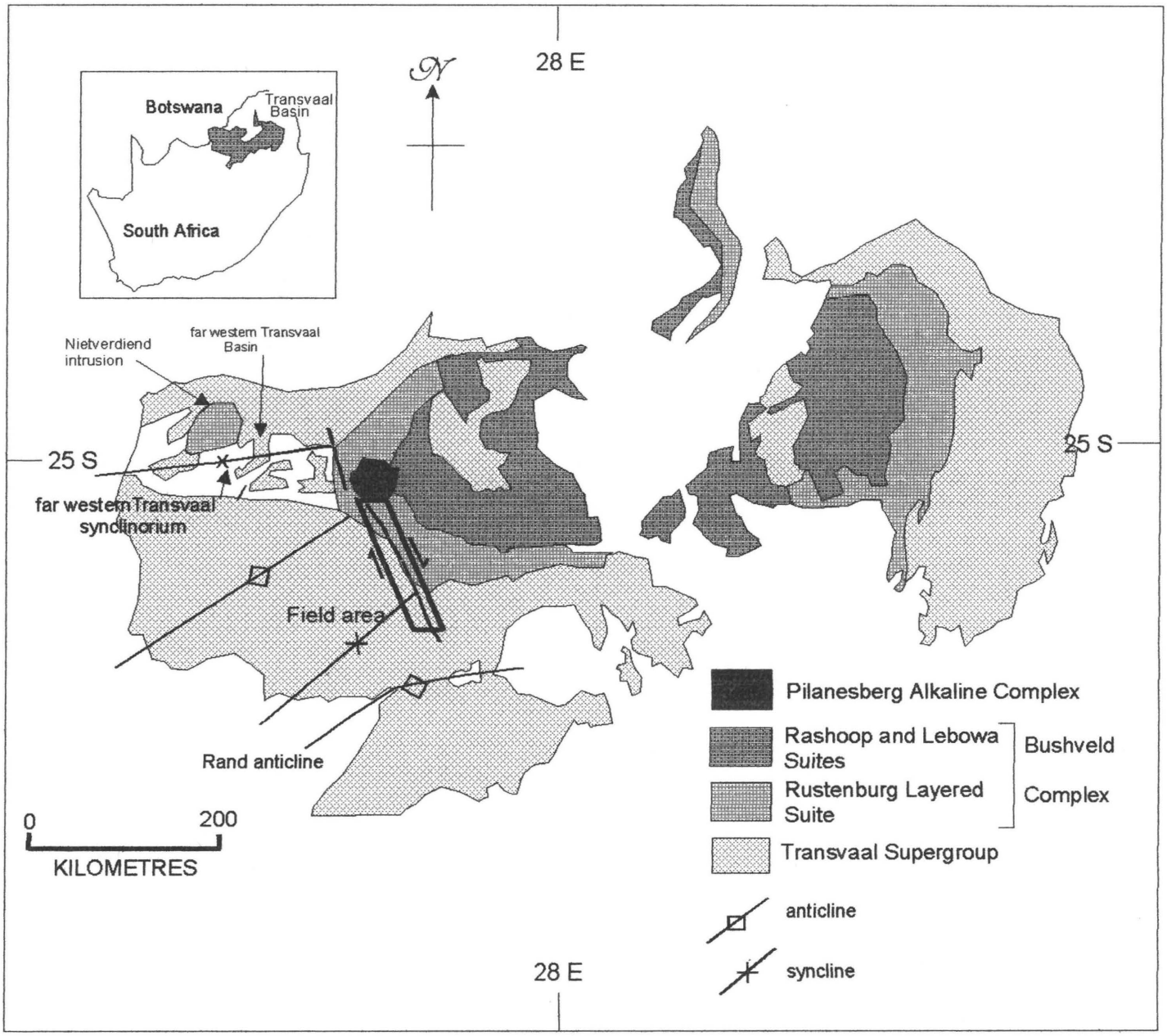

Figure 4.10: Geological map of the Transvaal Basin, showing compression of the far-western Transvaal Basin, as indicated by E.N.E.-W.S.W. to N.E.-S.W. trending folds. (after Dietvorst, 1991; Eriksson et al., 1995.)

5: CONCLUSIONS.

Field and microscopic examination of the outcrops adjacent to the Rustenburg Fault has enabled the history of the Fault to be constrained in considerable detail. The timing of movement of the Fault proposed in this work has further enabled a new model for the inversion of the far-western Transvaal basin to be constructed. A summary of proposed events which have occurred along the Fault zone and on a regional scale will be presented in this chapter, along with a table of reconstructed events (Table 5.1).

The earliest record for the movement of the Rustenburg Fault can be seen in the Daspoort Formation, which shows evidence for syn-sedimentary normal faulting, with downthrow to the west, creating a deeper basin which was filled with sediment. Movement may also have occurred during deposition of later Pretoria Group formations, though there is little evidence for this.

After lithification of the Pretoria Group, but before the onset of Bushveld magmatism, the field area was affected by a deformational event (D_1) with maximum compression in a N.E.-S.W. direction, which generally caused F_1 folding in the Pretoria Group adjacent to the Fault, with a fold axis trending N.W.-S.E.. The area was probably susceptible to folding due to pre-existing basement weakness beneath the Fault zone. This first deformational event was followed by a second (D_2), possibly due to the start of accretion of Kheis terranes on the N.W. margin of the Kaapvaal craton. Maximum compression was directed N.W.-S.E.. Initially this caused large-scale folding west of the Fault, with the fold axis orientated N.E.-S.W., and this compression inverted the far western Transvaal basin, by the creation of an anticlinorium in the upper Pretoria Group rocks. Folds of similar D_2 orientation were imposed adjacent to the Rustenburg Fault, often causing interference folding with the F_1 folds, leading to the creation of transitional Type 1-Type 2 interference structures. Continued pressure in the D_2 direction caused reactivation of the Rustenburg Fault, causing up to 10 km of dextral strike-slip movement, producing a Fault zone several hundred metres wide. Movement along the Fault released much of the D_2 stress in the region, preventing rocks east of the Fault from being effected by the deformation. The emplacement of the Bushveld intrusion caused contact metamorphism of the Pretoria Group, and circulation of quartz-rich fluids through the underlying Magaliesberg quartzite. The permeable Rustenburg Fault zone proved particularly exploitable by these fluids, and was intensely

recrystallised, destroying most characteristics of the pre-existing Fault rock. The less permeable Magaliesberg quartzite was also recrystallised to various degrees.

Burial beneath continued pulses of Bushveld magma lead to pressure solution at grain or crystal boundaries in all Pretoria Group sandstones and quartzites. The previously inverted far-western Transvaal basin could not be intruded by the Bushveld magmas, due to the continuous D_2 compressional regime in that area.

Continued post-Bushveld D_2-directed compression failed to reactivate the Fault again, due to its rheological strengthening by having had the Bushveld solidify across the Fault zone. However, some stress was accommodated by deformation within the quartz crystals along the Fault zone, though little net movement occurred. Beneath the Bushveld, where the Fault zone was still rheologically weak, some accommodation of D_2 occurred by movement, as shown by occasional brecciation of the metamorphosed Pretoria Group lithologies.

Age	Sedimentation and Igneous events	Tectonic Event
	Thermal collapse of Bushveld Complex	Continued D_2: Undulose extinction of Fault quartzite. Some reactivation of Fault in areas away from the Bushveld Complex
	Continued pulses of magma	Burial beneath Bushveld Complex: Pressure Solution
~2050 Ma	Bushveld intrusion	Recrystallisation of Magaliesberg and Fault rock. Contact metamorphism of Pretoria Group
		Eburnian (Kheis) orogeny causes D_2 folding (N.E.-S.W. fold axis) and up to about 10 km of dextral reactivation of the syn-sedimentary Rustenburg Fault.
		D_1 folding (N.W.-S.E. fold axis)
	Intrusion of Pre-Bushveld sills	Burial and partial lithification of Pretoria Group
c.2400-c.2200 Ma	Pretoria Group Sedimentation	Syn-sedimentary normal faulting

Table 5.1: Summary of reconstructed events along the Rustenburg Fault.

6: ACKNOWLEDGEMENTS.

R.T.Z. Mining and Exploration Ltd. are gratefully acknowledged for their financial and technical support during this work. In particular, Scott Jenkins, Cesar Ferreira and Dr. Rob Taylor are thanked for their support. Laura Regaldo of R.T.Z. Mining and Exploration painstakingly digitised the field maps.

Prof. Pat Eriksson and Dr. Roelof van der Merwe are thanked for their good humoured supervision of this work, and the remainder of the staff at the Department of Geology, University of Pretoria, are thanked for their technical support.

Thanks are also due to Duncan Lee, of St. Andrews University, Scotland, who acted as a field assistant between July and August 1996.

7: REFERENCES:

Altermann, W.A. & Nelson, D.R, in press: Basin analysis, sedimentation rates and regional correlations as implied by precise U-Pb zircon ages from volcanic sediments of the Neoarchaean Campbellrand Subgroup of the Kaapvaal craton. Sedimentary Geology.

Armstrong, R.A., Compston, W., Retief, E.A., Williams, I.S. & Welke, H.J. 1991: Zircon ion microprobe studies bearing on the age and evolution of the Witwatersrand triad. Precambrian Research **53**, p. 243-266.

Barton, J.M. & Van Reenen, D.D. 1992: When was the Limpopo Orogeny? Precambrian Research **55**, p. 7-16.

Barton, J.M., Compston, W., Williams, I.S., Bristow, J.W., Hallbauer, D.K. & Smith, C.K. 1989: Provenance ages for the Witwatersrand Supergroup and the Ventersdorp contact reef: constraints from ion microprobe (U-Pb) ages of detrital zircons. Economic Geology **84** p. 2012-2019.

Beukes, N.J. & Cairncross, B. 1991: A lithostratigraphic-sedimentological reference profile for the Late Archaean Mozaan Group, Pongola sequence: application to sequence stratigraphy and correlation with the Witwatersrand Supergroup. South African Journal of Geology **94**, p. 44-69.

Bloy, P.D. 1986: The Rustenburg Fault. Unpublished B.Sc. honours dissertation, University of Natal.

Brock, B.B. & Pretorius, D.A. 1964: Rand basin sedimentation and tectonics. In: Houghton, S.H. (ed.) The geology of some ore deposits in southern Africa. Vol. 1. Geological Society of South Africa, Johannesburg, p. 549-599.

Burke, K., Kidd, W.S.F. & Kusky, T. 1985: Is the Ventersdorp rift system of southern Africa related to a continental collision between the Kaapvaal and Zimbabwe cratons at 2.64 Ga ago? Tectonophysics **115**, p. 1-24.

Burke, K., Kidd, W.S.F. & Kusky, T. 1986: Archaean foreland basin tectonics in the Witwatersrand, South Africa. Tectonics **5**, p. 439-456.

Button, A. 1973. A regional study of the stratigraphy and development of the Transvaal basin in the eastern and northeastern Transvaal. Unpublished Ph.D. thesis, University of Witwatersrand.

Callaghan, C.C., Eriksson, P.G. & Snyman, C.P. 1991: The sedimentology of the Waterberg Group in the Transvaal, South Africa: and overview. Journal of African Earth Sciences **13**, p. 121-139.

Cawthorn, R.G., Davies, G., Clubley-Armstrong, A. & McCarthy, T.S. 1981: Sills associated with the Bushveld Complex, South Africa: an estimate of parental magma composition. Lithos **14**, p.1-15.

Clendenin, C.W. 1989: Tectonic influence on the evolution of the early Proterozoic Transvaal Sea,

Sea, southern Africa. Unpublished Ph.D. thesis, University of Witwatersrand.

Coertze, F.J. 1962: The Rustenburg Fault as a controlling factor of ore-deposition southwest of Pilansberg. Transactions of the Geological Society of South Africa **65**, p.253-262.

Cousins, C.A. 1959: The structure of the mafic portion of the Bushveld Complex. Transactions of the Geological Society of South Africa **62**, p. 179-201.

Cousins, C.A.1962: Discussion of paper presented by F.J. Coertze on 'The Rustenburg Fault as a controlling factor of ore-deposition southwest of Pilansberg'. Transactions of the Geological Society of South Africa **65**, p. 253-262.

Coward, M.P. Spencer, R.M. & Spencer, C.E. 1995: Development of the Witwatersrand Basin, South Africa. In: Coward, M.P. & Ries, A.C. (eds.): Early Precambrian Processes. Geological Society Special Publications no. **95**, p. 243-269.

Daly, R.A. 1928: Our mobile earth. Charles Scribner, New York.

Davis, G.H. & Reynolds, S.J. 1996: Structural geology of rocks and regions, second edition. John Wiley & Sons, New York.

de Wit, M.J., Roering, C., Hart, R., Armstrong, R.A., de Ronde, C.E.J., Green, R.E.W., Tredoux, M., Peberdy, E. & Hart, R.A. 1992: Formation of an Archaean continent. Nature **357**, p. 553-562.

Dietvorst, E.J.L. 1991: Instability and basin formation on the Kaapvaal Craton, southern Africa. Journal of African Earth Sciences **13**, p. 359-365.

Du Plessis, C.P., & Walraven, F. 1990: The tectonic setting of the Bushveld Complex in southern Africa, Part 1. Structural deformation and distribution. Tectonophysics **179**, p. 305-319.

Engelbrecht, J.P. 1976: Metasediments of the Pretoria Group in the Enzelsberg area, Marico District. Transactions of the Geological Society of South Africa **79**, p. 61-75.

Engelbrecht, J.P. 1986: Die Bosveldkompleks en sy vloergesteentes in die omgewing van Nietverdiend, Wes-Transvaal. Unpublished Ph.D. thesis, University of Pretoria.

Eriksson, P.G. & Cheney, E.S. 1992: Evidence for the transition to an oxygen-rich atmosphere during the evolution of red beds in the lower Proterozoic sequences of southern Africa. Precambrian Research **54**, 257-269.

Eriksson, P.G. & Reczko, B.F.F. 1995: The sedimentary and tectonic setting of the Transvaal Supergroup floor rocks to the Bushveld Complex. Journal of African Earth Science **21**, p. 487-504.

Eriksson, P.G., Schreiber, U.M. & van der Neut, M. 1991: A review of the sedimentology of the early Proterozoic Pretoria Group, Transvaal Sequence, South Africa: implications for tectonic setting. Journal of African Earth Sciences **13**, p. 107-119.

Eriksson, P.G., Hattingh, P.J. & Altermann, W.A. 1995: An overview of the geology of the Transvaal Sequence and Bushveld Complex, South Africa. Mineralium Deposita **30**, p. 98-111.

Eriksson, P.G., van der Merwe, R. & Bumby, A.J. under review: The early Proterozoic Woodlands Formation (Transvaal Supergroup) of eastern Botswana - northwestern South Africa: lithostratigraphy and relationship with Transvaal basin inversion structures. Journal of African Earth Sciences.

Eriksson, P.G., Reczko, B.F.F., Corner, B. & Jenkins, S.L. 1996: The Kanye axis, Kaapvaal craton, southern Africa: a postulated Archaean crustal architectural element inferred from three-dimensional basin modelling of the lower Transvaal Supergroup. Journal of African Earth Sciences **22**, p. 223-233.

Eriksson, P.G., Schweitzer, J.K., Bosch, P.J.A., Schreiber, U.M., van Deventer, J.L. & Hatton, C.J. 1993: The Transvaal Sequence: an overview. Journal of African Earth Sciences **16**, p. 25-51.

Fleuty, M.J. 1964:The description of folds: Geological Association Proceedings **75**, p. 461-492

Friese, A.E.W., Charlesworth, E.G. & McCarthy, T.S. 1995: Tectonic processes within the Kaapvaal craton during the Kibaran (Grenville) orogeny: Structural, geophysical and isotopic constraints from the Witwatersrand basin and environs. University of Witwatersrand, Johannesburg, Economic Geology Research Unit information circular no. 292.

Grobler, D.F., and Walraven, F. 1993: Geochronology of Gabarone Granite Complex extensions in the area north of Mafikeng, South Africa. Chemical Geology (Isotope Geoscience Section) **105** p. 319-337.

Hargraves, R.B. 1961: Shatter cones in the rocks of the Vredefort Ring. Transactions of the Geological Society of South Africa **64**, p. 147-162.

Harmer, R.E., & Von Gruenewaldt, G. 1991: A review of magmatism associated with the Transvaal basin - implications for its tectonic setting. South African Journal of Geology **93**, p. 104-122.

Hartzer, F.J. 1995: Transvaal Supergroup inliers: tectonic development and relationship with the Bushveld complex, South Africa. Journal of African Earth Science **21**, p. 521-547.

Hatton, C.J. 1995: Mantle plume origin for the Bushveld and Ventersdorp magmatic provinces. Journal of African Earth Sciences **21**, p. 571-577.

Hegner, E., Kroner, A. & Hoffmann, A.W. 1984: Age and isotope geochemistry of the Archaean pongola and Usushwana suites in Swaziland, southern Africa: a case for crustal contamination of mantle-derived magma. Earth and Planetary Science Letters **70**, p. 267-279.

Leeb-du Toit, A. 1986: The Impala Platinum Mines. In Anheusser, C.R., & Maske, S., (eds.): Mineral Deposits of Southern Africa 2, p. 1091-1106. Geological Society of South Africa.

Mineral Deposits of Southern Africa 2, p. 1091-1106. Geological Society of South Africa.

Lurie, J. 1986: Mineralisation of the Pilansberg Alkaline Complex. In Anheusser, C.R., & Maske, S. (eds.): Mineral Deposits of Southern Africa 2, p. 2215-2220. Geological Society of South Africa.

Martini, E.J. 1978: Coesite and stishovite in the Vredefort dome, South Africa. Nature **272**, p. 715-717.

Meadon, H.M. 1973: Die geologie en petrologie van die Wonderfonteingang. Unpublished M.Sc. thesis, University of Potchefstroom.

McCourt, S. 1995: The crustal architecture of the Kappvaal crustal block, South Africa, between 3.5 and 2.0 Ga. Mineralium Deposita **30**, p. 89-90.

Nell, J.1985: The Bushveld metamorphic aureole in the Potgietersrus area: Evidence for a two-stage metamorphic event. Economic Geology **80**, p 1129-1152.

Oberholzer, J.D.1995: Die geologie van die piroklastiesegesteentes in die Hekpoort Formasie, Transvaal Opeenvolging. Unpublished M.Sc. thesis, University of Pretoria.

Potgieter, G.J. 1992: Tektonisme langs die noordoostelike rand van die Bosveldkompleks, Suid Afrika. Unpublished Ph.D. thesis, University of Pretoria.

Ramsay, J.G. 1967: Folding and fracturing of rocks. McGraw-Hill Book Company, NewYork.

Reczko, B.F.F., Antoine, L.A.G. & Eriksson, P.G. in press: Three-dimentional computer-assisted basin modelling to generate exploration target areas: an example from the late Archaean-early Proterozoic Transvaal Supergroup, South Africa. Mineralium Deposita **32.**

Reczko, B.F.F., Oberholzer, J.D., Res, M., Eriksson, P.G. & Schrieber, U.M. 1995: A re-evaluation of the volcanism of the Palaeoproterozoic Pretoria Group (Kaapvaal craton) and a hypothesis on basin development. Journal of African Earth Sciences **21**, p. 505-519.

Reimold, W.U. & Gibson, R.L. 1996: Geology and evolution of the Vredefort Impact Structure, South Africa. Journal of African Earth Sciences **23** p. 125-162.

Robb, L.R., Davies, D.W. & Kamo, S.L. 1991: Chronological framework for the Witwatersrand basin and environs: towards a time constrained geological model. South African Journal of Geology **94** p. 86-95.

Roering, C., Barton, J.M. & Winter, H. de la R. 1990: The Vredefort structure: A perspective with regard to new tectonic data from adjoining terranes. Tectonophysics **171**, p. 7-22.

S.A.C.S. (South African Committee for Stratigraphy) 1980: Stratigraphy of South Africa. Part 1 (ed. Kent, L.E.). Lithostratigraphy of the Republic of South Africa, South West Africa/Namibia, and the Republics of Boputhatswana, Transkei and Venda. Handbook of the Geological Survey

of South Africa 8.

Schmidt, W. 1925: Gefügestatistik. Tschermaks mineralog. petrog. Mitt. **38**, p. 395-399.

Schreiber, U.M. 1991: A palaeoenvironmental study of the Pretoria Group in the Eastern Transvaal. Unpublished Ph.D. thesis, University of Pretoria.

Schreiber, U.M., Eriksson, P.G. & Snyman, C.P. 1990: Shale geochemistry of the Proterozoic Pretoria Group, Transvaal Sequence, South Africa: implications for source material. Abstracts for the 13th International Sedimentological Congress, Nottingham, p.482.

Schreiber, U.M., Eriksson, P.G., van der Neut, M. & Snyman, C.P. 1992: Sedimentary petrography of the early Proterozoic Pretoria Group, Transvaal Sequence, South Africa: implications for tectonic setting. Sedimentary Geology **80**, p. 89-103.

Schürmann, L.W. 1991: The geochemistry and Petrology of the Upper Critical zone in the Boshoek section of the western Bushveld Complex. Unpublished M.Sc. thesis, University of Pretoria.

Shand, S.J. 1916: The pseudotachylite of Parijs (Orange Free State) and its relation to "trapshotten gneiss" and "flinty crushrock". Quarterly Journal of the Geological Society of London **72**, 198-217.

Sharpe, M.R. 1982: The floor contact of the eastern Bushveld Complex: Field relations and petrography. University of Pretoria Institute for Geological Research on the Bushveld Complex Research Report No.36.

Sibson, R.H. 1977: Fault rocks and fault mechanisms. Journal of the Geological Society of London **133** p. 191-213.

Spry, A. 1969: Metamorphic textures, Pergamon Press, Oxford.

Stanistreet, I.G. & McCarthy, T.S. 1991: Changing tectono-sedimentary scenarios relevant to the development of the Late Archaean Witwatersrand Basin. Journal of African Earth Sciences **13**, p. 65-81.

Thomas, R.J., von Veh, M.W. & McCourt, S. 1993: The tectonic evolution of southern Africa: an overview. Journal of African Earth Sciences **16**, p. 5-24.

Truter, F.C. 1955: Modern concepts of the Bushveld Complex. Publ.Comn. Cooperation Technique en Afrique, Southern Reg. Comn. Géol. Salisbury, p. 77-91.

Van der Neut, M. 1990: Afsettingstoestande van die Pretoria Groep gesteentes in die Pretoria-Bronkhorstspruit-Delmas gebeid. Unpublished M.Sc. thesis, University of Pretoria.

Vermaak, C.F. 1970: The geology of the lower portion of the Bushveld Complex and its relationship to the floor rocks in the area west of the Pilansberg, western Transvaal. In: Visser,

D.J.L. & von Gruenewaldt, G. (eds.) 1970: Symposium on the Bushveld Igneous Complex and other layered intrusions. The Geological Society of South Africa Special Publication no.1, p. 242-265.

Verwoerd, W.J. 1963: Die geologiese struktuur van die Krokodilrivierfragment. Transactions of the Geological Society of South Africa **66**, p. 49-74.

Viljoen, M.J. & Hieber, R. 1986: The Rustenburg section of Rustenburg Platinum Mines Limited, with reference to the Merensky Reef. In Anheusser, C.R., & Maske, S., (eds.): Mineral Deposits of Southern Africa 2, p. 1107-1134. Geological Society of South Africa.

Von Gruenewaldt, G. & Harmer, R.E. 1993: Tectonic setting of Proterozoic layered intrusions with special reference to the Bushveld Complex. In: Condie, K.C. (ed.) Proterozoic crustal evolution. Elsevier, Amsterdam, p. 181-213.

Wager, L.A. & Brown, G.M., 1967: Layered Igneous Rocks. Oliver & Boyd, Edinburgh.

Wagner, P.A. 1927: The geology of the north-eastern part of the Springbok Flats and surrounding country. Explanation sheet 17 (Springbok Flats). Geological Survey South Africa, Pretoria.

Wallmach, T., Hatton, C.J. & Droop, G.T.R. 1989: Extreme facies of contact metamorphism developed in calc-silicate xenoliths in the eastern Bushveld Complex. Canadian Mineralogist **27**, p. 509-523.

Walraven, F. 1981: The geology of the Rustenburg area. Explanation sheet 2526. Geological Survey South Africa, Pretoria.

Willemse, J. 1959: The "floor" of the Bushveld Igneous Complex and its relatioships, with special relationships to the eastern Transvaal. Proceedings of the Geological Society of South Africa **62**, xxii-lxxxiii.